Extracellular Electron Transport in Microbial Electrochemical Cells

by

Bipro Ranjan Dhar

A thesis

presented to the University of Waterloo

in fulfillment of the

thesis requirement for the degree of

Doctor of Philosophy

in

Civil Engineering

Waterloo, Ontario, Canada, 2016

AUTHOR'S DECLARATION

I hereby declare that I am the sole author of this thesis. This is a true copy of the thesis, including any required final revisions, as accepted by my examiners.

I understand that my thesis may be made electronically available to the public.

Abstract

Microbial electrochemical cells (MxCs) are engineered biological systems that use microbial metabolism of anode-respiring bacteria (ARB) to catalyze electron transfer from a soluble electron donor to the anode via extracellular electron transfer (EET). Although several EET mechanisms (via direct contact, mediators, and conduction) have been proposed, understanding of EET in biofilm anodes generating high current density is limited. Recent findings suggested that electrical conduction would be a key EET pathway in MxCs producing high current density, in which biofilm conductivity (K_{bio}) would mainly regulate EET kinetics. However, there is no clear understanding of the influence of various environmental factors, such as anode potential, local pH, and substrate limitation in biofilm anodes on EET kinetics and K_{bio}. In addition, scalable, economical designs of MxCs producing high current density still need improvement for deployment of MxCs in field, such as multi-anode MxCs. Hence, the goals of this study were to systematically characterize the effects of (a) anode potential (E_{anode}), (b) local pH in biofilm anodes and (c) substrate limitations on EET kinetics and K_{bio} for a key fundamental aspect of MxCs, and develop scalable, economical MxCs using multi-anode configurations in an engineering aspect of MxCs.

A biofilm anode enriched with *Geobacter* spp. showed high K_{bio} (0.96-1.24 mS/cm) to E_{anode} change from -0.2 V to +0.2 V vs. standard hydrogen electrode (SHE), while the steady-state current density varied significantly in the MxC. Change of E_{anode} shifted population of *Geobacter* genus in the biofilm anode, influencing intracellular electron transfer (IET) kinetics. However, high K_{bio} was consistently kept in the biofilm at E_{anode} change. This result suggests that EET kinetics would be relatively insensitive to E_{anode} dynamics. A step-wise decrease in phosphate buffer concentration from 100 to 2.5 mM caused pH gradient of ~0.5 pH unit between the outmost and inmost layers of a biofilm anode, showing a pH of 6.5-6.7 near the anode in a thick (>100 μm) biofilm. This pH gradient substantially dropped current density from 2.38 to 0.64 A/m^2 in an MxC, and K_{bio} decreased by 69% for the 2.5 mM phosphate buffer. These results imply that the metabolic activity of ARB inhibited by acidic pH is closely associated with conductive nature of biofilm anodes and EET kinetics. In a steady-state MxC, K_{bio} dynamically decreased from 0.53 mS/cm to 0.14 mS/cm during the long starvation (4-5 days) lacking exogenous electron donor. However, the poor K_{bio} was recovered to 0.55 mS/cm after acetate spiking, indicating that ARB's

activity profoundly influences K_{bio} and EET kinetics. A multi-anode MxC equipped with three anode modules showed a non-linear increase of current density to the number of anodes. The anode closest to a reference electrode (i.e., low ohmic energy loss) contributed to 65% of the overall current density of 9.15 A/m^2 from the multi-anode MxC, where *Geobacter* species were dominant at 87% and half saturation potential (-0.251 to -0.242 V vs. SHE) was lowest among all anode electrodes. In comparison, the current density from the other two anodes distant from the reference electrode was as small as 1.4-1.7 A/m^2, along with negligible population of *Geobacter* species. These results suggest that E_{anode} changed by ohmic energy losses in individual anodes can shift microbial communities, and lead to different electron transfer kinetics and current density on each anode.

Acknowledgements

I would like to express my sincere gratitude to my supervisor Dr. Hyung-Sool Lee, for giving me the opportunity to work on such a fascinating area of research. It was truly a great privilege to work with him. His dedication and passion to research always inspired me to dig into fundamentals more. Definitely, this work wouldn't have become what it is without his continuous influence, guidance and support in last four years. His honest criticism and evaluations always helped me to improve my research quality throughout my Ph.D. program at Waterloo.

I am thankful to my Ph.D. committee members: Dr. Raymond Legge, Dr. James R. Craig, Dr. Youngki Yoon, and Dr. César I. Torres for their valuable advice, and feedback. I would like to thank our research collaborators at United State Environmental Protection Agency (USEPA) and Arizona State University (ASU).

Thanks to all my teachers, mentors, and supervisors who have enlightened me since my childhood. I cannot possibly say enough thanks to Dr. Elsayed Elbeshbishy, for his friendship, help, and advice since I started my journey as a graduate student at Western in 2009. My profound thanks go to Dr. Junyoung An, for his friendship, and sharing his knowledge through valuable discussions related to my project. I am very grateful to all of former and current members at Waterloo Environmental Biotechnology Laboratory (WEBL). A very special thanks to Junyoung Sim, particularly for his generous help in last eight months. Thanks to Dr. Yaohuan Gao and Hyeongu Yeo, for their assistance, when I first joined WEBL in 2012. I would like to thank Mark Sobon and Mark Merlau for their technical assistance.

A very special word of gratitude goes to Sudhan Banik and Sharmishtha Banik for their unconditional support and encouragement during my early days in Canada. I would also like to thank all of my friends in Canada and Bangladesh. I would like to thank all members of Bangladeshi Cultural Society at KW, specially Nahid Naznin Nita and Asadur Rahman Joarder.

And last but certainly not least, I wish to express my deepest gratitude to my parents, my wife, my daughter, and my sisters. I am blessed to have such great parents who always support and encourage my major decisions in life. I would like to thank my wife, Bipasha, for her encouragement, and for accepting my busy life. Thanks to my beloved daughter, Biday, for her smile.

Dedication

R. S.

To my parents, wife, and daughter

Table of Contents

x

List of Tables

List of Figures

Nomenclature

η	Local potential (V)
ARB	Anode Respiring Bacteria
COD	Chemical Oxygen Demand (g/m^3 or mg/L)
CV	Cyclic Voltammetry
E_{anode}	Anode potential (V or mV)
EET	Extracellular Electron Transfer
E_{KA}	Half-saturation potential (V or mV)
E_{OMP}	Redox potential of OMPs (V)
E_{Sub}	Redox potential of NADH (V)
F	Faraday's constant (96,485 C/mol e$^-$)
f_s^o	Fraction of electron used for cell synthesis
G	Conductance (mS)
HRT	Hydraulic Residence Time (h)
j	Current density (A/m^2)
j_{max}	Maximum current density (A/m^2)
K_{bio}	Biofilm conductivity (mS/cm)
K_s	Substrate half-saturation concentration of acetate (g COD/m^3 or mg/L)
L_f	Biofilm thickness (μm or m)
LSCV	Low Scan Cyclic Voltammetry
MxC	Microbial Electrochemical Cell
n	Number of electrons transferred per reaction
OMP	Outer Membrane Protein
q_{max}	Maximum specific substrate utilization rate (g COD/g VS-d)
R	Ideal gas constant (8.314 J/mol-K)
S	Substrate concentration (g COD/m^3 or mg/L)
SHE	Standard Hydrogen Electrode
T	Operating temperature (K)
VSS	Volatile suspended solids (g/m^3 or mg/L)
X_f	Concentration of active ARB in anode biofilm (g VS/m^3)

Chapter 1

Introduction

1.1   Background

The need for energy-efficient wastewater treatment has increased, as energy security, climate change and sustainability issues become a major concern worldwide. As a result, there has been a growing interest in anaerobic wastewater treatment technologies that are able to recover energy or value-added products from organic wastes and wastewaters. These technologies include anaerobic digestion, dark biohydrogen fermentation, and microbial electrochemical cells (MxCs) (Logan and Rabaey, 2012; Rabaey and Rozendal, 2010; Lee et al., 2010; Torres, 2014; Zhang et al., 2014). Among them, MxCs represent an emerging anaerobic biotechnology that combines metabolism of anode-respiring bacteria (ARB) with electrochemistry to capture electrons directly from biodegradable organic matter in waste or wastewater. This feature allows us to manipulate the recovered electrons into electric power or other chemicals (e.g., hydrogen gas, hydrogen peroxide, acetate, ethanol, caustics, and butanol) (Logan and Rabaey, 2012; Rabaey and Rozendal, 2010; Logan et al., 2006; Lee et al., 2010; Schröder et al., 2015).

In MxCs, microorganisms capture energy by transferring electrons derived from a donor substrate to the anode. The microorganisms that are responsible for this electron transport process typically form a biofilm on the anode surface where they oxidize donor substrates, and release electrons, protons, and CO_2. The released electrons are transferred to outer membrane proteins (OMPs) via diffusible intracellular electron carriers (i.e., NAD^+/NADH) and membrane-bound electron transfer systems. The electron transport from the electron donor to the OMPs is called intracellular electron transfer (IET). Ultimately, the electrons transfer from the OMPs to the anode electrode via a process known as extracellular electron transfer (EET). Thus, the electron transfer from a donor substrate to the electrode involves three major steps: microbial oxidation, transfer of electrons from the intracellular electron carrier to the OMPs, and EET. Most researchers postulate that the kinetics of the first two steps (IET) mainly limit current generation (Torres et al., 2008a, 2009; Marcus et al., 2007; Yoho et al., 2014; Renslow et al., 2013a, 2013b; Sun et al., 2015), although the EET mechanism and kinetics are still ambiguous.

Earlier studies have proposed that EET can occur either via direct contact of the OMPs with the electrode or via mediators (Hernandez and Newman, 2001; Bond and Lovely, 2003; Kim et al., 2002; Marsili et al., 2008; Rabaey et al., 2005). However, recent studies have shown that these two mechanisms cannot produce a high current density (>10 A/m^2) due to diffusion limitations of mediators and limited surface area for direct contact. Instead, microorganisms use conduction-based EET to produce high current density (Marcus et al., 2007; Torres et al., 2008b, 2010; Renslow et al., 2013b; Malvankar et al., 2011, 2012; Marcus et al., 2007). The conduction-based EET is not well understood, although many studies suggest the significance of conductive EET in biofilm anodes generating high current density (> 10 A/m^2). Three conceptual pathways were suggested for this conductive EET, including microbial nanowires (or pili), electron superexchange (or electron hopping), and conductive biofilm matrix (Malvankar and Lovley, 2014; Malvankar et al., 2011, 2012; El-Naggar et al., 2010; Strycharz-Glaven et al., 2011; Snider et al., 2012; Marcus et al., 2007; Reguera et al., 2005; Pirbadian and El-Naggar, 2012; Pirbadian et al., 2014; Reguera et al., 2005; Gorby et al., 2006). Although significant research is underway to explore these conductive EET pathways, it seems reasonable that biofilm conductivity (K_{bio}) would represent EET kinetics in biofilm anodes (Marcus et al., 2007; Torres et al., 2010, 2008a; Malvankar et al., 2011, 2012). A few studies have suggested that metabolic activity of ARB, anode potential, substrate concentration, and proton mass transfer limitations may influence conductive EET (Malvankar et al., 2012; Liu and Bond, 2012; Renslow et al., 2013b; Torres et al., 2008b, 2009, 2007; Marcus et al., 2007). Yet, there are no studies evaluating the role of these factors on the K_{bio} and EET kinetics quantitatively. To succeed in MxC application we should better understand inter-correlations between important parameters (e.g., pH, ARB's activity, etc.) and EET kinetics characterized by K_{bio}.

Although significant advances in engineering designs for MxC have been developed over the last few years (Logan et al., 2015; Logan and Rabaey, 2012; Rabaey and Rozendal, 2010; Torres, 2014), these technologies are still at the laboratory scale. One of the major bottlenecks to MxC commercialization is the small energy output (current/voltage). For instance, power density achieved from millilitre-scale MxCs operated with acetate ranges from 1 to 6.9 mW/m^2 of anode surface area (Logan et al., 2015); no studies have demonstrated good performance of large-scale MXCs with wastewater. The research focus of MxCs has been shifted from electric power to resource recovery (e.g., hydrogen gas, hydrogen peroxide, acetate, ethanol, caustics,

and butanol) with an aid of exogenous power supply to improve the benefits of MxCs. For external energy-dependent MxCs, current density (proportional to the rate of resource recovery) is significant for success in field application, along with an acceptable range of electric power. It is yet to define an acceptable range of exogenous energy inputs, since this range depends on the economic value of recovered resources against electric power costs. Given that the economic benefit from resource recovery is much larger than input energy costs, the success of the MxCs needs the production of high current density. The literature has shown an increase of current density up to 25 A/m^2 using nanomaterials and conductive polymers (Xie et al., 2012; He et al., 2012; Li et al., 2011), but it is doubtful to deploy these approaches in large scale, due to cost and scale-up issues (Zhou et al., 2011; Butti et al., 2016). We need to explore more scalable and economical approaches to realize deployment of the MxCs, such as multi-anode MxCs. Anode kinetics mainly limit current density for MxCs run in the mode of exogenous energy supply (Lee et al., 2009; Torres et al., 2008a). Hence, multi-anode MxCs can be very efficient for improving current density. Unfortunately, the literature has commonly observed non-linear or trivial increases of current density in multi-anode MxCs (Jiang et al., 2011; Jiang and Li, 2009; Lanas and Logan, 2013; Hutchinson et al., 2011), although increased surface area of anodes can improve ARB biofilm formation and mass transfer in multiple-anode configurations (Fan et al., 2011; An and Lee, 2013; Dewan et al., 2008). Previous work has suggested that ohmic losses from electrode distance might limit current density from multi-anode MxCs (Lanas and Logan, 2013; Hutchinson et al., 2011; Jiang et al., 2011; Jiang and Li, 2009), but this information is relatively sparse. A more mechanistic approach is needed to understand limiting factors for the poor increase of current density in multi-anode MxCs, which will catalyze MxC scale-up.

1.2   Scope and Objectives

The overall objective of this study was to characterize EET kinetics and biofilm conductivity (K_{bio}) in mixed-culture biofilm anodes. The thesis comprises four specific research areas:

(1) Anode potential effects on IET and EET kinetics and K_{bio};
(2) EET kinetics and K_{bio} in acidic and neutral pH biofilms;
(3) EET kinetics and K_{bio} in substrate limiting and non-limiting conditions;
(4) Ohmic resistance effects on anod e kinetics in a multi-anode MxC;

This research was carried out at Waterloo Environmental Biotechnology Laboratory at the University of Waterloo. Several laboratory scale microbial electrochemical cells (MxCs) equipped with special anode electrodes for *in situ* K_{bio} measurement were fabricated and operated for this research. The unique aspect of this study is the systematic characterization of EET combining electrochemical, microbiological, microscopic, and other advanced engineering tools such as *in situ* measurement of K_{bio} using a source meter, and measurement of pH gradient throughout anode biofilms using microelectrodes.

1.3   Thesis Outline

This dissertation is divided into seven chapters, references, and six appendices. Chapter 1 (current chapter) provides background information on the research topic under investigation and summarizes the specific goals of the proposed research. Chapter 2 presents an overview of the available literature related to the proposed research. Chapter 3, 4, 5, and 6 are the main research chapters, presented in article format. Chapter 7 summarizes the findings focusing on scientific and engineering implications of the results, and provides recommendations for future research.

Chapter 2

Literature Review

2.1 General Features of Microbial Electrochemical Cells (MxCs)

Microbial electrochemical cells (MxCs) are devices that are able to convert chemical energy stored in organic compounds to electrical energy through the metabolism of microorganisms (mainly bacteria). The microbes that catalyze the electron transfer from soluble electron donors to the anode have been called exoelectrogens (Logan et al., 2006), electrocigens (Lovley, 2006), anode-respiring bacteria (ARB) (Torres et al., 2007), or electrochemically active bacteria (EAB) (Kim et al., 2004).

Figure 2-1 shows schematic of a dual-chamber MxC. In the anode chamber, ARB gain energy through anaerobic respiration that transfers electrons from an electron donor to the anode. ARB oxidize donor substrate anaerobically, and produce electrons, protons, and carbon-dioxide. In the cathode, the electrons transferred to the anode by ARB move to react with a terminal electron acceptor (e.g., oxygen, protons, H_2O, CO_2, etc.), and the overall reaction from the electron donor to the terminal electron acceptor is complete. Equation (2-1) describes a half reaction for acetate (CH_3COO^-) used as the electron donor to ARB:

$$CH_3COO^- + 3H_2O \rightarrow CO_2 + HCO_3^- + 8H^+ + 8e^- \qquad (2\text{-}1)$$
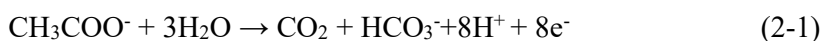
Electrons released by ARB's oxidation are transferred to the anode and then move to the cathode through an external circuit driven by the potential gradient between the two electrodes. When the potential gradient is positive (energy-generating reactions), MxCs produce electrical power. For each electron that is released from the anode, protons or other counter ions equivalent to the electron must transfer between the two electrodes through the separator (e.g., membrane) to meet charge neutrality (Figure 2-1).

MxCs can be used to synthesize value-added products on the cathode by manipulating terminal electron acceptors and providing exogenous energy (Figure 2-1). For instance, the electrons generated from organic wastewater can be used to reduce protons to form hydrogen gas on the cathode under anaerobic conditions with the supply of applied voltage.
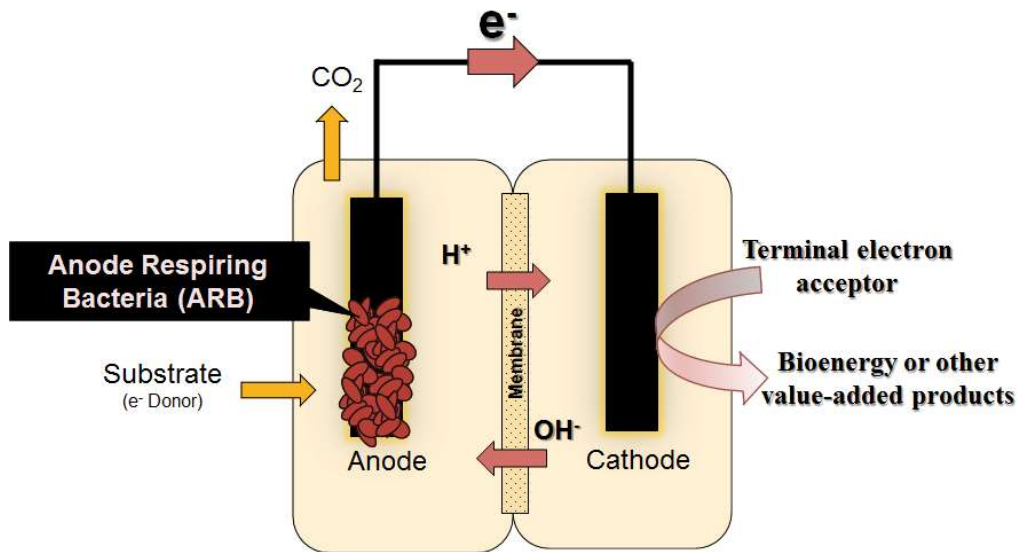
Figure 2-1. Schematic of a dual chamber MxC.

2.2 Electron Transfer from an Electron Donor to the Anode

The two major steps involved in the electron transfer from an electron donor to the anode include intracellular electron transfer (IET) and extracellular electron transfer (EET) (see Figure 2-2). This section describes the fundamentals involved in this cascade electron transfer process. IET consists of several biochemical reactions. Initially, ARB oxidize the electron donor, and produce electrons, protons, and CO_2 via the anaerobic tricarboxylic acid (TCA) cycle (Torres et al., 2010). The released electrons move to diffusible intracellular electron carriers (IEC), such as nicotinamide adenine dinucleotide (NAD^+/NADH). Then, the released electrons are transferred from NAD^+/NADH pools to the outer membrane proteins (OMPs) via membrane-bound electron transport systems (ETS) (Korth et al, 2015). The electrons transfer from the OMPs to the anode extracellularly; this is called EET (Lovley et al., 2006; Mehta et al., 2005; Reguera et al., 2005).

Several environmental or operating factors can influence IET, such as concentration and biodegradability of substrate, anode potential, microbial community (syntrophy and competition), proton accumulation, and substrate mass transfer limitations (Torres et al., 2007, 2008a, 2008b, 2009; Pant et al., 2010; Marcus et al., 2007, 2010, 2011; Renslow et al., 2013a,

2013b; Lee et al., 2009; Nam et al., 2011; Alterman et al., 2008; Franks et al., 2009; Parameswaran et al., 2009, 2010, 2011, 2012; Babauta et al., 2012, 2011; Gao et al., 2014a, 2014b; Dhar et al., 2013, 2015). The substrate-utilization kinetics mainly governs the IET kinetics and hence IET can be well described with the Monod equation .
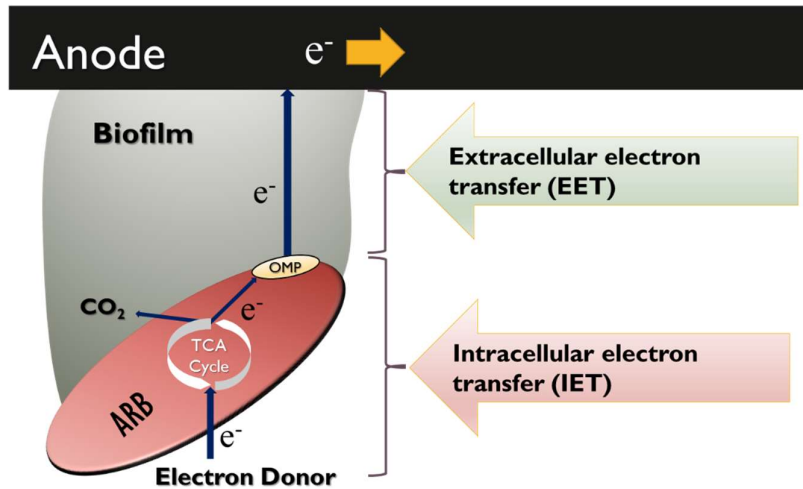
Figure 2-2. Electron transport from the substrate to the anode in MxCs.

There are several EET mechanisms, such as direct contact, mediators, conduction, or a combination of these pathways (Lovley and Malvankar, 2015; Malvankar et al., 2011, 2012a, 2012b, 2012c; El-Naggar et al., 2010; Strycharz-Glaven et al., 2011; Snider et al., 2012; Marcus et al., 2007; Reguera et al., 2005; Pirbadian and El-Naggar, 2012; Torres et al., 2010; Hernandez and Newman, 2001; Bond and Lovely, 2003; Kim et al., 2002; Marsili et al., 2008). EET kinetics is enigmatic, although understanding of EET mechanisms has been improved (Pirbadian et al., 2014; Malvankar et al., 2011, 2012a, 2015; Snider et al., 2012; Boyd et al., 2015). Recent studies have commonly suggested that conductive EET would only account for high current density over several A/m^2 in MxCs, while multi EET mechanisms might occur. Production of high current density is essential for MxC application in the field, which means that we should well comprehend the rate of electron transfer from the electron donor to the anode (IET and EET kinetics). The following sections summarize influential parameters and key fundamentals on IET and EET.

2.3   Intracellular Electron Transfer (IET)

2.3.1   Substrate Affinity of ARB

The amount of electrons captured from a donor substrate are critical for energy efficiency of MxCs: the more electrons are recovered, the higher the energy efficiency is. The amount of substrate consumed by ARB for current generation can be expressed with coulombic efficiency (CE (%) = coulombs/consumed substrate ×100). Many studies have investigated coulombic efficiency in MxCs treating a variety of organic compounds, waste and wastewater (Pant et al., 2010; Torres et al., 2007; Ren et al., 2014; Yong et al., 2013; Friman et al., 2013; Lee et al., 2008; Feng et al., 2008). Briefly summarizing, ARB prefer to oxidize simple forms of organic compounds, such as acetate, hydrogen, formate, ethanol, etc. (Pant et al., 2010; Torres et al., 2007; Lee et al., 2008). Relatively high CE from 60 to 100% have been reported in MxCs fed with acetate, while it was as low as 8-50% using fermentable substrate as the electron donor (Parameswaran et al., 2009; Lee et al., 2008; Torres et al., 2007). The literature has commonly shown that acetate is the best substrate for ARB (Pant et al., 2010; Torres et al., 2007; Lee et al., 2008; 2010): coulombic efficiency 65-98% and current density 10-25 A/m^2 (Logan and Rabaey et al., 2012; Pant et al., 2010; Xie et al., 2012; He et al., 2012). Although ARB can produce current from complex forms of substrate including glucose, sewage, industrial wastewater, leachate, and animal manure, agricultural waste (Ren et al., 2014; Yang et al., 2013; Lee et al., 2008; Feng et al., 2008; Mahmoud et al., 2016), coulombic efficiency is very low at 15–50%, along with negligible current density (Kim et al., 2015; Ahn and Logan, 2010; Mahmoud et al., 2016). Literature has suggested that such complex substrates should be fermented to acetate, H$_2$, and propionate, and then ARB should use the fermented products (e.g., acetate and H$_2$) as the electron donor (Parameswaran et al., 2009; 2010; 2011; 2012; Lee et al., 2008; Torres et al., 2007; Dhar et al., 2013, 2015; Gao et al., 2014a). Due to such limited availability of ARB for complex organics, researchers have studied syntrophic interactions between fermenters and ARB in mixed-culture MxCs to generate current from complex forms of substrate (Parameswaran et al., 2009, 2010, 2011, 2012; Gao et al., 2014a; Dhar et al., 2013, 2015). Hence, understanding microbial community structure in biofilms is significant for producing high current density from complex organics-fed MxCs.

2.3.2 Microbial Competition and Syntrophy in Biofilm Anodes

Competition for an electron donor between ARB and the other microorganisms (e.g., fermenters or methanogens) can limit current generation. In MxCs, the most competitive electron sink to coulombs is methane. Literature shows that methane formation can account for 26-53% of substrate electrons in MxCs fed with fermentable substrates (ethanol, glucose, etc.) (Parameswaran et al., 2009, 2010, 2011, 2012; Chae et al., 2010). Sulfate- or nitrate-reducing bacteria can outcompete ARB for donor substrate, but sulfate and nitrate are typically negligible in MxC environments (Lee et al., 2008; Chae et al., 2010; Parameswaran et al., 2009, 2010, 2011). Hence, the competitive relationship between ARB and sulphate/nitrate-reducing bacteria are not a major concern. Although the presence of non-ARB reduces coulombic efficiency, they actually help ARB generate current from more complex forms of organic compounds, due to poor utilization of ARB for the complex organics. For this reason, ARB need syntrophic partners for current production from the organics, despite the sacrifice of coulombic efficiency (Freguia et al., 2008; Parameswaran et al., 2009; Lu et al., 2012; Dhar et al., 2013, 2015; Gao et al., 2014a). Propionate, ethanol or butyrate, which is fermentable substrate, would be fermented to acetate and H_2 and ARB oxidize them to generate current in biofilm anodes (Torres et al., 2007; Dhar et al., 2013, 2014, 2015; Gao et al., 2014a). Fermentation of propionate, ethanol, and butyrate is not thermodynamically favourable at standard conditions, but the consumption of acetate and H_2 by ARB drives the fermentation reactions that are more thermodynamically favorable (Dhar et al., 2013, 2015; Gao et al., 2014a). These reactions indicate the syntrophy between fermenters and ARB. However, we should balance populations of fermenter and ARB in biofilm anodes to generate high current density in MxCs fed with complex organics. (Lee et al., 2008; Freguia et al., 2008; Lu et al., 2012; Gao et al., 2014a; Dhar et al., 2013, 2015). The presence of methanogens was solely considered ARB competitors in terms of coulombic efficiency. However, methanogens are able to act as "H_2 scavengers" accumulated in the fermentation of complex organics if ARB are poor at utilizing H_2 as substrate. In this case, hydrogenotrophic methanogens can drive fermentation reactions to acetate and H_2, which allows ARB to access acetate for current generation. In a similar manner, homoacetogens can be ideal syntrophic bacteria to ARB because they transform H_2 to acetate, the best substrate for ARB (Parameswaran et al., 2011; 2012; Gao et al., 2014a). Hence, mixed-culture biofilm anodes should be well balanced to

ferment complex organics into acetate and H_2 that are readily consumed directly or indirectly by ARB for current generation.

2.3.3 Substrate Utilization Kinetics

It has been well accepted that the current generated in MxCs is significantly influenced by the intracellular kinetics, i.e., the substrate-utilization rate. Current profiles to substrate concentration may be described using the Monod equation when the substrate concentration is rate-limiting for current, given that ARB directly utilize substrate, such as acetate (Lee et al., 2009; Torres et al., 2007). Then, current density increases with increasing substrate concentration until a saturation point, which is expressed with the Monod equation for biofilm anodes (Torres et al., 2008b; Lee et al., 2009):

$$j = j_{max} \frac{S}{K_s+S} = 0.14 \, (1 - f_s^o) q_{max} X_f L_f \frac{S}{K_s+S} \tag{2-2}$$

where, j is the current density (A/m^2), j_{max} is the maximum current density (A/m^2), 0.14 is the conversion factor for converting substrate flux to current density (0.14 A= 1 g COD/d), f_s^o in the fraction of electrons used for cell synthesis, q_{max} is the maximum specific substrate utilization rate (g COD/g VSS-d), X_f is the concentration of active ARB in the anode biofilm (g VSS/m^3), L_f is the biofilm thickness (m), K_s is the half-saturation concentration of acetate (g COD/m^3), S is the effluent substrate concentration (g COD/m^3). Eq. (2-2) indicates that current density depends on substrate concentration and current density is saturated at $S \gg K_s$. The relationship between substrate concentration and current density does not always follow the Monod equation when ARB cannot directly oxidize substrate for current generation. For instance, current density to substrate concentration will deviate from the Monod pattern when fermentation is rate-limiting for current density (Torres et al., 2007; Dhar et al., 2013). Other parameters (e.g., anode potential, or pH) can limit current density in biofilm anodes and in this case current density to substrate concentration does not follow the Monod equation. Ion transfer rate for charge neutrality or cathodic reaction rate can be sluggish, which can deviate current density profile to substrate. For instance, slow O_2 reduction rates on the cathode often limit current density in microbial fuel cells (MFCs) (Rismani-Yazdi et al., 2008; Harnisch et al., 2009). Hence, we should evaluate substrate-utilization rate of ARB after creating non-limiting conditions for other factors described above. We are able to meet these delicate,

10

complicated requirements for substrate kinetic study using a potentiostat and high buffer concentrations in the substrate medium (Lee et al., 2009).

2.3.4   Substrate Mass Transfer Limitation

When substrate concentration is rate-limiting for current, Eq. (2-2) can be used to express the relationship between current density and substrate concentration, simply employing the substrate concentration in bulk liquid. However, it should be awared that current generation occurs in a biofilm anode: ARB typically form a biofilm on the anode surface for EET. In biofilm environments, the substrate gradient is readily built and the substrate concentration in bulk liquid may not well represent the substrate-utilization rate of ARB throughout the biofilm (Marcus et al., 2007; Lee et al., 2009; Atci et al., 2016; Renslow et al., 2013a). ARB activity can be significantly inhibited in thick biofilms where the local substrate concentration can be too small to support ARB growth, creating inactive zones, as depicted in Figure 2-3. Experimental studies also confirmed the creation of such metabolically inactive zones near the anode where the substrate concentration was negligible (Atci et al., 2016; Renslow et al., 2013a). Hence, it is important to understand the relationship between biofilm thickness, substrate concentration profile, and substrate-utilization rate throughout biofilm anodes. Substrate diffusion within anode biofilms can be mathematically expressed by Fick's law and the Monod equation, which can provide the profiles of substrate concentration and substrate-utilization rate throughout the biofilms (Marcus et al., 2007; Lee et al., 2009).

There is limited information on optimum biofilm thickness to generate the maximum current density with negligible inactive zones, although researchers have successfully simulated substrate profiles in the anode biofilms, or measured significant depletion of substrate near the anode (Marcus et al., 2007; Lee et al., 2009; Renslow et al., 2013a). One reason for the limited information is the lack of knowledge on electron transfer mechanisms and kinetics from a soluble electron donor to the anode. Another reason is the complicated nature of biofilm anodes where a number of factors limit current. For instance, the pH gradient throughout anode biofilms creates inactive zones close to the anode, due to proton accumulation in ARB catabolism (Torres et al., 2008a; Franks et al., 2009; Babauta et al., 2012, 2011); the activity of ARB metabolism is seriously inhibited by low pH (Torres et al., 2008a; Franks et al., 2009). As a result, an acidic pH inside the anode biofilm is unavoidable unless extremely high buffer concentrations (~100 mM phosphate buffer) are used in the growth medium (Torres et al.,

2008a; Babauta et al., 2011). Therefore, the knowledge on concentration gradients of substrate and protons throughout the anode biofilms is essential for determination of optimum biofilm thickness.
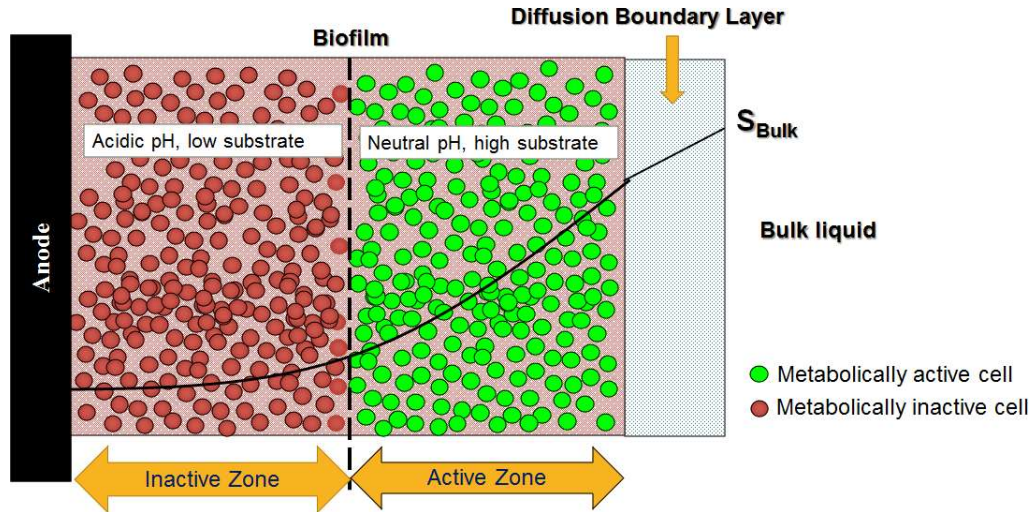
Figure 2-3. Conceptual schematic of metabolically active and inactive zones in biofilm anode. [Note. Figure drawn based on the concept or experimental results proposed by Torres et al. (2008a), Marcus et al. (2010 and 2011), Lee et al. (2009), Renslow et al. (2013a), and Atci et al. (2016)]

2.3.5   Proton Transport Limitations

As summarized above, protons are critical for ARB metabolism because the substrate-utilization rate of ARB is seriously inhibited at acidic pH (Torres et al., 2008a; Franks et al., 2009; Babauta et al., 2012; Kim and Lee, 2010), and current density is substantially decreased (Franks et al., 2009; Torres et al., 2008a) at low pH. Hence, quantifying the pH gradient throughout biofilm anodes is one of the important factors to define inactive zones and optimal biofilm thickness.

Proton accumulation inside the biofilms is indispensable because ARB only transfer substrate electrons to the anode, as described in Eq. 2-1. Theoretically, protons should migrate from the anode to the cathode for charge neutrality, but other cations (e.g., Mg^{2+}, Ca^{2+}, Na^+) in extremely higher than proton concentration in an anode chamber are moved to the cathode. Hence, protons readily accumulate in the biofilm anodes. To avoid proton accumulation in biofilm

anodes, bases should transfer to the biofilms for acid-base neutralization, such as carbonate or phosphate ions (Torres et al., 2008a). As a result, the pH decrease will be alleviated in biofilm anodes. For this reason, diffusion of buffer ions from the bulk liquid to biofilm anodes (e.g., carbonate or phosphate buffer solutions) is critical for the pH gradient. When diffusion rate of buffer ions to the biofilms is limited, pH inhibition zones will be created, as shown in Figure 2-3 (Torres et al., 2008a; Marcus et al., 2010, 2011). Hence, understanding of the pH gradient within the biofilms is very important to optimize ARB metabolism and increase current density.

To maintain neutral pH throughout the biofilms, the growth medium typically is supplemented with high concentration of buffer solutions (e.g., 50-100 mM phosphate or bicarbonate buffer) (Fan et al., 2007; Torres et al., 2008a). Some wastewaters have high buffer concentrations (e.g., animal manure, or protein-rich wastewater), but dilute wastewaters (e.g., domestic wastewater) do not. For instance, the alkalinity concentration in municipal wastewater ranges from 50 to 250 mg/L as $CaCO_3$, equivalent to 1-5 mM bicarbonate buffer (Dhar and Lee, 2014), which can easily acidify biofilm anodes and significantly reduce current density in MxCs treating domestic wastewater. Despite of significance of local pH in biofilm anodes, only a few studies have experimentally evaluated pH gradient in biofilm anodes (Franks et al., 2009; Babauta et al., 2012b). Franks et al. (2009) reported 0.8 of pH unit between the outmost layer of a biofilm anode (pH=6.8) and the inmost layer (pH=6) in a 70 µm thick *G. sulfurreducnes* biofilm anode, which led to a decrease of current density by 50% in an MxC. Babauta et al. (2012b) also observed a gradient of 0.4 pH unit (pH 6.7 to pH 6.3) for a relatively thick (~200 µm) *G. sulfurreducnes* biofilm, producing ~1 A/m^2 of steady-state current density. Hence, understanding of pH gradient throughout biofilm anodes is essential for improving current density and engineering MxCs for field application.

2.3.6 Role of Anode Potential on ARB Growth

The electron transport from an electron donor (e.g., acetate) to OMPs is a stepwise redox reaction, generating energy-rich compounds (e.g., ATP) for ARB growth. Therefore, the redox potential of OMPs determines the energy generation in catabolism of ARB, as expressed with Eq. (2-3).

$$\Delta G = -nF\Delta E = -nF(E_{OMP} - E_{Sub}) \qquad (2\text{-}3)$$

where, ΔG is the change of Gibbs free energy at pH 7 and 25°C (J/mol e⁻), n is the number of electrons transferred per reaction, F is Faraday's constant (96,485 C/mol e⁻), E_{OMP} is the redox potential of OMPs (V), E_{Sub} is the redox potential of the substrate (V), ΔE is the potential difference between the electron acceptor and the donor (V). The redox potential of acetate is -0.28 V vs. SHE at pH 7. Eq. (2-3) clearly shows that more positive E_{OMP} can provide more energy for ARB given at fixed substrate and electron acceptor (Marcus, 2007).

From an ARB growth point of view, ARB would prefer to increase E_{OMP} as much as possible to conserve more energy. In contrast, we intend to proliferate ARB having less positive E_{OMP} in biofilm anodes to maximize energy capture from a given electron donor. Therefore, comprehension of influential parameters (e.g., X_f term in Eq. 2-2) for E_{OMP} is significant for improving current density in MxCs. It is not clear how ARB are able to manipulate E_{OMP}, but the electrode potential seems to affect E_{OMP} in biofilm anodes directly or indirectly (Alterman et al., 2008; Torres et al., 2009, Marcus et al., 2007). For ARB to transfer electrons from OMPs to the anode spontaneously, E_{OMP} must be more negative than the anode potential (E_{anode}). Therefore, the assumption that E_{anode} would affect E_{OM} seems reasonable (Alterman et al., 2008; Torres et al., 2009).

To improve current density in MxCs, we need to engineer biofilm anodes for enriching kinetically efficient ARB, such as *Geobacter* genus. To proliferate ARB on the biofilms, the energy requirements for ARB growth must be met. Thus, optimization of E_{anode} should consider both current generation (energy recovery) and ARB growth. There are several references that estimate ΔG or quantified observed yield of ARB against E_{anode} (Wei et al., 2010; Yoho et al., 2014). The literature commonly reported that the change of ΔG is not significant to E_{anode} variation, since ARB are oligotrophic. Then, we must concentrate kinetically efficient ARB in biofilm anodes, which are able to produce high current density with small energy loss. Several literatures reported that the IET kinetics and intracellular energy loss depends on type of ARB (Alterman et al., 2008; Wei et al., 2010; Torres et al., 2009). For instance, *Geobacter* genus showed current saturation of ~ 10 A/m² at -0.3 V to -0.25 V (vs. Ag/AgCl) of E_{anode} under acetate non-limiting conditions (Torres et al., 2009; Commault et al., 2013). In comparison, kinetically inefficient ARB would lose significant energy for saturated current density much lower than 10 A/m². For this reason, understanding IET kinetics at different E_{anode} will be significant for better engineering MxCs.

2.4   Extracellular Electron Transfer (EET)

To transport substrate electrons from OMPs to the anode is the final step (i.e., EET) to complete ARB's catabolism and produce current in MxCs. To date, at least three (3) mechanisms have been proposed for EET (Figure 2-4). This section summarizes the important features of these mechanisms and their ability to explain high current density (>10 A/m^2) in MxCs.
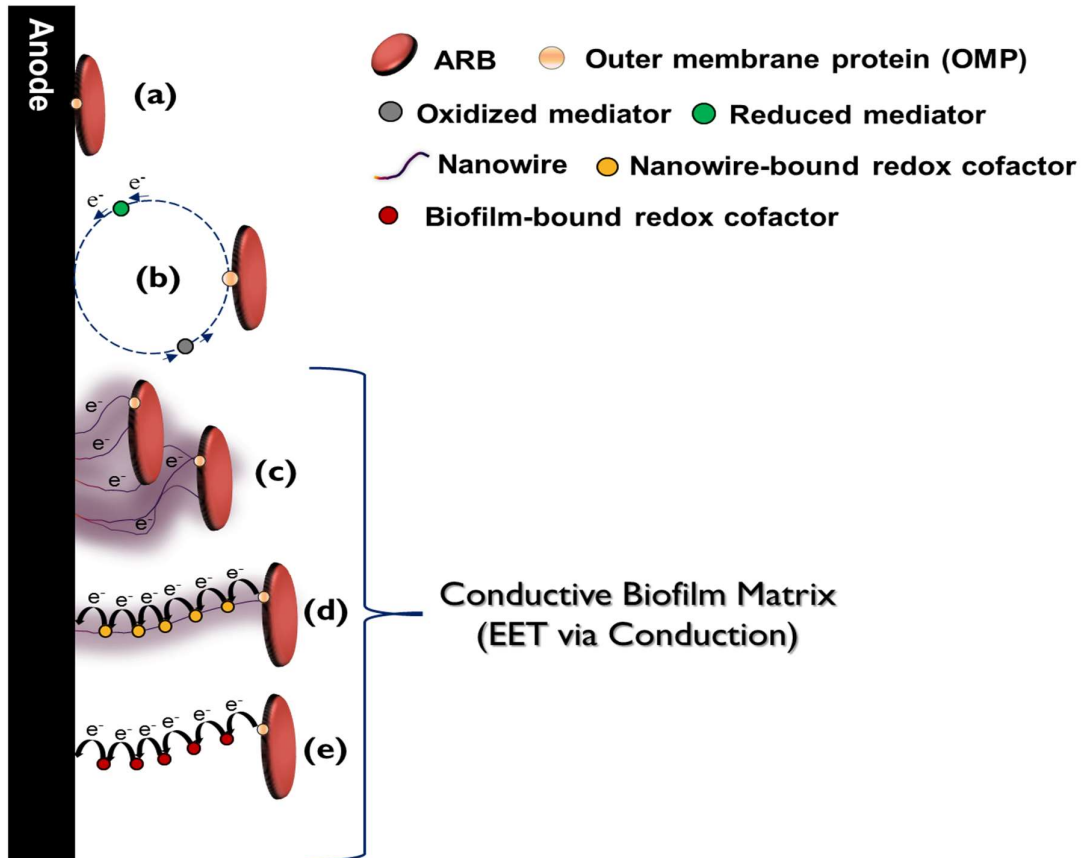
Figure 2-4. Extracellular electron transfer via: (a) direct contact, (b) mediators, (c) conductive pili or nanowire, (d) electron hopping via redox cofactor aligned through microbial nanowire, and (e) electron hopping via biofilm-bound redox cofactors. [Note. Figure drawn based on the concept, model, and experimental results proposed by Reguera et al. (2005), Marcus et al. (2007), El-Naggar et al. (2010), Malvankar et al. (2011), Strycharz-Glaven et al. (2011), Snider et al. (2012), Kim et al. (2002), Marsili et al. (2008), and Torres et al. (2010)]

2.4.1 Direct Contact Mechanism

Earlier EET studies proposed that EET would occur via direct contact of OMPs with the anode surface (Kim et al., 2002; Bond and Lovely, 2003; Torres et al., 2010). For this mechanism, the key assumption is the formation of a mono-layer biofilm on the anode surface (Figure 2-4a). However, anode biofilms that generate high current density consist of several dozen to hundred layers given that a single layer is close to 1 μm. If EET is possible only through the direct-contact mechanism, the current density from the mono-layer biofilm should be similar to multi-layer biofilms. However, literature has reported substantially high current densities (10-25 A/m^2) from relatively thick (20-80 μm) multi-layer ARB biofilms (Torres et al., 2010, 2008a; Malvankar et al., 2012a; Lee et al., 2009), while the maximum current density is as small as 0.16-0.24 A/m^2 for 2-3 μm thin biofilms (Reguera et al; 2006). These results clearly show that EET mechanisms other than the direct contact must exist to account for such high current density.

2.4.2 EET via Redox Mediators

Studies have shown that long-range EET can occur via some redox-active, diffusible, soluble compounds (Marsili et al., 2008; Nguyen et al., 2012; Mehta-Kolte and Bond, 2012; Schmitz et al., 2015; Rabaey et al., 2004; 2005; Von Canstein et al., 2008; Okamoto et al., 2014a, 2014b). These compounds are typically known as mediators or shuttling compounds. The mediators (originally oxidized forms) are reduced by accepting electrons from OMPs in ARB, and are subsequently oxidized on the anode surface by transferring electrons to the anode (Figure 2-4b). In MxCs, mediator-based EET can occur via both exogenous mediators (non-biodegradable synthetic mediators such as neutral red and methylene blue) and endogenous mediators (mediators secreted by the microbes such as flavin, riboflavin, pyocyanin, and or phenazine-1-carboxamide) (Marsili et al., 2008; Velasquez-Orta et al., 2010; Brutinel and Gralnick, 2012; Nguyen et al., 2012; Schmitz et al., 2015; Rabaey et al., 2004; 2005; Von Canstein et al., 2008; Okamoto et al., 2014a, 2014b).

To date, various EET-capable microbes *Geobacter sulfurreducens*, *Shewanella oneidensis, Pseudomonas* sp. have been identified to produce mediators to conduct mediated EET (Marsili et al., 2008; Velasquez-Orta et al., 2010; Brutinel and Gralnick, 2012; Nguyen et al., 2012; Okamoto et al., 2014a, 2014b). The presence of mediators can be qualitatively identified using cyclic voltammetry (CV) techniques, since a redox peak can be observed at the standard

reduction potential of a specific mediator (Mehta-Kolte and Bond, 2012; Marsili et al., 2008; Nguyen et al., 2012). For instance, the presence of flavin in a biofilm should give a redox peak between -0.39 V to -0.42 V vs. Ag/AgCl, since flavin's standard redox potential is within this range (Nguyen et al., 2012). Such a qualitative approach, however, does not provide useful information on EET kinetics because the unmeasured concentration of mediators is responsible for current density. Mediator-based EET is a diffusion-driven mechanism. Therefore, the theoretical current density via this mechanism can be calculated using Fick's first law (Torres et al., 2010). The calculation using the Fick's law indicates that the oxidized flavin concentration should be within mM range in a 100 μm thick biofilm anode to produce high current density (~10 A/m^2) (Torres et al., 2010). However, the literature shows that the flavin concentration was extremely small at 0.25-0.65 μM in biofilm anodes (Marasili et al., 2008; Nguyen et al., 2012). Thus, the mediator-dependent EET mechanism cannot explain the high current density close to 10 A/m^2 in MxCs. There is other indirect evidence to support that mediator-dependent EET would not account for high current density. Mediators are soluble, which means that they readily diffused out to the bulk liquid. Hence, mediators would be washed out in continuous MxCs. Mehta-Kolte and Bond (2012) qualitatively identified the contribution of mediators in EET from the current drop after replacement of the anolyte with the fresh substrate medium during fed-batch operation of MxCs. These results undoubtedly indicate the presence of other robust mechanisms for EET.

2.4.3 Conductive EET

Conduction is considered as the most efficient mechanisms for electron transport and mitigating energy loss in EET within biofilm anodes. For conduction-based EET, biofilm anodes have been considered as conductive biofilm matrix (Marcus et al., 2007; Torres et al., 2008a). To date, at least two mechanisms have been proposed or confirmed for conductive EET, which includes (1) metal-like (i.e., Ohmic) conduction via microbial nanowires (Figure 2-4c), and (2) electron hopping or superexchange via nanowire-bound (Figure 2-4d) or biofilm-bound extracellular redox cofactors (Figure 2-4e) (Reguera et al., 2005; Marcus et al., 2007; El-Naggar et al., 2010; Malvankar et al., 2011; Strycharz-Glaven et al., 2011; Snider et al., 2012; Pirbadian and El-Naggar, 2012). In Ohmic conduction, it is proposed that ARB produce and use conductive nanowires to conduct EET to conductive solids or insoluble electron acceptors (Reguera et al., 2005; Marcus et al., 2007; Malvankar et al., 2011). In contrast, for multi-step "electron hopping" or "super-exchange", electrons are transported to the anode by a

succession of oxidation-reduction reactions among the nanowire-bound or biofilm-bound extracellular redox cofactors (e.g., c-type cytochromes) located in 1-2 nm, as shown in Figure 2-4d and 2-4e (Strycharz-Glaven et al., 2011; Snider et al., 2012; Pirbadian and El-Naggar, 2012; El-Naggar et al., 2010). The two EET mechanisms would be based on electrical conduction, but the potential gradient and related parameters (e.g., concentration of extracellular cofactors and conductivity of nanowires or the cofactors) are enigmatic. Table 2-1 presents a brief timeline summarizing main findings on the conduction based EET, and the following sections will critically review these findings.

Table 2-1. A summary of major developments towards the fundamental understanding of the conduction based EET in MxCs.

Year	Fundamental findings	Reference
2005	Conductive microbial nanowires production by *Geobacter sulfurreducens*	Reguera et al. (2005)
2006	Conductive microbial nanowires production by *Shewanella oneidensis MR-1*	Gorby et al. (2006)
2007	Conduction based Nernst-Monod model for EET	Marcus et al. (2007)
2008	Experimental validation of Nernst-Monod model for EET	Torres et al. (2008b)
2010	Conceptual model for electron hopping via cytochrome aligned through nanowire produced by *Shewanella oneidensis* MR-1	El-Naggar et al. (2010)
2011	First experimental measurement of the biofilm conductivity for *Geobacter* species	Malvankar et al. (2011)
2011	Conceptual model proposed for electron hopping via nanowire-bound cytochrome for *Geobacter* species	Strycharz-Glaven et al. (2011)
2012	First experimental measurement of the biofilm conductivity for mixed-culture	Malvankar et al. (2012c)
2012	Conceptual model proposed for redox driven EET via biofilm-bound redox extracellular cofactors for *Geobacter* species	Snider (2012)
2014	Identification of *S. oneidensis* MR-1 nanowires as extensions of the outer membrane and periplasm, rather than pilin-based structures found in *Geobacter* species	Pirbadian et al. (2014)

Production of nanowires (hair like extracellular appendages) by ARB represents a unique strategy for conductive EET (Reguera et al., 2005; Gorby et al., 2006; El Naggar et a., 2010). Previously it was believed that nanowires are mainly pilin-based (protein or aromatic amino acids) structures in both *Geobacter* and *Shewanella* species (Reguera et al., 2005; Gorby et al., 2006; El Naggar et a., 2010). However, recent findings suggested that physical properties and functions of these nanowires can depend on ARB type (Pirbadian et al., 2014). The nanowires produced by *Geobacter* species have been primarily identified as type IV pili (Reguera et al., 2005), while nanowires produced by *Shewanella* species are have been identified as an extension of cytochrome-rich outer membranes and periplasm, rather than pili (Pirbadian et al., 2014). However, both nanowires have semi-conductive nature (Reguera et al., 2005; El Naggar et a., 2010; Malvankar et al., 2011).

Table 2-2. Conductivity of different anode biofilms.

Microbial community	Biofilm conductivity (mS/cm)	Reference
G. Sulfurreducens KN400	5	Malvankar et al. (2012a)
G. Sulfurreducens BEST	1	Malvankar et al. (2012a)
G. Sulfurreducens ST	1	Malvankar et al. (2012a)
G. Sulfurreducens WT-DL1	0.5	Malvankar et al. (2012b)
G. Sulfurreducens Fumarate DL-1	0.2	Malvankar et al. (2012a)
Mixed-culture[*]	0.25	Malvankar et al. (2012c)

[*]*Geobacteraceae* family accounted for almost half the microbial community

Table 2-2 shows experimental measurements of biofilm conductivity (K_{bio}) for *Geobacter* biofilms. Pili filaments produced by *Geobacter* species were mainly responsible for highly conductive biofilms (Malvankar et al., 2011), while pilin-deficient mutants were also able to produce small current in MxCs (Reguera et al., 2006). Malvankar et al. (2011) reported a linear correlation between abundance of piliA and K_{bio} for different *Geobacter* species. Furthermore, pili filaments extracted from biofilm anodes showed "metal-like" behaviour, such as a decrease in conductivity with increasing temperature over 25°C (Malvankar et al., 2011). Therefore, the conductivity of *Geobacter* enriched biofilms is typically refereed in the literature as intrinsic "metal like" conductivity (Malvankar et al., 2011). To date, both experimental and modeling

approaches support the importance of high K_{bio} to produce a high current density in MxCs (Marcus et al., 2007; Torres et al., 2008b, 2010; Renslow et al., 2013b; Malvankar et al., 2012a). For instance, a simulation study by Renslow et al. (2013b) showed that conduction-based EET can produce 25 A/m^2 of current density in a 100 μm ARB biofilm with K_{bio} of 0.5 mS/cm, while mediator-dependent EET can only produce current density of ~0.2 A/m^2 in presence of 1μM flavin. Malvankar et al. (2012a) reported that the conductivity of anode biofilms was 5 mS/cm in an MxC generating ~10 A/m^2 of current density. Simulation studies showed that K_{bio} over 0.5 mS/cm can account for 10 A/m^2 from biofilm anodes under substrate non-limiting conditions (Marcus et al., 2007; Torres et al., 2008b).

For *Shewanella* species, redox chains formed by multi-heme c-type cytochromes aligned through nanowires have been identified to contribute to the conductivity of nanowires and high current density (El Naggar et a., 2010). This observation suggests the possibility of electron hopping among c-type cytochromes. Spatial organization of cytochromes within a small distance (1-2 nm) may facilitate such redox-driven EET via multi-step electron hopping (cytochrome-to-cytochrome) (El Naggar et a., 2010; Pirbadian and El-Naggar, 2012). Interestingly, *Geobacter* species also have such outer membrane c-type cytochromes aligned through pili, which have been identified to be important for Fe (III) reduction (Mehta et al., 2005); however, there is no solid evidence on a role of outer membrane c-type cytochrome in current generation in MxCs. Interestingly, a conceptual electron-hopping model for *Geobacter* species has been proposed like the electron hopping for *Shewanella* species (Strycharz-Glaven et al., 2011). However, the distance between c-type cytochromes in *Geobacter* pili have been found to be too large (30-200 nm) to facilitate electron hopping (Malvankar et al., 2012b). Furthermore, experimental measurement showed an insignificant contribution of cytochromes to K_{bio} for *Geobacter* biofilms (Malvankar et al., 2012b). Therefore, the strategy for conduction based EET can be different between *Geobacter* and *Shewanella* species, due the biophysical differences in nanowires. To date, there is no report on K_{bio} of *Shewanella oneidensis* MR-1, since the method typically used for K_{bio} measurement (two or four-probe measurements with electrodes separated by a non-conductive gap) could not be used for *Shewanella* species due to poor biofilm formation (Malvankar et al., 2011).

The second mechanism on electron hopping describes EET to the anode via as a series of redox reactions among biofilm-bound redox cofactors, such as extracellular cytochromes (Snider et al., 2012). This mechanism postulates that potential gradient built in multiple redox cofactors throughout biofilm anodes may regulate EET kinetics. Confocal Raman microscopic analysis

showed the redox gradient of extracellular c-type cytochromes throughout a biofilm anode (Lebedev et al., 2014). However, there is no quantitative data to correlate the concentration of extracellular cofactors (oxidation and reduction states) and current density for assessment of EET kinetics.

2.5   Nernst-Monod Model for Anode Kinetics

Microbial kinetics can be limited by the availability of the electron donor, electron acceptor, or both terms, which can be expressed by the dual limitation Monod equation (Bae and Rittmann, 1996). Given that electrons transfer from OMPs to the anode via conductive biofilm matrix, Marcus et al. (2007) proposed that the concentration of OMPs can be replaced with electric potential using the Nernst equation, as expressed with Eq. (2-4); a detailed derivation of the model is available in Marcus et al. (2007).

$$j = 0.14 \, (1 - f_s^o) \, q_{max} X_f L_f \frac{S}{S+K_s} \left[\frac{1}{1+\exp\left(-\frac{nF}{RT}(E_{Anode}-E_{KA})\right)} \right] \qquad (2-4)$$

where, j is the current density (A/m^2), S is the substrate concentration (g COD/m^3), K_S is the substrate half-saturation concentration (g COD/m^3), 0.14 is the conversion factor for converting substrate flux to the current density (0.14 A= 1 g COD/d), q_{max} is the maximum specific substrate utilization rate (g COD/g VSS-d), X_f is the concentration of active ARB in anode biofilm (g VSS/m^3), f_s^o in the fraction of electron used for cell synthesis, E_{anode} is the anode potential (V), E_{KA} is the midpoint potential or half-saturation anode potential where $j=j_{max}/2$ (V), R is the ideal gas constant (8.314 J/mol-K), F is the Faraday's constant (96485 C/mol e$^-$), T is the operating temperature (K), n is the number of electrons transferred. The E_{KA} is an empirical parameter like K_s, and can depend on the microbial community structure in the biofilm anode and the metabolic activity of a specific ARB biofilm. The term (E_{anode}-E_{KA}) in Eq. (2-4) is also referred to as the local potential (η). The Nernst-Monod term in Eq. (2-4) indicates that the local potential (η) should be 0.0574 V for 90% saturated current density under substrate non-limiting condition (Figure 2-5). For instance, a set E_{anode} at -0.4 V vs. Ag/AgCl, the E_{KA} value should be -0.46 vs. Ag/AgCl for 90% of j_{max}. The E_{KA} can be estimated from the current response at different anode potentials under electron donor non-limiting conditions (S>>K_s) (Torres et al., 2008b).

The Nernst-Monod model indicates that kinetically efficient ARB should have low E_{KA}. In comparison, kinetically inefficient ARB will have high E_{KA}. The Nernst-Monod Model assumes EET via Ohmic conduction. Hence, the Nernst-Monod model can be extended for interpreting the rate of EET. For instance, the simulated current density with the Nernst-Monod model should fit the observed current density to different anode potential (CV pattern) when EET is not rate-limiting. However, we can observe significant deviations between simulated and observed CV patterns when EET limits current density (Marcus et al., 2007; Torres et al., 2008b, 2009; Lee et al., 2009). It seems that *Geobacter*-enriched biofilm would have negligible energy loss in EET, which means that the conductivity of the biofilm (K_{bio}) is relatively high (Marcus et al., 2007; Torres et al., 2008b; Lee et al., 2009). However, there are no publications to clearly prove the relationship between E_{KA} and K_{bio}, while model studies would indirectly support the reciprocal correlation between E_{KA} and K_{bio}. Hence, quantification of E_{KA} and K_{bio} is required to solidify the correlation, which will substantially improve understanding of EET.
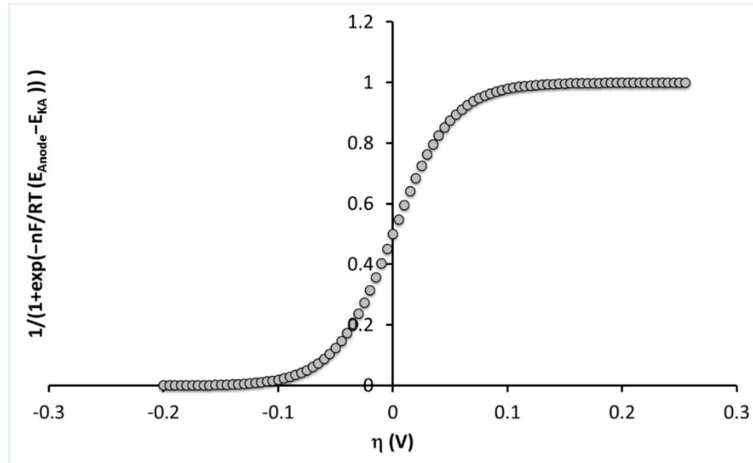
Figure 2-5. Pattern of Nernst-Monod term with local potential. [Note. Figure drawn with modification after Lee et al. (2009)]

Considering biofilm as a linear metal-like conductor, Marcus et al. (2007) estimated theoretical conductivity of biofilm anode with Ohm's law:

$$j = K_{bio}\left(\frac{E_{anode}-E_{OMP}}{L_f}\right) = K_{bio}\left(\frac{\eta}{L_f}\right) \qquad (2\text{-}5)$$

Where, K_{bio} is the biofilm conductivity (S/cm), L_f is the biofilm thickness (cm), ($\eta = E_{anode} - E_{OMP}$) is the potential loss between the OMPs and the anode or EET potential loss (V). Marcus et al. (2007) assumed that the local potential (η) would limit EET due to the poor biofilm conductivity (K_{bio}). Therefore, the local potential ($\eta = E_{anode} - E_{KA}$) could well represent the potential loss associated with the EET process. Nernst-Monod modeling results suggested that the conductivity of an ARB biofilm must be higher than 10^{-3} mS/cm to allow conduction (Marcus et al., 2007). Furthermore, experimental validation of the model suggest that biofilm conductivity should be higher than 0.5 mS/cm to produce a current density of 10 A/m^2 (Torres et al., 2008b). Interestingly, experimental measurements by Malvankar et al. (2011) also supported the semi-conductive (0.25-5 mS/cm) nature of the ARB biofilms (Table 2-2).

2.6   Factors Limiting EET Kinetics

There are several publications that have used modelling or experimental approaches to explore effects of anode potential, substrate or proton mass transfer limitations on IET kinetics and current density in biofilm anodes (Torres et al., 2007, 2008a, 2008b, 2009; Pant et al., 2010; Marcus et al., 2007, 2011; Renslow et al., 2013a, 2013b; Lee et al., 2009; Nam et al., 2011; Alterman et al., 2008; Liu et al., 2010; Franks et al., 2009; Parameswaran et al., 2009, 2010, 2011; Babauta et al., 2012a, 2011). In contrast, there is limited information on the impacts of these parameters on EET kinetics and K_{bio}. Several reports in the literature indicate that EET kinetics or K_{bio} can be influenced by substrate or proton mass transfer limitations (Malvankar et al., 2012a; Liu and Bond, 2012; Ishii et al., 2013; Torres et al., 2009; Matsuda et al., 2011), but there are no direct, solid data to quantitatively evaluate these important relationships. For instance, Malvankar et al. (2012a) compared biofilm conductivity, current density and biofilm thickness for different strains (KN400, BEST, DL-1, Fumarate DL-1) of *Geobacter* species. The lowest biofilm conductivity (0.25 mS/cm) and current density (2 A/m^2) was observed for the thickest biofilm (130 μm) of Fumarate DL-1 strain of *Geobacter* species, as compared to thin biofilms (Malvankar et al., 2012a), indicating mass transfer limitations may influence K_{bio}. Liu and Bond (2012) found an accumulation of reduced c-type cytochromes in outer membrane c-type cytochromes in a relatively thick biofilm anode, implying sluggish EET by mass transport limitation.

Since various OMPs such as c-type cytochromes are typically denatured at acidic pH, Bond et al. (2012) proposed that acidic pH may hinder EET. However, Malvankar et al. (2011) separated nanowires from a *G. sulfurreducens* biofilm, measured the conductivity of nanowires

at different pH (2-10), and showed the highest conductivity of 100 μS/cm at pH 2 against 1 μS/cm at pH 10. Sun et al. (2015) recently found that ARB far from the anode can respire across metabolically inactive zones located near the anode, indicating mass transfer limitations may not restrict EET.

Several studies showed indirect evidence of E_{anode} effects on EET kinetics (Torres et al., 2009; Liu et al., 2010; Matsuda et al., 2011; Srikanth et al., 2010; Snider et al., 2012; Ishii et al., 2013). Torres et al. (2009) compared EET kinetics for biofilm anodes grown at different E_{anode}, based on the conduction based Nernst-Monod equation for EET, and reported better EET kinetics (i.e., low E_{KA}) at E_{anode} –0.15 V than that at E_{anode} +0.37 V. Literature reported changes in gene expression levels of outer membrane c-type cytochromes for ARB at different E_{anode} conditions (Ishii et al., 2013; Matsuda et al., 2011). Furthermore, several studies suggested multiple EET mechanisms at more positive E_{anode} conditions (Torres et al., 2009; Liu et al., 2010; Matsuda et al., 2011; Srikanth et al., 2010; Marsili et al., 2008; Bond and Lovley, 2005; Rabaey et al., 2005). However, there is no report on E_{anode} effects on experimentally measured K_{bio} in biofilm anode.

The aforementioned literature did not provide any quantitative information on EET parameters (e.g., K_{bio}), which is important to establish the role of mass transfer limitations and E_{anode} in EET kinetics or K_{bio}. Therefore, to unravel the complex, cascade of electron transfers mechanisms from the electron donor to the anode, a comprehensive approach including biological, electrochemical, and EET parameters is required. EET parameters should be systematically studied with precise approaches to explicate the impact of environmental factors (e.g., substrate, pH, anode potential).

2.7   Multi-anode Configurations for Scaling up MxCs

In the last decade, a significant research effort has been devoted towards developing MxC based engineering concepts for recovery of various resources from organic waste and wastewater. However, MxCs has not been commercialized yet. One main reason is inadequate power output for practical application. For instance, maximum power density from acetate fed microbial fuel cell (MFC) is reported to be ~7 W/m^2 of anode surface area (Logan et al., 2015). For external energy dependent MxCs for resource recovery, the current density has been substantially improved up to 25 A/m^2, using advanced anode materials (e.g., nanomaterials, conductive polymers) (Xie et al., 2012; He et al., 2012; Li et al., 2011). These advanced electrode materials can be used for miniaturized MxCs for lab on a chip or biosensor

application (Ren et al., 2015), while high manufacturing cost limits their economic feasibility for large-scale MxCs (Zhou et al., 2011; Logan et al., 2015). For sustainable scale-up of MxCs, the capital cost should be significantly reduced along with improved current density.

Among various electrode materials, low-cost electrode materials having high surface area per unit volume (e.g., carbon brush, carbon fiber) have received significant attention by MxC researchers (Logan, 2015; An and Lee, 2013; Zhou et al., 2011). For scale-up, a number of studies proposed multi-electrode configurations of MxCs with these low-cost electrode materials (Ahn and Logan, 2012; Lanas and Logan, 2013; Hutchinson et al., 2011; Ren et al., 2014; Ghadge and Ghangrekar, 2015; Ahn et al., 2014; Jiang et al., 2011). However, most of these studies reported only a slight improvement in power density with increasing anode surface area or a number of electrodes in multi-anode configurations. For instance, Lanas and Logan (2013) reported comparable power densities (1.25-1.15 W/m^2 of anode surface area) from single-chamber air-cathode MFCs having different numbers of carbon brush anodes (1, 3, and 6). Hutchinson et al. (2011) also reported that up to 65% of the carbon brush can be removed without disturbing the power density from a single chamber MFC. Furthermore, Jiang et al. (2011) demonstrated a non-linear increase in power densities with increasing the number of electrodes in a multi-anode/cathode microbial fuel cells due to increased internal resistance. However, none of these studies investigated the influence of biofilm anode kinetics or microbial community on individual anode electrodes, and primarily focused on minimizing internal resistances. Thus, understanding of the factors limiting energy output from multi-anode MxCs is still limited, which is one of the major bottlenecks for commercialization of MxCs. Hence, anode kinetics should be optimized for multi-anode MxCs.

2.8   Outlook

To engineer MxCs, limiting factors impeding the anodic electron transfer processes should be well understood. The literature indicates that EET via conduction could be critical for producing high current density from MxCs, and different conduction based EET mechanisms have been proposed. However, it is not well understood yet how the EET kinetics and K_{bio} are affected by other factors such as mass transfer limitations and anode potential. The research findings in the literature have raised many unexplored questions and conflicting hypotheses due to the lack of systematic approaches. Moreover, apart from a few recent studies, most of the studies did not measure the EET parameters, specially K_{bio}. Due to limited experimental

data, most of the mathematical modeling and simulation studies have made assumptions about upstream operating parameters, and thus, the existing simulation results may not fairly represent the EET via conduction. In summary, identification of the limiting factors for EET is needed to improve the fundamental understanding as well as the development of a unified theory on the EET in biofilm anode. Therefore, a significant research effort with systematic, comprehensive approaches is required to characterize anode kinetics including EET more explicitly avoiding the existing inconsistencies. In addition to the fundamental understanding of EET kinetics, the techno-economically feasible design of MxCs is essential for sustainable scale-up of resource recovery technologies. Although several multi-anode configurations have been proposed in the literature, the non-linear improvement in power density with increasing the number of electrodes demonstrated the importance of optimization of anode kinetics on individual anode electrodes in multi-anode configurations. Hence, future development of multi-anode MxCs should incorporate investigation of biofilm anode kinetics.

Chapter 3

High Biofilm Conductivity Conserved to Change of Anode Potential in a *Geobacter*-enriched Biofilm Anode

A version of this chapter, co-authored by Dhar, B.R., Ryu, H., Santo Domingo, J. W., Ren, H., Chae, J., and Lee, H.S., has been submitted to ChemSusChem for peer-review and publication.

Contributions statement: Dhar, B.R. designed the study, fabricated the reactors, performed all laboratory experiments and analyses, and contributed to data interpretation and manuscript preparation. Ryu, H. and Santo Domingo, J. W conducted microbial community analysis. Ren, H. and Chae, J. fabricated micro-sized gold electrodes with non-conductive gap. Lee, H.S. supervised this project.

3.1   Introduction

Extracellular electron transfer (EET) is a unique electron transfer step for anode-respiring bacteria (ARB) to complete anaerobic respiration using conductive solids (Torres et al., 2010; Reguera et al., 2005; Lovley et al., 2008). This specific electron transfer is important for bioremediation of hazardous contaminants such as toxic metals, halogenated, and radioactive compounds in subsurface environments (Yun et al., 2014; Wardman et al., 2014), resource recovery wastewater treatment technologies (Logan and Rabaey, 2012; Rabaey and Rozendal, 2010), and bioelectronics (Malvankar et al., 2011; Malvankar and Lovley, 2014). Among them resource-recovering wastewater treatment using microbial electrochemical cells (MxCs) has significant attention in environmental engineering as energy, water, and environment issues become significant in recent society: moving toward sustainable wastewater treatment.

High current density, proportional to rate of resource recovery, is essential for improving benefits of MxCs-utilized wastewater treatment, but identification of a rate-limiting step is still unclear due to complex electron transfer processes in biofilm anodes. Electron transfer from a soluble electron donor to solid conductors can be divided into intracellular electron transfer (IET) and extracellular electron transfer (EET). The IET kinetics is commonly characterized with Monod equation (Marcus et al., 2007; Lee et al., 2009; Parameswaran et al., 2013; Torres et al., 2008a, 2007). Several studies reported IET kinetic parameters with apparent half-saturation substrate concentration ($K_{s,app}$), apparent maximum specific substrate utilization rate ($q_{max,app}$), or $q_{max,app}$ multiplied with biofilm density (X_f), $q_{max,app}X_f$ term, for biofilm anodes (Lee et al., 2009; Parameswaran et al., 2013; Torres et al., 2008a, 2007; Esteve-Núñez et al., 2005). To obtain high current density from MxCs, biofilm anodes should be enriched with

ARB having small $K_{s,app}$ and high $q_{max,app}X_f$. For instance, $K_{s,app}$ and $q_{max,app}X_f$ values range from 119-176 g COD/m^3 and 8×10^5-1×10^6 g COD/m^3-d, respectively, in *Geobacter*-enriched biofilm anodes generating high current density $\sim$ 10 A/m^2 (Lee et al., 2009; Parameswaran et al., 2013; Torres et al., 2008a, 2007).

Many parameters can influence the IET kinetics, including pH, substrate type, substrate concentration, anode potential (E_{anode}), anode materials and configurations, and the presence of exogenous electron acceptors (sulfate, O_2, nitrate, etc.) (Lee et al., 2009; Torres et al., 2007, 2008b, 2009; Commault et al., 2013; Aelterman et al., 2008; Kumar et al., 2013; Logan et al., 2015; Sherafatmand and Ng, 2015; Xia et al., 2015; Franks et al., 2009). pH mainly affects ARB activity (Franks et al., 2009; Torres et al., 2008b; Kim and Lee, 2010). In comparison, most of other factors directly or indirectly change microbial community structures on biofilm anodes, indirectly influencing the IET kinetics (Torres et al., 2009; Commault et al., 2013; Kumar et al., 2013; Chae et al., 2009). Among them, E_{anode} is known to be a critically important parameter for selection of kinetically efficient ARB, such as *Geobacter* genus, from mixed culture (Torre et al., 2009; Commault et al., 2013; Kumar et al., 2013). Literature has shown that negative E_{anode} (-0.05 to -0.15 V vs. SHE) enriched *Geobacter* spp. from mixed culture (Torre et al., 2009; Commault et al., 2013). In comparison, more diverse microbial communities in biofilm anodes were established at positive E_{anode} (+0.02 to +0.37 V) where IET kinetics becomes slow (Torre et al., 2009; Commault et al., 2013). For instance, Hamelers et al. (2011) reported an increase in apparent K_s from 0.37 mM to 2.2 mM acetate for E_{anode} increase from -0.2 V to -0.1 V vs. standard hydrogen electrode (SHE); however, they did not report other biological kinetic parameter (q_{max}) and microbial community. There is no clear evidence on why and how E_{anode} shifts biofilm community. Recent literature has suggested that more diverse ARB built at positive E_{anode} would diversify EET pathways (e.g., outer membrane proteins involved in EET, endogenous production of mediators), along with decrease of current density (Torres et al., 2009; Liu et al., 2010; Matsuda et al., 2011; Srikanth et al., 2010; Marsili et al., 2008; Bond and Lovley, 2005; Rabaey et al., 2005). There are limited studies quantitatively evaluating the effects of E_{anode} on IET kinetics, simultaneously with biofilm community analysis, inspite of significant E_{anode} impacts on the both parameters considerably influencing current density in MxCs.

Several EET mechanisms (direct contact, mediator, conduction, or combined routes) have been proposed (Torres et al., 2010; Reguera et al., 2005; Lovley et al., 2008; Marsili et al., 2008),

but most of the recent studies have commonly indicated the importance of conductive EET in biofilm anodes to produce high current density over several A/m^2 (Torres et al., 2008a; 2010; Malvankar et al., 2011, 2012a; Marcus et al., 2007; Strycharz-Glaven et al., 2011, 2012; Snider et al., 2012). Biofilm anodes enriched with *Geobacter* pure- and -enriched cultures generating relatively high current densities of 0.9-10 A/m^2 showed high biofilm conductivity (K_{bio}) ranging from 0.25 to 5 mS/cm (Malvankar et al., 2011, 2012a, 2012b), which indicates that Ohmic conduction plays a vital role of EET in the biofilm anodes. Modeling studies often supports the importance of Ohmic conduction for EET in the biofilm anodes (Marcus et al., 2007; Renslow et al., 2013), such as the Nernst-Monod equation. The Nernst-Monod equation, which assumes Ohm's law governs EET (Marcus et al., 2007), characterizes EET kinetics with half-saturation anode potential (E_{KA}). This equation well matches sigmoidal patterns of current density to E_{anode} change under substrate non-limiting conditions (Marcus et al., 2007; Lee et al., 2009; Torres et al., 2008a). Literature reports that E_{KA} ranges from -0.12 V to -0.24 V for biofilm anodes producing high current density (Lee et al., 2009; Torres et al., 2008a, 2008b, 2009; Miceli et al., 2012). The Nernst-Monod equation suggests that K_{bio} must be higher than 0.5 mS/cm for highly conductive biofilm anodes generating ~ 10 A/m^2 (Torres et al., 2008a). Although many studies have reported significant impact of E_{anode} on current density in MxCs (Torre et al., 2009; Commault et al., 2013; Kumar et al., 2013), the information on E_{anode} effects on EET kinetics is very limited. Torres et al. (2009) compared E_{KA} and cyclic voltammograms for biofilm anodes grown at different E_{anode} conditions, based on the Nernst-Monod equation for EET, and indirectly demonstrated better EET kinetics for the biofilm anode grown at E_{anode} –0.15 V than that at E_{anode} + 0.37 V only with E_{KA}; more detailed information on EET kinetics is required to comprehend E_{anode} effects on EET. No studies have experimentally assessed K_{bio} of biofilm anodes for different E_{anode}, while E_{anode} could change K_{bio}. There are no comprehensive works quantitatively assessing E_{anode} effects on IET and EET kinetics, along with biofilm community analysis to our knowledge.

To improve understanding of kinetic change by E_{anode}, this study evaluates IET kinetic parameters (apparent $K_{s,app}$ and $q_{max,app}X_f$), microbial community structures and EET kinetic parameters (K_{bio} and E_{KA}) at steady-state current density in a MxC as E_{anode} was changed stepwise. The implications of the IET and EET kinetic parameters are discussed, along with biofilm community structures, to identify kinetic bottlenecks for current density in the MxC.

3.2   Methodology

3.2.1   MxC Configuration and Operation

Two identical dual-chamber MxCs were constructed with plexiglass (Figure 3-1a). Two gold anode electrodes (width 9.5 mm × length 15 mm× thickness 10 μm) on a glass base with a non-conductive gap of 50 μm was designed and fabricated specifically to measure the biofilm conductivity (Figure 3-2b and 3-2c); total geometric surface area of the anodes was 2.85 cm^2. A porous graphite plate (Isomolded Graphite Plate 203101, Fuel Cell Earth, USA) was used as the cathode and anion exchange membrane (AMI-7001, Membranes International Inc., USA) was placed between the anode and the cathode chambers as a separator. The working volumes of both chambers were 15 mL. A reference electrode (Ag/AgCl reference electrode, MF-2052, Bioanalytical System Inc., USA) was placed within less than 1 cm distance from the anodes to control the E$_{anode}$ during experiments. All anode potentials were reported versus standard hydrogen electrode (SHE).

The MxC was inoculated with 10 mL of anolyte from a mother MxC that had been operated for over 1.5 years, and was fed with sodium acetate medium (2,628±76 mg COD/L) supplemented with 100 mM phosphate buffer (medium pH 7.25-7.4). The cathode chamber was filled with tap water, producing hydrogen gas. The literature provides information on the composition of the medium (Dhar et al., 2013). After inoculation, the anode chamber was sparged with ultra-pure nitrogen (99.999%) for 5 min, and then the E$_{anode}$ was set at -0.2 V using a potentiostat (BioLogic, VSP, Gamble Technologies, Canada). Current was recorded at every 120 s using EC-Lab for windows v 10.32 software in a personal computer connected with the potentiostat (BioLogic, VSP, Gamble Technologies, Canada).   After operation in batch mode for 12 days, the acetate medium was fed in continuous mode at a flow rate of 5.8 mL/h using a cartridge-type peristaltic pump (Master Flex® L/S digital drive, Model 7523-80, Cole-Parmer, Canada) to maintain hydraulic residence time (HRT) of 2.6 h in the anode chamber (substrate non-limiting conditions).   After the steady-state current density was achieved, E$_{anode}$ was changed from -0.2 V to +0.2 V. The MxC was operated in a temperature-controlled room at 26±2°C.
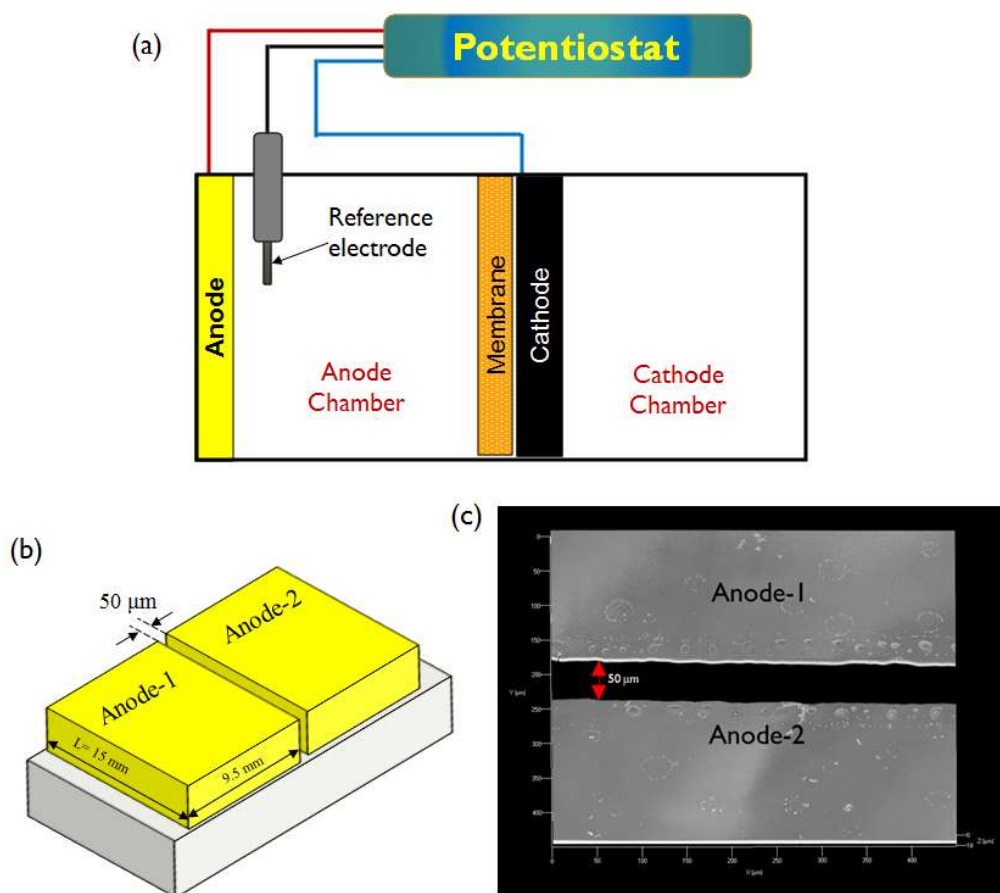
Figure 3-1. Schematic of (a) a dual chamber MxC, (b) two gold anodes on the glass base with a non-conductive gap of 50 μm, and (c) a microscopic image of non-conductive gap between two gold electrodes.

3.2.2   Biofilm Conductivity Measurements

The biofilm conductivity (K_{bio}) was quantified for each E_{anode} according to Eq. 3-1 and measured biofilm conductance using the two-probe measurement method (Malvankar et al., 2011). For the biofilm conductance measurement, the anode electrodes and the cathode were disconnected temporarily (open circuit mode) (Appendix B). Then, a small voltage ramp of 0-50 mV in steps of 25 mV was applied across two gold electrodes using a source meter (Keithley 2400, Keithley Instruments, Inc., USA), and the current data was recorded. Observed biofilm conductance ($G_{Biofilm\ (obs)}$, mS) was calculated from the current-voltage response (I-V characteristics). The ionic conductance ($G_{control}$, mS) was also quantified with an identical

31

control MxC to account for ionic current across the non-conductive gap using the acetate medium. Intrinsic biofilm conductance ($G_{Biofilm} = G_{Biofilm\ (obs)}$-$G_{control}$, mS) was used for calculation of biofilm conductivity (K_{bio}, mS/cm). Then, K_{bio} was computed from the biofilm conductance ($G_{biofilm}$) using conformal mapping (Schwarz-Chris toffel transformation) (Kankare and Kupila, 1992):

$$K_{bio} = \left. G_{Biofilm} \frac{\pi}{L} \middle/ ln\left(\frac{8L_f}{\pi a}\right) \right. \qquad (3-1)$$

Where, L_f is the biofilm thickness (μm), L is the length of the electrodes (1.5 cm), and a is half of the non-conductive gap between two electrodes (25 μm).

3.2.3 Biofilm Thickness Measurement

Biofilm thickness (L_f) was measured using the method proposed by Bonanni et al. (2013) using the change of resistance between the surface of the biofilm and the anode electrode. A stainless steel needle with a tip diameter of 100 μm was used as the microelectrode for biofilm thickness measurement. The microelectrode connected to a motorized micromanipulator (MM33, Unisense A/S, Denmark) was positioned very close to the surface of the biofilm and then stepwise moved toward the gold electrodes (see Figure 3-2). A step size of 5 μm was controlled using Unisense SensorTrace Suite software (Unisense A/S, Denmark). The anode chamber was disclosed and anolyte was removed with a syringe, which means that the anode biofilms were open to the air for the access of the microelectrode. When the microelectrode was open to air away from the biofilm, resistance was close to infinite value (open circuit). High resistance in MΩ ranges was observed when the microelectrode touched the outermost layer of the biofilm, mainly due to the water content in the biofilm. Resistance substantially decreased at <1 Ω when the microelectrode touched the anode surface. The biofilm thickness was quantified by monitoring the change of resistance in the microelectrode using a multimeter (Fluke 179/TPAK, Fluke Electronics Canada LP, Mississauga, ON, Canada) connected to the microelectrode, as shown in Figure 3-2. During measurements, drops of the substrate medium were added to the surface of the biofilm to avoid dehydration. To mitigate O_2 inhibition effects on ARB, quadruplicate measurements of biofilm thickness were completed in 20 min. Then, the MxC was quickly assembled, and operated under potentiostat mode. Current density was immediately recovered to the steady state. The biofilm thickness was measured at steady-state current density for two E_{anode} conditions.
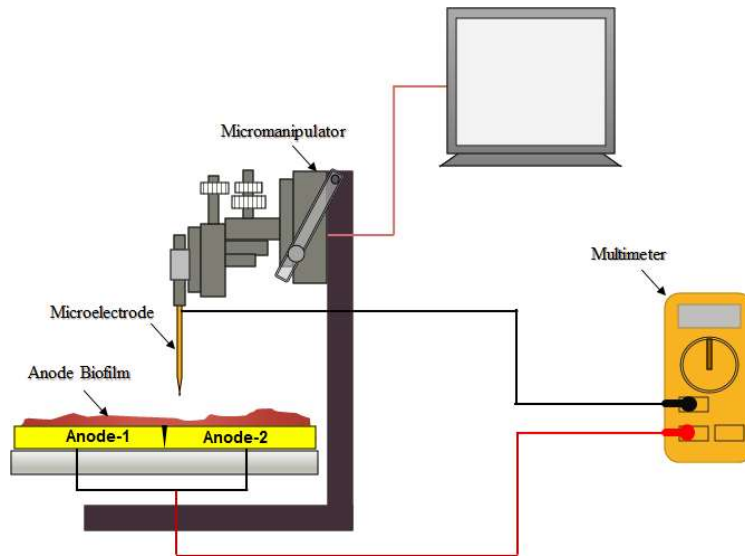
Figure 3-2. Set-up for biofilm thickness measurement.

3.2.4   Estimation of E_{KA}, $K_{s,app}$, and $q_{max,app}X_f$

Under substrate non-limiting conditions, the E_{KA} of the biofilm anode was estimated at E_{anode} - 0.2 V and +0.2 V with low-scanning cyclic voltammetry at a scan rate of 1 mV/s (Lee et al., 2009; Torres et al., 2008a). E_{anode} was ramped between -0.4 to +0.4 V at a scan rate of 1 mV/s using the potentiostat. The current and anode potential were recorded at every 5 s using EC-Lab for windows v 10.32 software in a personal computer connected with the potentiostat. To ensure the reproducibility of the low scanning cyclic voltammetry (LSCV) data, each test was conducted at least in triplicates, and the average data is reported. LSCV tests were performed under substrate non-limiting conditions (2,628±76 mg COD/L and HRT 1.3 h).

The $K_{s,app}$ and $q_{max,app}X_f$ values for ARB were estimated from current density at different acetate concentrations (11-2,750 mg COD/L). According to the Nernst-Monod equation (Eq. 3-2) (Lee et al., 2009; Parameswaran et al., 2013; Torres et al., 2008a), the best-fit apparent $K_{s,app}$ (g COD/m^3) and $q_{max,app}X_f$ (g COD/m^3-d) were estimated with the relative least squares method using MS 2016 MS Excel solver as described in literature (Lee et al., 2009; Parameswaran et al., 2013).

33

$$j = 0.14 \, (1 - f_s^o) \, q_{max,app} \underbrace{X_f L_f \, \frac{S}{K_{s,app} + S}}_{IET} \underbrace{\left[\frac{1}{1 + \exp\left(-\frac{F}{RT} \, (E_{anode} - E_{KA}) \right)} \right]}_{EET} \qquad (3-2)$$

Where, j is the current density (A/m^2), 0.14 is the conversion factor for converting substrate flux to the current density (0.14 A= 1 g COD/d), f_s^o in the fraction of electron used for cell synthesis (f_s^o =0.1) (Lee et al., 2009; Torres et al., 2008a), $q_{max,app}$ is the maximum specific substrate utilization rate (g COD/g VSS-d), X_f is the concentration of active ARB in anode biofilm (g VSS/m^3), L_f is the biofilm thickness (m), L_f is the biofilm thickness (m), $K_{s,app}$ is the apparent half-saturation concentration of acetate (mg COD/L), S is the effluent acetate concentration (mg COD/L), E_{anode} is the anode potential (V), E_{KA} is half-saturation potential of biofilm anode at $j=j_{max}/2$ (V), R is the ideal gas constant (8.3145 J/mol-K), F is the Faraday's constant (96,485 C/mol e$^-$), T is temperature (298.15, K), n is the number of electrons transferred.

3.2.5 Microbial Community Analysis

The biofilm samples were collected with a sterilized spatula when the current density reached at steady state for each E_{anode}. Microbial community structures were analyzed by targeting 16S rRNA. Total RNA were extracted from the biofilm samples as previously described with some minor modifications (Pitkänen et al., 2013). Briefly, the AllPrep DNA/RNA Mini Kit (Qiagen GmbH, Hilden, Germany) was used to extract total nucleic acid. RNA was further purified using Ambion TURBO DNA-free DNase kit (Life Technologies, Grand Island, NY). The concentration and purity of RNA were determined using Qubit RNA assay kits and the Qubit 2.0 Fluorometer (Life Technologies). Barcoded 16S rRNA gene targeting primers (i.e., 515F and 806R) and the targeted product (i.e., 291 bp) was sequenced in both directions using an Illumina MiSeq PE250 approach (Caporaso et al., 2011). Sequence reads (16S rRNA-based) were processed and analyzed using Mothur software (Schloss et al., 2009). Sequence reads that did not fit the following criteria were discarded from further analyses: did not form contigs, deviated considerably from the expected PCR size product, identified as chimeras, had ambiguous bases, and had homopolymers greater than 7 bases long. Sequence reads were grouped at a 97 % similarity and the consensus sequences were then identified using Mothur and the Silva database as a reference (Quast et a., 2013). MS Excel was used to determine the overall relative abundance of representative sequences at different taxonomic levels (e.g., class, order, family, genus). Rare members (less than 10 sequences) were excluded for the calculation

of the relative abundance. Sequences were analyzed using Blast (http://www.ncbi.nlm.nih.gov/BLAST) and RDP classifier (Wang et al., 2007) further confirm their phylogenetic affiliation and to classify sequences at a low taxonomic level (genus and species) whenever possible.

3.2.6 Liquid Analysis

Acetate concentration was analyzed using a gas chromatography (GC) (Model: Hewlett Packard HP 5890 Series II) equipped with flame ionization detector (FID) (Dhar et al., 2013). All samples were analyzed in triplicate. The detection limit of acetate was 1.5 mg COD/L. The pH values were measured with a pH benchtop meter (PHB-600R, OMEGA, Canada) connected with a microprobe pH electrode (RK-55500-40, Accumet® MicroProbe™ combination electrode, Cole-Parmer, Canada).

3.3 Results

3.3.1 Current Density, Biofilm Thickness and Biofilm conductivity

The steady-state current density was 2.05±0.05 A/m^2 at E_{anode} -0.2 V (Figure 3-3). The current density significantly decreased to 0.35±0.004 A/m^2 at E_{anode} +0.2 V, although equivalent operating conditions were kept, except for E_{anode}. An average biofilm thickness was 34±5 μm at E_{anode} -0.2 V, which was comparable to an average of 39±9 μm at E_{anode} +0.2 V (Table 3-1). Biofilm conductivity (K_{bio}) was 1.24±0.24 mS/cm at E_{anode} -0.2 V, which slightly reduced to 0.96±0.21 mS/cm at E_{anode} +0.2 V. High conductivity of the biofilm anode was kept against E_{anode} change, although the steady-state current density decreased substantially at E_{anode} +0.2 V.

3.3.2 Microbial Community Analysis

Biofilm community structures were identified with a total of 158,565 rRNA sequences. Detailed information on the microbial community analysis result was provided in Appendix C. *Geobacter* genus, one of the most kinetically efficient ARB, was predominant (96%) for the biofilm anode at E_{anode} -0.2 V. *Geobacter*'s population substantially decreased to 44% in the biofilm at E_{anode} +0.2 V in which population of *Treponema* spp. became significant (40%) in

35

the biofilm, along with small numbers of *Pseudomonadaceae* family (5.3%) and *Aminiphilus* genus (3.3%) (see Figure 3-4).

3.3.3 Estimation of Half-saturation Potential

Figure 3-5 shows sigmoidal shapes of cyclic voltammetries (CVs) for two E_{anode} conditions. The half-saturation potential (E_{KA}) was determined at -0.230±0.003 V at E_{anode} -0.2 V and it slightly increased by -0.197±0.008 V at E_{anode} +0.2 V (see Table 3-1). This small change of E_{KA} is consistent to K_{bio} trend, implying that EET would not limit electron transfer rate from a soluble electron donor to the anode in a highly conductive biofilm anode, despite of substantial decline in current density.

3.3.4 Monod Kinetic Parameters

The best-fit values for Monod kinetic parameters of $K_{s,app}$ and $q_{max,app}X_f$ were estimated using Eq. 3-2 and measured parameters of effluent acetate concentration, biofilm thickness, half-saturation potential, and current density. At E_{anode} -0.2 V, the best-fit $K_{s,app}$ was 156 g COD/m^3, which was 67 g COD/m^3 at E_{anode} +0.2 V. The best-fit $q_{max,app}X_f$ was 6.4×10^5 g COD/m^3-d at E_{anode} -0.2 V, but it was very small at 6.9×10^4 g COD/m^3-d at E_{anode} +0.2 V.

Table 3-1. Measured and estimated biofilm conductivity, biological and electrochemical kinetic parameters.

E_{anode} (V vs. SHE)	L_f (µm)	K_{bio} (mS/cm)	E_{KA} (V)	$K_{s,app}$ (g COD/m^3)	$q_{max,app}X_f$ (g COD/m^3-d)
-0.2 V vs. SHE	34±5	1.24±0.24	-0.230±0.003	156	648,152
+0.2 V vs. SHE	39±9	0.96±0.21	-0.197±0.008	67	69,591
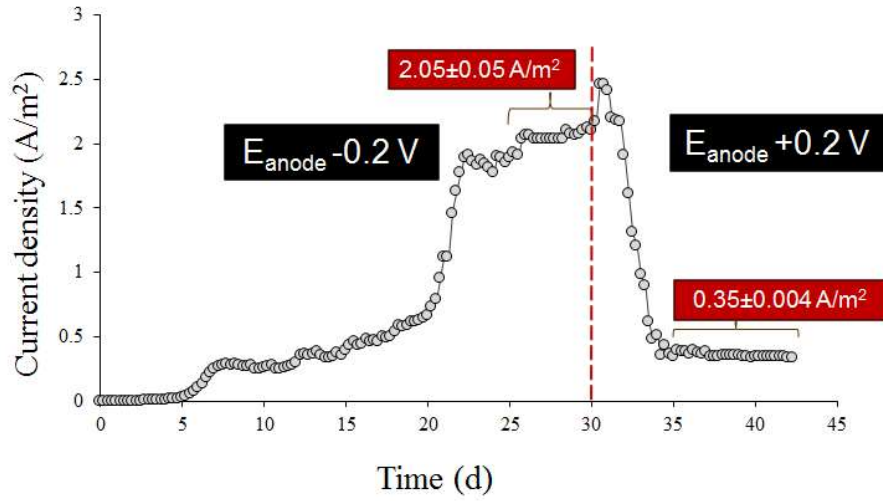
Figure 3-3. Current density over time during operation of MxC at two different anode potentials.
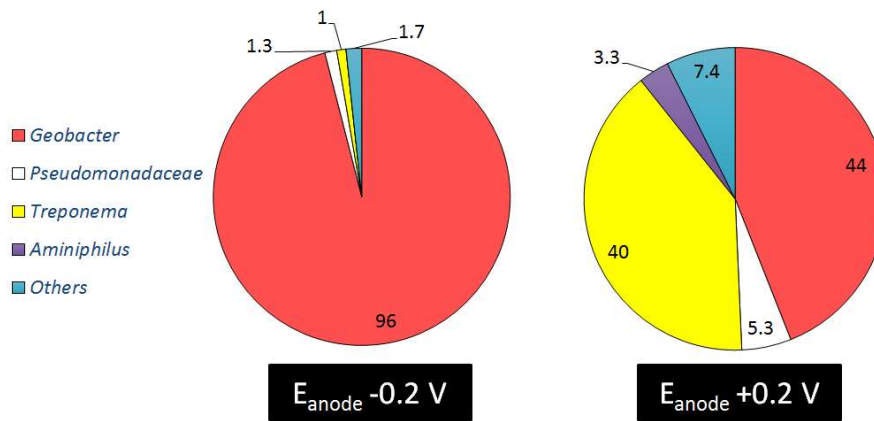
Figure 3-4. Microbial community structures at different anode potentials.

3.4   Discussion

3.4.1   Shifts of Microbial Community in the Biofilm Anode

Microbial community in the biofilm anode shifted from *Geobacter*-dominant (96%) to relatively diverse structure (*Geobacter* 44%, *Treponema* 40%, and *Aminiphilus* (3.3%) and *Pseudomonadacea* (5.3%) after E_{anode} was changed from -0.2 V to +0.2 V. This substantial change of microbial community occurred only in 2 weeks. Abundance of *Geobacter* spp. at E_{anode} -0.2 V is consistent to the literature reporting enrichment of *Geobacter* spp. from mixed-culture at negative E_{anode} (-0.05 to -0.2 V) (Torre et al., 2009; Commault et al., 2013; Kumar et al., 2013). There are no studies clearly proving EET for *Treponema* spp., but they have been frequently identified in biofilm anodes (Rismani-Yazdi et al., 2007; Ishii et al., 2008; Gao et al., 2014a, 2014b; Patil et al., 2009; Wang et al., 2015). Due to limited understanding of *Treponema*'s EET, previous work interpreted the presence of *Treponema* in biofilm anodes as non-EET function, such as homoacetogenesis (Rismani-Yazdi et al., 2007; Gao et al., 2014a, 2014b; Patil et al., 2009). In this study, the dual-chamber MxC was operated with acetate medium, so H_2 was almost unavailable for *Treponema* genus in the biofilm. H_2 might diffuse from the cathode to the anode. This small H_2 diffused to the anode, however, would have commonly occurred for the two E_{anode} conditions, which cannot account for the substantial increase of *Treponema*'s population only for E_{anode} +0.2 V. Hence, this result implies that *Treponema* spp. would be one of the main EET players at positive E_{anode}, although further research is required to prove the hypothesis.

3.4.2   Intracellular Electron-Transfer (IET) Kinetics

The estimated $K_{s,app}$ (156 g COD/m^3) for *Geobacter*-enriched biofilm at E_{anode} -0.2 V falls within K_s values from 119 to 176 g COD/m^3 for biofilm anodes dominated with *Geobacter* spp. (Lee et al., 2009; Torres et al., 2008a; Ren et al., 2015). The estimated $q_{max,app}X_f$ of 6.4×10^5 g COD/m^3-d was close to $q_{max,app}X_f$ values from 8×10^5 to 1×10^6 g COD/m^3-d in *Geobacter*-enriched biofilm anodes (Lee et al., 2009; Torres et al., 2008a). X_f is computed at 29,460 g VSS/m^3 for the biofilm anode, given that $q_{max,app}$ is 22 g COD/g VSS-d for *Geobacter* spp. (Lee et al., 2009; Esteve-Núñez et al., 2005). This relatively low X_f, which is ~ 60% of X_f of 50,000 g VSS/m^3 in the literature (Lee et al., 2009), would partially account for the low maximum current density of 2.05±0.05 A/m^2 as compared to ~ 10 A/m^2 in the literature (Lee et al., 2009; Torres et al., 2008a). In addition, this small X_f of *Geobacter* spp. estimated for the biofilm

anode accords to less biocompatibility of gold electrodes for *Geobacter* biofilm (Crittenden et al., 2006). Assuming $q_{max,app}$ of 22 g COD/g VSS-d for *Geobacter* enriched biofilm (Lee et al., 2009; Esteve-Núñez et al., 2005) and 50% of active biomass cell (i.e., VSS) is protein (Marsili et al., 2010; Lee et al., 2008), the electron transfer rate was estimated at 2.6×10^{16} electrons/mg proteins-sec, which is comparable to literature values ranging from 1×10^{16} to 5×10^{16} electrons/mg proteins-sec for pure-culture *Geobacter sulfurreducens* biofilms (Malvankar et al., 2012a). This calculation supports high metabolic activity of *Geobacter* genus in the biofilm anode.

At higher E_{anode} +0.2 V, the best-fit $K_{s,app}$ and $q_{max,app}X_f$ were small at 67 g COD/m^3 and 6.9×10^4 g COD/m^3-d, respectively. The $K_{s,app}$ term controls how early current density is saturated to substrate concentration. In comparison, the $q_{max,app}X_f$ term regulates the maximum current density. Hence, the small $K_{s,app}$ and $q_{max,app}X_f$ terms at E_{anode} +0.2 V indicate kinetic advantages of ARB only at current density smaller than the saturated current density of 0.35 A/m^2. Due to diverse community structure in the biofilm anode at E_{anode} +0.2 V, it could not be identified which parameter (q_{max} or X_f) primarily limits current density. However, this result clearly indicates that $q_{max,app}X_f$ is a main rate-limiting factor for low current density at E_{anode} +0.2 V. Illumina sequencing data suggests that the increase population of *Treponema* spp. (40%) would be related to low $K_{s,app}$ and $q_{max,app}X_f$ for the biofilm anode at E_{anode} +0.2 V.

3.4.3. Extracellular Electron Transfer (EET) Kinetics

High K_{bio} was measured at 0.96-1.24 mS/cm for the biofilm anode, which is higher than 0.25 mS/cm in mixed-culture biofilm anode enriched with *Geobacteraceae* family (Malvankar et al., 2012b). The high K_{bio} supports Ohmic conduction for EET in the biofilm anode (Marcus et al., 2007; Torres et al., 2008a; Malvankar et al., 2011, 2012a). This study clearly showed that EET kinetics were not changed much to E_{anode} change. High K_{bio} (0.96 mS/cm) and negative E_{KA} (-0.197 V) were observed at E_{anode} +0.2 V, although biofilm community structures and IET kinetic parameters were significantly changed at +0.2 V (see Table 3-1). This result suggests that biofilm community structures and related IET kinetics do not significantly influence EET kinetics in a highly conductive biofilm anode governed by Ohm's law. Substantial change of microbial community in biofilm anodes would affect EET mechanisms or kinetics (Torre et al., 2009; Kumar et al., 2013). However, relatively constant EET kinetics were observed when the population of *Geobacter* spp., a main ARB player, was shifted from 96% to 44%.

As compared to the biofilm anode at E_{anode} -0.2 V, the experimental CV for E_{anode} +0.2 V was deviated from the CV simulated with the Nernst-Monod equation (Eq. 3-2), despite of high K_{bio} (Figure 3-5). The Nernst-Monod equation assumes Ohm's law for EET, and hence the deviation between experimental and simulated CVs at E_{anode} +0.2 V implies EET mechanisms other than Ohmic conduction. Literature reported multiple EET mechanisms at more positive E_{anode} (Torres et al., 2009; Liu et al., 2010; Matsuda et al., 2011; Srikanth et al., 2010; Marsili et al., 2008; Bond and Lovley, 2005; Rabaey et al., 2005). Significant increase of *Treponema*'s population in the biofilm anode and the CV deviation at E_{anode} +0.2 V suggest that *Treponema* spp. might use non-Ohmic conduction mechanism for EET, while high K_{bio} was kept in the biofilm, probably due to *Geobacter* genus (44%).
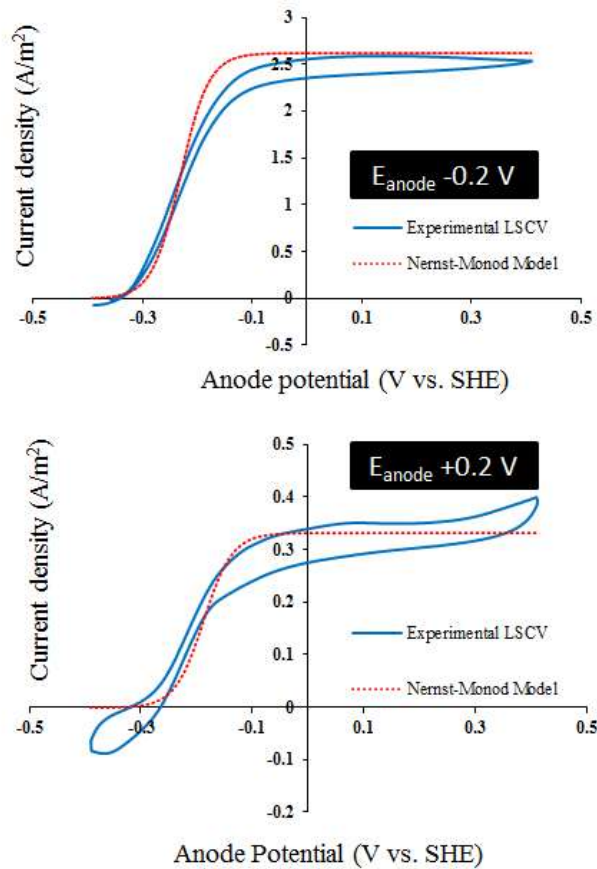
Figure 3-5. Low-scanning cyclic voltammetry (LSCV) and Nernst-Monod model simulation. The blue line: the experimental LSCVs (1 mV/s), the dotted red line: Nernst-Monod model simulation.

3.5   Conclusions

E_{anode} increase significantly reduced the steady-state current density from 2.05 to 0.35 A/m^2 in the MxC. However, E_{anode} increase did not affect EET kinetics much. E_{KA} and K_{bio} values at E_{anode} +0.2 V only decreased by 17 and 29%, respectively, as compared to those at E_{anode} -0.2 V. In comparison, $q_{max,app}X_f$ at E_{anode} +0.2 V decreased approximately ten-fold less than that at E_{anode} -0.2 V, along with significant shift of bacterial community in the biofilm anode. Despite high K_{bio} kept at E_{anode} +0.2 V, CV experiments and simulations indicate that EET might occur via mechanisms other than Ohmic conduction at E_{anode} +0.2 V, implying the involvement of multiple EET mechanisms at this positive E_{anode}. This result suggests that fast EET kinetics can be conserved in a highly conductive biofilm anode for E_{anode} dynamic conditions, although IET kinetics becomes slow, mainly due to change of dominant ARB (i.e., *Geobacter* genus) in biofilm anodes.

Chapter 4

Proton Accumulation Deteriorates Conductivity of Biofilm Anodes

A manuscript based on this chapter, co-authored by Dhar, B.R., Sim, J., Ren, H., Chae, J., and Lee, H.S., is under preparation for submission to a refereed journal for peer-review and publication.

Contributions statement: Dhar, B.R. designed the study, fabricated the reactors, performed all laboratory experiments and analyses, and contributed to data interpretation and manuscript preparation. Sim, J. assised in conducting experiments. Ren, H. and Chae, J. fabricated micro-sized gold electrodes with non-conductive gap. Lee, H.S. supervised this project.

4.1   Introduction

Extracellular electron transfer (EET) is the terminal electron transfer step for catabolism of anode-respiring bacteria (ARB) in MxCs (Torres et al., 2010; Yang et al., 2012). Various EET mechanisms (e.g., direct contact, mediator, conduction, and their combination) have been proposed, but only a conductive EET mechanism can account for generation of high current density from microbial electrochemical cells (MxCs) capable of recovering value-added products from organic waste and wastewater (Malvankar et al., 2011, 2012a; Marcus et al el., 2007; Torres et al., 2008a, 2010; Renslow et al., 2013a). The literature proved electrical conductivity of anode biofilm and it was as high as 5 mS/cm (Malvankar et al., 2011, 2012a). Modeling approaches also validated the significance of biofilm conductivity (K_{bio}) for conduction based EET (Marcus et al., 2007; Renslow et al., 2013a). In these studies, the Nernst-Monod equation was used to characterize electron transfer from a donor substrate to the anode with half-saturation potential of biofilm (E_{KA}), given that Ohm's law controls EET (Marcus et al., 2007): the lower E_{KA} is, the less energy loss becomes. We can experimentally produce a relationship between current density (j) to anode potential (E_{anode}) in biofilm anodes, which is called j-E profile. The Nernst-Monod equation can simulate j-E profile, and the simulations match experimental cyclic voltammetry (CV) at substrate non-limiting conditions, supporting the validity of the Nernst-Monod equation and conductive EET. At substrate limiting conditions, j-E profile deviate from experimental CVs because the substrate-utilization rate by ARB limits current density. Hence, understanding of the substrate-utilization rate is important for improving current density in MxCs.

Different from other environmental factors, ARB have two limiting parameters in biofilm environments: availability of donor substrate and proton accumulation. Mass transfer limitations for electron donor and protons in biofilm anodes can affect the substrate-utilization rate and current density (Torres et al., 2008b; Lee et al., 2009; Marcus et al., 2010, 2011; Babauta et al., 2011, 2012; Renslow et al., 2013b; Marcus et al., 2010, 2011; Franks et al., 2009). The proton transfer limitation is more critical than substrate limitations for the substrate oxidation rate, since acidic pH seriously inhibits metabolism of ARB (Marcus et al., 2010, 2011; Gao et al., 2014; Franks et al., 2014; Torres et al., 2009; Renslow et al., 2013b). ARB typically grow well at neutral pH, although some extreme ARB (e.g., *Geoalkalibacter* spp.) which proliferate at alkaline pH have been identified (Yoho et al., 2015; Pierra et al., 2015). For instance, the growth rate of *Geobacter* spp. at pH 6 was decreased to 80% over pH 7 (Franks et al., 2009). Ironically, protons are accumulated in biofilm anodes during ARB's catabolism because only electrons transfer to the anode. Protons conceptually migrate to the cathode for meeting charge neutrality in MxCs, but in reality other cations move to the cathode, due to concentration effects. The concentration of the cations (Na^+, K^+, Ca^{2+}, Mg^{2+}, NH_4^+) present in growth medium or wastewater is typically between several and dozens mM, which is several orders of magnitude higher than the proton concentration (10^{-4} mM) (Torres et al., 2009; Dhar and Lee, 2013). Accumulated protons acidify biofilm anodes, which can seriously inhibit ARB metabolism and decrease current density in MxCs (Torres et al., 2009; Marcus et al., 2010, 2011; Franks et al., 2009). Frank et al. (2009) clearly showed acidic pH close to the anode in a biofilm anode. To mitigate acidic biofilm anodes a high buffer concentration (e.g., 50-100 mM carbonate or phosphate buffer) has been used in the growth medium (Torres et al., 2009; Marcus et al., 2010, 2011; Franks et al., 2009). However, buffer concentrations in most wastewaters are much less than those in growth medium, ranging from 1 to 5 mM bicarbonate buffer (Dhar and Lee, 2014), which indicates that proton accumulation can significantly limit current density for MxCs treating wastewater.

Despite the significance of pH for current density, studies of pH effects on EET are very limited in the literature. Malvankar et al. (2012a) only reported significantly lower K_{bio} (0.25 mS/cm) and current density (2 A/m^2) for a thick biofilm (130 μm) as compared to thin biofilms (40-60 μm), suggesting that mass transfer limitations of protons or substrate might decrease K_{bio} and current density. Interestingly, the nanowires produced by *Geobacter* spp. showed higher electrical conductivity at pH 2 than pH 10 (Malvankar et al., 2011). This result suggests the

increase of K_{bio} with decreasing pH, given that the nanowires mainly accounts for K_{bio} in biofilm anodes; Dr. Lovley' group has insisted that nanowires (or called pili-like appendages) are responsible for EET in *Geobacter* biofilm anodes (Malvankar et al., 2011, 2012b, 2012c, 2012d; Malvankar and Lovley, 2012; Xiao et al., 2016). These conflicting results confuse understanding of K_{bio} and EET kinetics at acidic pH in biofilm anodes.

In this study, the effects of proton accumulation on EET kinetics was evaluated at steady-state current density in an MxC run with three different phosphate buffer concentrations. pH gradients throughout a anode biofilm were established with a micro-sensor system for the three phosphate buffer conditions. Confocal laser scanning microscopic analysis was carried out to qualitatively evaluate the metabolic activity of ARB within the biofilm. Finally, experimentally measured K_{bio} and E_{KA} of the biofilm anode at the three buffer concentrations were determined.

4.2   Materials and Methods

4.2.1   MxC Configuration and Operation

Two dual-chamber MxCs were constructed with plexiglass: one biotic and one abiotic MXC. Two gold anode electrodes (width 9.5 mm × length 15 mm× thickness 10 μm) on a glass base with a non-conductive gap of 50 μm was designed and fabricated specifically to measure the biofilm conductivity; total geometric surface area of the anodes was 2.85 cm^2. A porous graphite plate (Isomolded Graphite Plate 203101, Fuel Cell Earth, USA) was used as the cathode and anion exchange membrane (AMI-7001, Membranes International Inc., USA) was placed between the anode and the cathode chambers as separator. The working volumes of both chambers were 15 mL. A reference electrode (Ag/AgCl reference electrode, MF-2052, Bioanalytical System Inc., USA) was placed within less than 1 cm distance from the anodes to fix E_{anode} during experiments.

The biotic MxC was inoculated with biofilms collected from a mother MxC that had been operated for over one year, and was fed with 25 mM acetate medium supplemented with 100 mM phosphate buffer (medium pH 7.25-7.4). The literature provides information on the composition of the medium (Dhar et al., 2013). The cathode chamber was filled with tap water, producing H_2 gas. After that, the anode chamber was sparged with ultra-pure nitrogen

(99.999%) for 5 min, and then E_{anode} was set at -0.2 V using a potentiostat (BioLogic, VSP, Gamble Technologies, Canada). Current was recorded at every 120 s using EC-Lab for windows v 10.32 software in a personal computer connected to the potentiostat (BioLogic, VSP, Gamble Technologies, Canada). After operation in batch mode for 5 days, the acetate medium was fed in continuous mode at a flow rate of 5.8 mL/h using a cartridge-type peristaltic pump (Master Flex® L/S digital drive, Model 7523-80, Cole-Parmer, Canada) to maintain hydraulic residence time (HRT) of 2.6 h in the anode chamber (substrate non-limiting conditions). After steady-state current density was reached, the phosphate buffer in the growth medium was stepwise decreased from 100 mM to 2.5 mM (medium pH 7.2-7.4). At steady-state current density for each buffer concentration, pH gradients throughout the biofilm anode, K_{bio}, E_{KA}, and biofilm thickness were measured.

4.2.2 Biofilm Conductivity

The conductivity of a biofilm anode grown at different phosphate buffer concentrations was measured using the two-probe measurement method (Malvankar et al., 2011). For the biofilm conductance measurement, the gold anodes and the cathode were disconnected temporarily (open circuit mode). Then, a small voltage ramp of 0-50 mV in a step of 25 mV was applied across two gold electrodes using a source meter (Keithley 2400, Keithley Instruments, Inc., USA), and the current data was recorded. Observed biofilm conductance ($G_{Biofilm\,(obs)}$, mS) was quantified from the current-voltage response. Ionic conductance ($G_{control}$, mS) was also measured with an abiotic MxC (control) to account for ionic current across the non-conductive gap using both acetate medium and MxC effluents. As shown in Appendix D (Figure D-2), the ionic conductance was constant at 0.07±0.01 mS. Intrinsic biofilm conductance ($G_{Biofilm}$ = $G_{Biofilm\,(obs)}$-$G_{control}$, mS) was used for calculation of biofilm conductivity (K_{bio}, mS/cm) with equation (4-1) (Kankare and Kupila, 1992).

$$K_{bio} = \frac{G_{Biofilm}\frac{\pi}{L}}{ln\left(\frac{8L_f}{\pi a}\right)} \qquad (4-1)$$

Where, L_f is the biofilm thickness (μm), L is the length of the electrodes (1.5 cm), and a is half of the non-conductive gap between two electrodes (25 μm).

4.2.3 Biofilm Thickness

Biofilm thickness (L_f) was measured with the method proposed by Bonanni et al. (2013) using the change of electrical resistance between the surface of biofilms and microelectrodes. Stainless steel needle with a tip diameter of 100 µm was used as the microelectrode for biofilm thickness measurement. The microelectrode connected with a motorized micromanipulator (MM33, Unisense A/S, Denmark) was positioned very close to the surface of the biofilm and then stepwise moved toward gold electrodes. A step size of 5 µm was controlled using Unisense SensorTrace Suite software (Unisense A/S, Denmark). The anode chamber was disclosed and anolyte was removed with a syringe, which means that the anode biofilms were open to the air for the access of the microelectrode. When the microelectrode was open to air away from the biofilm, resistance was close to infinite value (open circuit). High resistance in MΩ ranges was observed when the microelectrode touched the outmost layer of the biofilm, mainly due to water content in the biofilm. Resistance substantially decreased to less than 1 Ω when the microelectrode touched the anode surface. The biofilm thickness was quantified by monitoring the change of resistance in the microelectrode using a multimeter (Fluke 179/TPAK, Fluke Electronics Canada LP, ON, Canada) connected to the microelectrode. During measurements, drops of the substrate medium were added to the surface of the biofilm to avoid dehydration. To mitigate O_2 inhibition effects on ARB, quadruplicate measurements of biofilm thickness were completed in 45 min. Then, the MxC was quickly assembled, and operated under potentiostat mode. Current density was immediately recovered to the steady state. The biofilm thickness was measured at steady-state current density at different buffer concentrations.

4.2.4 pH Gradient Throughout a Biofilm Anode

The pH gradient within a biofilm anode at different phosphate buffer concentrations were measured with a pH microelectrode (Unisense pH-100, Unisense A/S, Denmark) with a tip diameter of 100 µm connected with a 4-channel microsensor multimeter (Microsensor Multimeter for Unisense Sensors, 2x pA, 1x mV and 1x Temp channel, Unisense A/S, Denmark). The pH microelectrode was used in combination with an external Ag/AgCl reference electrode (Unisense REF-10, Unisense A/S, Denmark). The reference electrode was used to develop a reference potential against the pH electrode. Prior to use, the pH microelectrode was calibrated with three standard pH buffer solutions (pH 4, 7, and 10). After

disassembling the reactor, the anode, the cathode and the reference electrode were transferred to a rectangular open-chamber filled with the acetate medium, and continuously purged with ultra-pure nitrogen (99.999%). During pH gradient measurement, the anode was poised at -0.2 V vs. SHE using the potentiostat. The pH microelectrode tip was positioned very close the surface of the biofilm, and then moved toward the biofilm at a step size of 5 μm using a motorized micromanipulator (Unisense MM33, Unisense A/S, Denmark) (see Figure 4-1). The pH was recorded using Unisense SensorTrace Suite software (Unisense A/S, Denmark). The pH profiles throughout the biofilm were acquired at least twice for each buffer concentration, and the average value is reported here. The measurements of the pH profiles were completed within 40 min. After that, the MxC was quickly assembled, and operated under potentiostat mode. Current density immediately recovered to the steady state following the measurments.
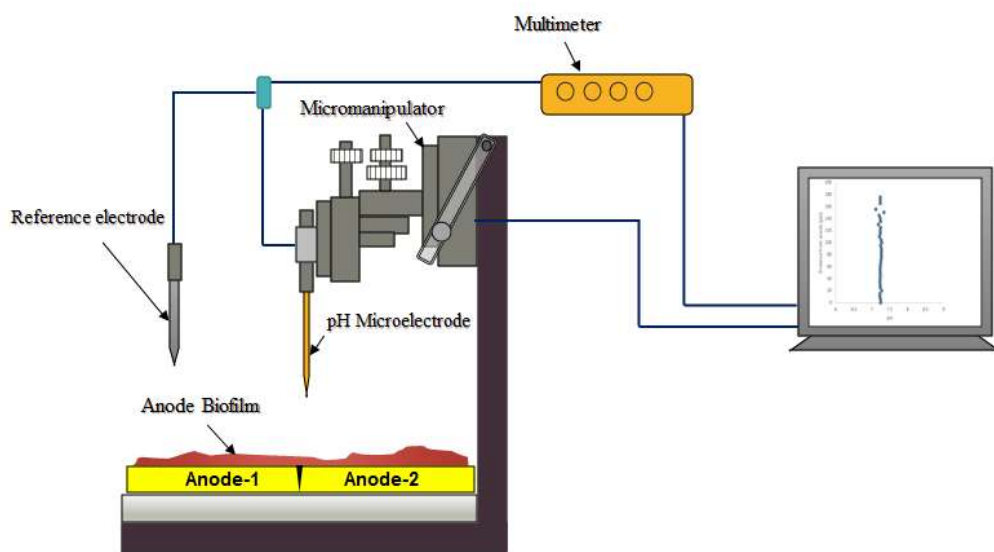
Figure 4-1. Set-up for pH gradient measurement throughout biofilm.

4.2.5 Visualization of Live and Dead Cells in a Biofilm Anode

Metabolic activities of ARB within a biofilm anode (2.5 mM and 100 mM phosphate buffer concentrations) were compared using a LIVE/DEAD cell imaging technique with a confocal laser scanning microscopy (CLSM) (Zeiss LSM 5 Duo Vario Microscope). After conducing all experiments at different phosphate buffer concentrations, the CLSM image of the biofilm was taken to evaluate the metabolic activity of ARB at 2.5 mM phosphate buffer. To evaluate the metabolic activity in a biofilm anode at 100 mM phosphate buffer concentration, an

47

identical MxC was operated under the same conditions (design of MxC, electrode materials, inoculum, HRT, and growth medium). The supplementary MxC inoculated with the biofilms collected from the same mother MxC was operated with 25 mM acetate medium supplemented with 100 mM phosphate buffer. After around 30 days of operation, the current density (2.14±0.2 A/m^2), biofilm thickness (107±20 μm), and K_{bio} (0.73±0.1 mS/cm) reached a steady-state comparable to the original MxC. Then, the biofilm from this supplementary MxC was imaged with the CLSM. The biofilms sampled from two MxCs were stained with Film Tracer™ LIVE/DEAD$^®$ biofilm viability kit (Life Technologies, ON, Canada) and washed with DI water after 30 minutes to remove excess dyes. The biofilm samples at 100 mM and 2.5 mM phosphate buffer were visualized with the CLSM with a 20x and 10x objective, respectively. The photos were taken with Zen Software (Zen 2009, Carl Zeiss AG, Jena Germany). The 2D images of the biofilms were reconstructed using the Bitplane Imaris Software (Bitplane USA, Concord MA). Moreover, the thickness of metabolically inactive zones within the biofilms (red color) was also approximately measured with Bitplane Imaris Software.

4.2.6 Liquid Analysis

Acetate concentration was analyzed using a gas chromatography (GC) (Model: Hewlett Packard HP 5890 Series II) equipped with flame ionization detector (FID) (Dhar et al., 2015). All samples were analyzed in triplicate. The pH values for bulk liquid or substrate medium were measured with a pH benchtop meter (PHB-600R, OMEGA, Canada) connected with a microprobe pH electrode (RK-55500-40, Accumet$^®$ MicroProbe™ combination electrode, Cole-Parmer, Canada).

4.2.7 Estimation of Half-Saturation Potential

At different buffer concentrations, E_{KA} for a biofilm anode was estimated with low-scanning cyclic voltammetry at a scan rate of 1 mV/s (Lee et al., 2009; Torres et al., 2008). E_{anode} was ramped between -0.4 to +0.4 V at a scan rate of 1 mV/s using the potentiostat. The current and anode potential were recorded at every 5 s using EC-Lab for windows v 10.32 software in a personal computer connected to the potentiostat. During LSCV tests, the acetate medium was fed to the biofilm anode with a HRT of 1.3 h to maintain substrate non-limiting conditions. To ensure the reproducibility of the LSCV data, each test was conducted at least in triplicate, and the average data is reported.

4.2.8   Nernst-Monod Model Simulation

After determination of E_{KA}, the current density in response to anode potential was fit to Nernst-Monod equation described in Eq. (4-2) (Lee et al., 2009; Torres et al., 2008a).

$$j = j_{max} \left[\frac{1}{1 + \exp\left(-\frac{F}{RT}\left(E_{anode} - E_{KA}\right)\right)} \right] \qquad (4-2)$$

Where, j is the current density (A/m²), j_{max} is the maximum current density (A/m²), E_{anode} is the anode potential (V), E_{KA} is half-saturation potential of biofilm anode at $j=j_{max}/2$ (V), R is the ideal gas constant (8.3145 J/mol-K), F is the Faraday's constant (96,485 C/mol e⁻), T is temperature (298.15, K).

4.3   Results and Discussion

4.3.1   Current Density and Biofilm Thickness

Figure 4-2 shows the current density observed in the original MxC over time at different buffer concentrations. After around 15 days of operation, the current density reached the maximum steady-state current density of 2.38±0.05 A/m² (100 mM phosphate buffer). The decrease of phosphate buffer concentration from 100 mM to 50 mM on day 34 caused a sharp decrease in the maximum current density and led to a steady-state current density of 1.53±0.03 A/m² (36% reduction compared to 2.38±0.05 A/m² at 100 mM phosphate buffer). At 2.5 mM phosphate buffer, the steady-state current density further decreased down to 0.64±0.04 A/m² (73% reduction as compared to 100 mM phosphate buffer). This consistent reduction of the steady-state current density to phosphate buffer concentration implies partial acidification of a biofilm anode due to protons accumulation (Torres et al., 2008b). Different from typical catabolism of bacteria using a soluble electron acceptor, ARB utilize the anode as the terminal electron acceptor. Hence, electrons transfer to the anode but protons accumulate in biofilm anode, acidifying the biofilms. Literature reported that the metabolic activity of ARB was seriously inhibited by acidic pH lower than 6.8 (Franks et al., 2009; Kim and Lee, 2010). Bases present in growth medium (phosphate buffer here) can only neutralize the protons and keep neutral pH throughout biofilm anodes. Hence, mass transfer of the bases determines pH profiles throughout biofilm anodes, as suggested by the literature (Torres et al., 2008b) showing

the decline of current density by 80% (10 A/m^2 to ~2 A/m^2) at phosphate buffer decreased from 100 mM to 12.5 mM in an MxC. In this work, biofilm thickness was constantly thick over 100 μm in the biofilm anode, as shown in Table 4-1, which means that inner biofilm can be readily acidified at low buffer conditions.
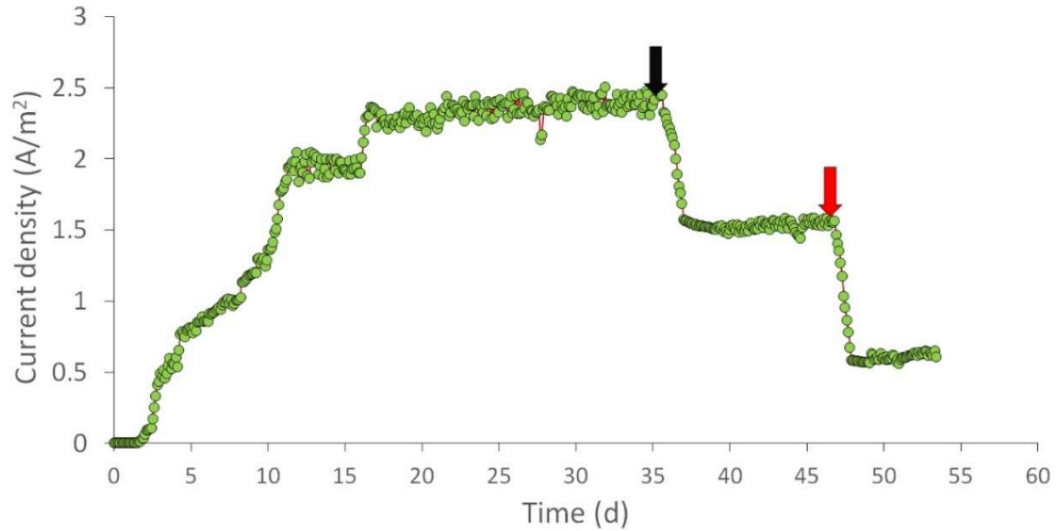
Figure 4-2. The steady-sate current density (A/m^2) in a microbial electrochemical cell operated in continuous mode. The black arrow indicates the day when the phosphate buffer in acetate medium was decreased from 100 mM to 50 mM, the red arrow indicates the day when the phosphate buffer in the medium was decreased from 50 mM to 2.5 mM.

Table 4-1. Measured biofilm thickness at different buffer concentrations.

Phosphate buffer concentration (mM)	Biofilm thickness (μm)
100	119±26
50	132±34
2.5	134±14

4.3.2 pH Gradient Throughout Biofilm Anodes

Figure 4-3 shows the measured pH gradients throughout the biofilm anode grown at different phosphate buffer concentrations. At 100 mM phosphate buffer, no pH gradient was observed within the biofilm, showing pHs from 7.1-7.35 (Figure 4-3a). The innermost pH was as high as 7.24 at 100 mM phosphate buffer. This result is consistent with the literature (Babauta et al., 2011) presenting no pH gradient in a 100 μm-thick biofilm anode at 100 mM phosphate buffer. In contrast, low phosphate buffer concentrations (both 50 and 2.5 mM phosphate buffer) caused large pH gradients throughout the biofilm anode with a pH difference of 0.3-0.4 units between the outermost and the inmost layers in the biofilm. The local pH in the biofilm was as low as ~6.5 with a 2.5 mM phosphate buffer (Figure 4-3c), which fall within a range of 0.3-0.8 pH units in biofilm anodes having 70-100 μm thickness in the literature (Babauta et al., 2012; Franks et al., 2009). The literature (Franks et al., 2009; Kim and Lee, 2010) reported that a local pH of 6.5-6.7 inhibited the metabolic activity of ARB. In my study, the pH gradients at 50 and 2.5 mM phosphate buffer concentrations were not different much, while the steady-state current density at 2.5 mM phosphate buffer significantly decreased by a factor of ~2.5 as compared to that at 50 mM phosphate buffer. Phosphate buffer concentration was stepwise decreased from 100 to 2.5 mM (see Figure 4-2), so it seems that the activity of ARB in part of the biofilm anode had been already inhibited at 50 mM phosphate buffer. For this reason, a substantial decrease of current density at 2.5 mM phosphate buffer might be observed over 50 mM phosphate buffer. Given that an inhibition pH is ~6.7, the inactive zones of the biofilm anode is estimated at 30-50 μm at 50 mM phosphate buffer and 60-75 μm at 2.5 mM phosphate buffer, respectively.
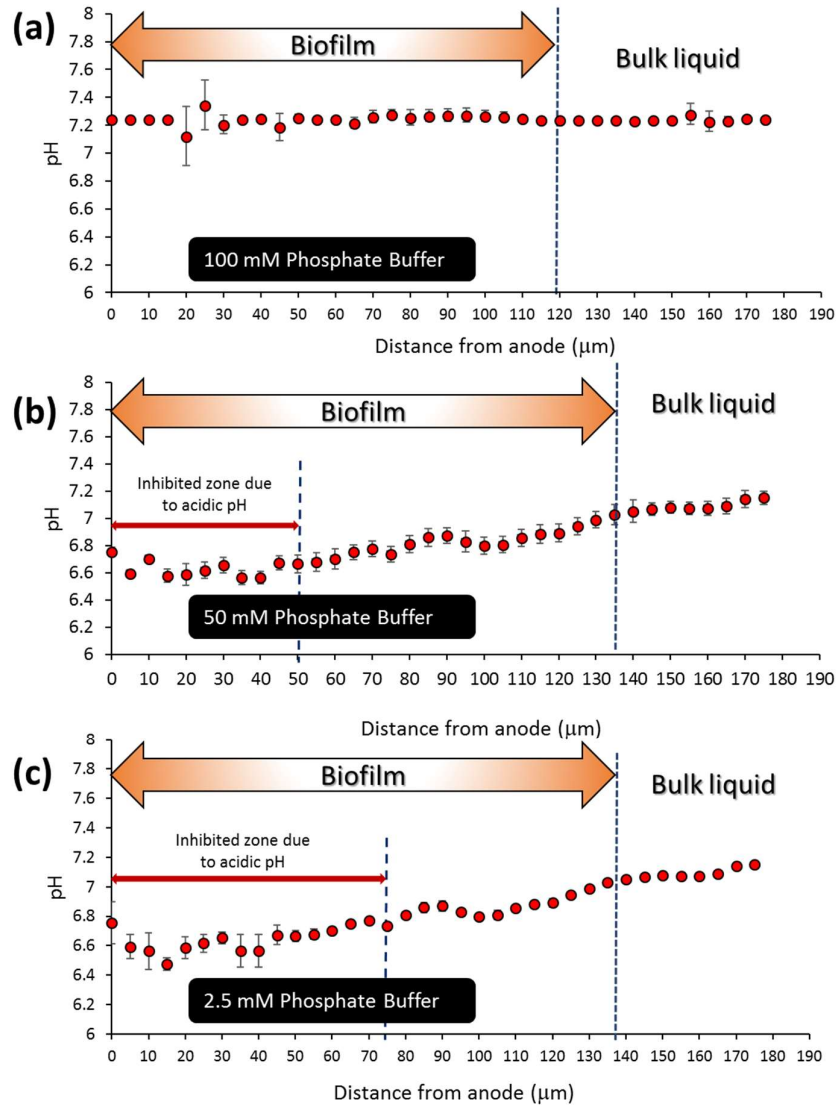
Figure 4-3. pH gradients within the biofilm at different phosphate buffer concentrations. (a) 100 mM, (b) 50 mM and (c) 2.5 mM.

4.3.3   Metabolic Activity of ARB throughout Biofilm Anodes

Figure 4-4 shows the representative 2D CLSM images of anode biofilms at 100 mM and 2.5 mM phosphate buffer. A biofilm anode grown at 100 mM phosphate buffer was entirely stained with green color, indicating that ARB were active throughout the biofilm with a small number of dead cells (red color) (Figure 4-4a). In comparison, an inner biofilm was inactive (red color) at 2.5 mM phosphate buffer where most of the metabolically active cells were located at outer layers of the biofilm, as shown in Figure 4-4b. The thickness of an inactive biofilm was as large

as ~80 μm, in CLSM image analysis, which is close to the thickness of inactive biofilm (60-75 μm) estimated with a pH profile (see Figure 4-3c). The CLSM live/dead cell image at 2.5 mM phosphate buffer proved that the metabolic activity of ARB was limited by acidic pH due to proton accumulation at an inner biofilm.
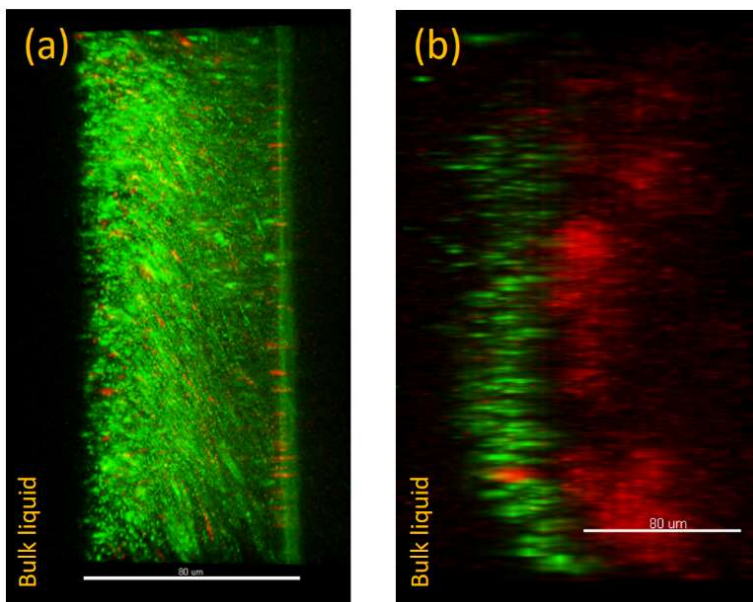
Figure 4-4. 2D Confocal laser scanning microscopy (CLSM) images of biofilm anodes at (a) 100 mM phosphate buffer (supplementary MxC), (b) 2.5 mM phosphate buffer (orignial MxC). Green (live cells) and red color (dead cells).

4.3.4 Biofilm Conductivity

At 100 mM phosphate buffer, K_{bio} was as high as 0.87 ± 0.03 mS/cm, consistent with a highly conductive biofilm anode. The K_{bio} gradually decreased with decreasing phosphate buffer concentration (Figure 4-5), and it was as small as 0.27 ± 0.03 mS/cm at 2.5 mM phosphate buffer. This K_{bio} trend accords to current density, as shown in Figure 4-5. Several literature has commonly reported a substantial decrease of current density in MxCs when pH became acidic in biofilm anodes (Torres et al., 2008b; He et al., 2008; Franks et al., 2009; Kim and Lee, 2010). Acidic pH inhibits the activity of ARB's catabolism (Franks et al., 2009), implying that acidic conditions would exacerbate intracellular electron transfer (IET) kinetics from a soluble electron donor (acetate) to outer membrane proteins (see Figure 2-2). In comparison,

there are no studies on pH effects on EET kinetics in biofilm anodes. Malvankar et al. (2011) reported that the conductivity of nanowire-like appendages produced from *Geobacter sulfurreducens* was increased with increasing proton concentration (pH decrease), claiming metal-like conduction for the appendages. Interestingly, Malvankar et al. (2012a) reported relatively lower current density (2 A/m^2) for a thick (130 μm) and poorly conductive biofilm (0.25 mS/cm) as compared to thin biofilms (40-60 μm), and suggested mass transfer limitations of protons or substrate might decrease the current density. If microbial nanowires are mainly responsible for K_{bio} in biofilm anodes (Malvankar et al., 2011), K_{bio} should increase as pH decreases. However, the results presented here clearly shows K_{bio} decrease with decreasing pH, which implies more EET mechanisms processes are involved in K_{bio} than the appendages. For instance, an acidic pH may denature outer membrane c-type cytochromes (Bond et al., 2012), possibly affecting K_{bio}. Extracellular cofactors (e.g., extracellular cytochrome c), associated with EET in biofilm anodes, are randomly distributed throughout biofilm anodes (Lebedev et al., 2014; Snider et al., 2012), and the cofactors would be related to K_{bio} (El-Naggar et al., 2010; Pirbadian et al., 2015). For example, the conductivity of ferricytochrome c ranges from 1.5×10^{-8} to 1.5×10^{-6} mS/cm (Nakahara et al., 1977, 1979), which implies that extracellular cofactors would have electrical conductivity. pH can transform the structure of extracellular cofactors, and hence, pH change would affect the conductivity of extracellular cofactors and consequently K_{bio} in biofilm anodes.
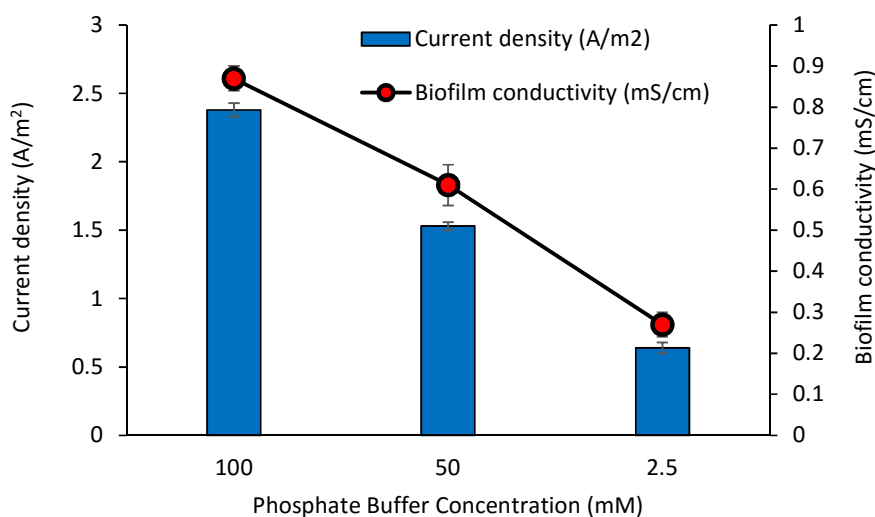
Figure 4-5. Average current density and biofilm conductivity at different phosphate buffer concentrations.

4.3.5 Half-saturation Potential of Biofilm Anode

Figure 4-6 shows LSCVs patterns at different phosphate buffer concentrations. The half-saturation potential (E_{KA}) values were comparable at different buffer concentrations, although K_{bio} and current density decreased significantly to buffer change. The E_{KA} was -225±11 mV at 100 mM phosphate buffer, and it only slightly increased to -191±11 mV at 2.5 mM phosphate buffer. Similar E_{KA} means small energy loss for saturated current density in biofilm anodes, despite of substantial decrease of K_{bio}. At 100 mM phosphate buffer where K_{bio} was the highest at 0.87±0.03 mS/cm, the experimental LSCV well matches the CV simulated with the Nernst-Monod equation (Figure 4-6). It seems like more deviations between the experimental and simulated LSCVs at 2.5 and 50 mM, but after reflecting different scales of current density in y-axis (Figure D-5 in Appendix), it seems that all simulations with the Nernst-Monod equation consistently match experimental LSCVs. These results suggest that K_{bio} would be still high for saturated current densities of 0.64-1.53 A/m^2 at the lower phosphate buffer concentrations.
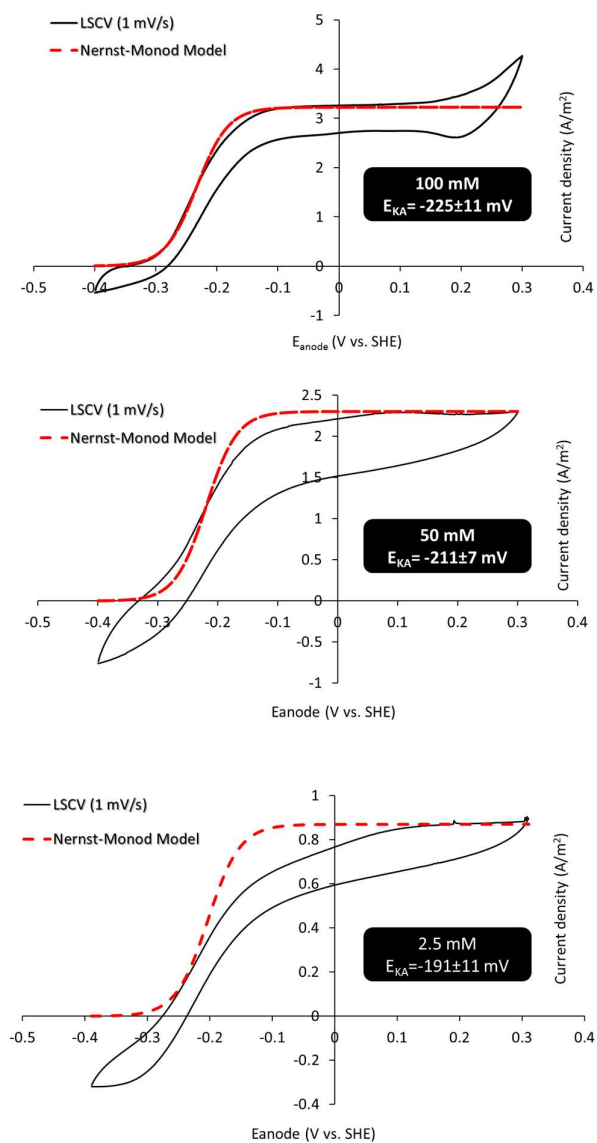
Figure 4-6. LSCVs and Nernst-Monod equation simulation at different phosphate buffer concentration.

4.4   Conclusions

The decrease of phosphate buffer in acetate medium from 100 mM to 2.5 mM caused a pH gradient throughout the biofilm anode and acidified the inner biofilm close to the anode. The pH gradient was as large as 0.4-0.5 units between the outmost layer and the inmost layer of the biofilm, which resulted in the significant decrease of current density from 2.38 to 0.64 A/m^2 in the MxC. CLSM images clearly proved metabolically inactive zones at the inner biofilm under 2.5 mM phosphate buffer, implying very slow IET kinetics. Along with that, the K_{bio} significantly decreased from 0.87 mS/cm to 0.27 mS/cm at the low phosphate buffer concentration. This work is first to demonstrate that acidic pH deteriorates IET and EET kinetics simultaneously in biofilm anodes under low buffer conditions.

Chapter 5

Change of Biofilm Conductivity by Substrate Limitations

A manuscript based on this chapter, co-authored by Dhar, B.R., Ren, H., Chae, J., and Lee, H.S., is under preparation for submission to a refereed journal for peer-review and publication.

Contributions statement: Dhar, B.R. designed the study, fabricated the reactors, performed all laboratory experiments and analyses, and contributed to data interpretation and manuscript preparation. Ren, H. and Chae, J. fabricated micro-sized gold electrodes with non-conductive gap. Lee, H.S. supervised this project.

5.1   Introduction

Microbial electrochemical cells (MxCs) are a unique biotechnology capable of transferring electrons in complex compounds to electrodes catalyzed by anode-respiring bacteria (ARB). This exclusive feature provides dual benefits for wastewater treatment: pollutant removal and electron recovery (e.g., H_2, CH_4, H_2O_2, etc.) (Logan and Rabaey, 2012; Rabaey and Rozendal, 2010; An and Lee, 2013; Escapa et al., 2016). Furthermore, no requirement for intensive air supply to MxCs would provide a clear advantage over conventional wastewater treatment technologies, such as activated sludge process (Dhar and Lee, 2014; Escapa et al., 2016). To promote MxCs as a sustainable technology in wastewater market, MxCs must demonstrate robustness against dynamic changes to various environmental factors along with high substrate utilization rate and current density.

Current density and wastewater treatment rate in MxCs can be limited by the kinetics of substrate utilization (i.e., intracellular electron transfer (IET)) and EET (Lee et al., 2009; Torres et al., 2008a; Marcus et al., 2007; Parameswaran et al., 2013). Substrate utilization rate in MxCs, typically expressed with Monod kinetics (e.g., half-saturation substrate concentration, K_s), depends on several factors including microbial community, substrate concentration, biofilm thickness, active biomass concentration, and mass transfer limitations for protons and substrate within biofilm anodes (Lee et al., 2009; Torres et al., 2008a, 2008b, 2007, 2009; Marcus et al., 2007, 2010, 2011; Parameswaran et al., 2013; Franks et al., 2009). Among them, substrate concentration is important for MxC application to wastewater treatment, since effluent should meet regulations; together with that, MxCs need to generate high current density for improving the benefit of resource reocvery. Substrate-utilization rate will be

saturated at high substrate concentration ($S \gg K_s$), which means non-limiting conditions of IET kinetics for current density. Under this circumstance, EET will control current density. In comparison, IET kinetics regulates current density in MxCs when the substrate concentration is low ($S \ll K_s$). For instance, the Monod term ($S/(K_s+S)$) becomes 0.14 when substrate concentration is 25 mg COD/L (assuming K_s of 156 mg COD/L for *Geobacter*-enriched biofilm anode), which means that the current density at 25 mg COD/L is only 14% of current density at substrate non-limiting condition ($S/(K_s+S) \sim 1$).

K_{bio}, which well represents EET kinetics in conductive biofilm anodes, might be independent of ARB's activity (Malvankar et al., 2011, 2012) or substrate concentration. However, we have often observed indirect evidence that K_{bio} would be associated with the activity of ARB. Steady-state current density has never recovered to a saturated value after changes of environmental and operational parameters, such as long-term starvation over several days, pH inhibition, temperature change, and so on. For instance, in one study, steady-state current density that had been close to 10 A/m^2 for an acetate-fed MxC (growth medium pH $\sim$ 8) significantly decreases by 5 A/m^2 at acidic growth medium ($\sim$ pH 6) (Rinaldi et al., 2008). After medium pH is increased by 8 and fed to the MxC, the current density does not rebound to 10 A/m^2 (Rinaldi et al., 2008). Although the metabolic activity of ARB could affect K_{bio}, the information of substrate effects on EET kinetics or K_{bio} is very limited. Malvankar et al. (2012a) only reported a trivial effect of short-term (> 24 hours) substrate limitations on K_{bio}. MxCs should be operated at substrate-limiting conditions for wastewater treatment to meet effluent standards (e.g., biochemical oxygen demand concentration > 25 mg/L). However, the relationship between substrate concentration (or ARB's activity) and K_{bio} is relatively unexplored as compared to IET kinetics, which limits understanding of substrate effects on current density in MxCs.

The goal of this study is to exclusively investigate substrate effects on K_{bio} in a biofilm anode. The experiments were performed in three stages. First, biological and extracellular kinetic parameters including K_{bio} were quantified for the biofilm anode at a steady-state current density in an MxC operated under substrate non-limiting condition. Second, K_{bio} was quantified at substrate-limited conditions in short-term period less than 6 h. Finally, the MxC was operated at long-term starvation period followed by acetate spiking to assess K_{bio} dynamics to substrate rich and endogenous decay conditions

5.2   Materials and Methods

5.2.1   MxC Configuration and Operation

Dual-chamber MxCs were constructed with plexiglass. Two gold anode electrodes (width 9.5 mm × length 15 mm × thickness 10 μm) on a glass base with a non-conductive gap of 50 μm was designed and fabricated specifically to measure the K_{bio}; the total geometric surface area of the two anodes was 2.85 cm^2. A porous graphite plate (Isomolded Graphite Plate 203101, Fuel Cell Earth, USA) was used as the cathode and anion exchange membrane (AMI-7001, Membranes International Inc., USA) was placed between the anode and the cathode chambers as separator. The working volumes of both chambers were 15 mL. A reference electrode (Ag/AgCl reference electrode, MF-2052, Bioanalytical System Inc., USA) was placed within less than 1 cm distant from the anodes to control anode potential (E_{anode}) during experiments. Here, all anode potentials are reported versus standard hydrogen electrode (SHE).

The MxC was inoculated with biofilms collected from a mother MxC that had been operated for over 2 years using acetate medium, and was fed with 25 mM acetate medium supplemented with 100 mM phosphate buffer (medium pH 7.2-7.4). The literature provides information on the composition of the medium (Dhar et al., 2013). The cathode chamber was filled with tap water, producing H_2 gas. After inoculation, the anode chamber was sparged with ultra-pure nitrogen (99.999%) for 5 min, and then E_{anode} was set at -0.2 V using a potentiostat (BioLogic, VSP, Gamble Technologies, Canada). Current was recorded at every 120 s using EC-Lab for windows v 10.32 software in a personal computer connected to the potentiostat (BioLogic, VSP, Gamble Technologies, Canada). After operation in batch mode for a week, the medium was continuously fed to the MxC at a flow rate of 5.8 mL/h using a cartridge-type peristaltic pump (Master Flex$^\circledR$ L/S digital drive, Model 7523-80, Cole-Parmer, Canada) to maintain hydraulic residence time (HRT) of 2.6 h in the anode chamber (substrate non-limiting conditions). After characterizing biological and electrochemical kinetic parameters, K_{bio}, and biofilm thickness at the steady-state current density, the effects of short- and long-term substrate depletion on EET kinetics were evaluated. At steady state, a short-term substrate limiting condition was created by continuous feeding of mineral medium lacking acetate to the anode chamber in order to decrease acetate concentration. A long-term substrate limitation was made by stopping medium feed for 7-9 days. After 4-5 days of starvation phase, approximately 10 mL of 25 mM acetate medium was spiked to the anode chamber. Starvation followed by acetate spiking was repeated at least 3 times in batch mode.

60

5.2.2   Biofilm Conductivity Measurement

K_{bio} was quantified from experimentally measured biofilm conductance using the two-probe measurement method (Malvankar et al, 2011). For measurements of biofilm conductance, the anodes and the cathode were disconnected temporarily (open circuit mode). Then, a small voltage ramp of 0-50 mV in a step of 25 mV was applied across two gold electrodes using a source meter (Keithley 2400, Keithley Instruments, Inc., USA), and the current data was recorded. Observed biofilm conductance ($G_{Biofilm\ (obs)}$, mS) was quantified from the current-voltage response. Ionic conductance ($G_{control}$, mS) was also measured with an abiotic MxC (control) to account for ionic current across the non-conductive gap using both acetate medium and MxC effluents. Intrinsic biofilm conductance ($G_{Biofilm} = G_{Biofilm\ (obs)}$-$G_{control}$, mS) was used for calculation of biofilm conductivity (K_{bio}, mS/cm) with equation (5-1) (Kankare and Kupila, 1992).

$$K_{bio} = \left. G_{Biofilm}\frac{\pi}{L} \middle/ ln\left(\frac{8L_f}{\pi a}\right) \right. \qquad (5-1)$$

Where, L_f is the biofilm thickness (µm), L is the length of the electrodes (1.5 cm), and a is half of the non-conductive gap between two electrodes (25 µm).

5.2.3   Biofilm Thickness Measurement

Biofilm thickness (L_f) was measured with the method proposed by Bonanni et al. (2013) using the change of resistance between the surface of biofilms and electrodes. A stainless steel needle with a tip diameter of 100 µm was used as the microelectrode for biofilm thickness measurement. The microelectrode connected with a motorized micromanipulator (MM33, Unisense A/S, Denmark) was positioned very close to the surface of the biofilm and then stepwise moved toward gold electrodes. A step size of 5 µm was controlled using Unisense SensorTrace Suite software (Unisense A/S, Denmark). The anode chamber was disclosed and anolyte was removed with a syringe, which means that the anode biofilms were open to the air for the access of the microelectrode. When the microelectrode was open to air away from the biofilm, resistance was close to infinite value (open circuit). High resistance in MΩ ranges was observed when the microelectrode touched the outmost layer of the biofilm, mainly due to water content in the biofilm.   Resistance substantially decreased at <1 Ω when the microelectrode touched the anode surface. The biofilm thickness was quantified by monitoring

the change of resistance in the microelectrode using a multimeter (Fluke 179/TPAK, Fluke Electronics Canada LP, Mississauga, ON, Canada) connected to the microelectrode. During measurements, drops of the substrate medium were added to the surface of the biofilm to avoid dehydration. To mitigate O_2 inhibition effects on ARB, triplicate measurements of biofilm thickness were completed in 35 min. Then, the MxC was quickly assembled, and operated under potentiostat mode. Current density was immediately recovered to the steady state.

5.2.4 Estimation of $K_{s,app}$, and $q_{max,app}X_f$

The best-fit $K_{s,app}$ and $q_{max,app}X_f$ for the biofilm anode were estimated from current density at different acetate concentration in the bulk liquid (8-2,650 mg COD/L). According to the Nernst-Monod equation (Eq. 5-2), the best-fit apparent $K_{s,app}$ (g COD/m^3) and $q_{max,app}X_f$ (g COD/m^3-d) were quantified with the relative least squares method using MS 2016 excel solver (Lee et al., 2009; Torres et al., 2008a).

$$ j = 0.14(1 - f_s^o)\, q_{max,app}X_fL_f\ \frac{S}{K_{s,app} + S} \left[\frac{1}{1 + \exp\left(-\frac{F}{RT}(E_{anode} - E_{KA})\right)} \right]\ (5-2) $$

Where, j is the current density (A/m^2), 0.14 is the conversion factor for converting substrate flux to the current density (0.14 A= 1 g COD/d), f_s^o in the fraction of electron used for cell synthesis (f_s^o =0.1) (Lee et al., 2009; Torres et al., 2008a), $q_{max,app}$ is the maximum specific substrate utilization rate (g COD/g VS-d), X_f is the concentration of active ARB in the anode biofilms (g VS/m^3), L_f is the biofilm thickness (m), $K_{s,app}$ is the apparent half-saturation concentration of acetate (mg COD/L), S is the acetate concentration (mg COD/L), E_{anode} is the anode potential (V), E_{KA} is the half-saturation potential at $j=j_{max}/2$ (V), R is the ideal gas constant (8.3145 J/mol-K), F is the Faraday's constant (96,485 C/mol e$^-$), and T is temperature (298.15, K).

5.2.5 Estimation of E_{KA}

The E_{KA} of the biofilm anode was estimated with low-scanning cyclic voltammetry (LSCV) at a scan rate of 1 mV/s (Lee et al., 2009; Torres et al., 2008a). E_{anode} was ramped between -0.4 to +0.4 V at a scan rate of 1 mV/s using the potentiostat. The current and anode potential were recorded at every 5 s using EC-Lab for windows v 10.32 software in a personal computer

connected with the potentiostat. To ensure the reproducibility of the LSCV data, each test was conducted in triplicates, and the average data is reported.

5.2.6 Liquid Analysis

The concentration of acetate was analyzed using a gas chromatography (GC) (Model: Hewlett Packard HP 5890 Series II) equipped with flame ionization detector (FID) (Dhar et al., 2015). All samples were analyzed in triplicate.

5.3 Results and Discussion

5.3.1 Steady-state Current Density, Biofilm Conductivity, and Kinetic Parameters

After around 10 days of operation, the current density (j) reached at the steady-state current density of 1.68 ± 0.06 A/m^2 (Figure 5-1). A relatively thick biofilm developed, with an average biofilm thickness (L_f) of 139 ± 11 μm. The average K_{bio} was 0.48 ± 0.05 mS/cm, which is enough to facilitate EET via Ohmic conduction (Marcus et al., 2007; Torres et al., 2008; Malvankar et al., 2012a). Steady-state LSCVs at 1 mV/s under substrate non-limiting conditions also showed sigmoidal Nernst-Monod pattern (Figure 5-2), which is another indication of conduction based EET (Marcus et al., 2007; Torres et al., 2008a; Renslow et al., 2013; Lee et al., 2009). The half-saturation potential, E_{KA}, was estimated at -246 ± 2 mV, indicating small energy loss for saturated current density. The best-fit of the Monod half-saturation substrate concentration, $K_{s,app}$ was estimated to be 168 g COD/m^3, and this falls within 119-176 g COD/m^3 in biofilm anodes showing high kinetics (Lee et al., 2009; Torres et al., 2008a). This low $K_{s,app}$ proves that 25 mM acetate medium (1610 ± 40 g COD/m^3) does not limit current density (substrate non-limiting conditions). The best-fit $q_{max,app}X_f$ of 1.26×10^5 g COD/m^3-d was relatively lower than $q_{max,app}X_f$ in a range of 8×10^5 to 1×10^6 g COD/m^3-d for biofilm anodes producing high current density ~10 A/m^2 (Lee et al., 2009; Torres et al., 2008). This low $q_{max,app}X_f$ is consistent to previous chapter (Chapter 3) in an MxC equipped with gold anodes, confirming that $q_{max,app}X_f$ could accounts for high current density in biofilm anodes.
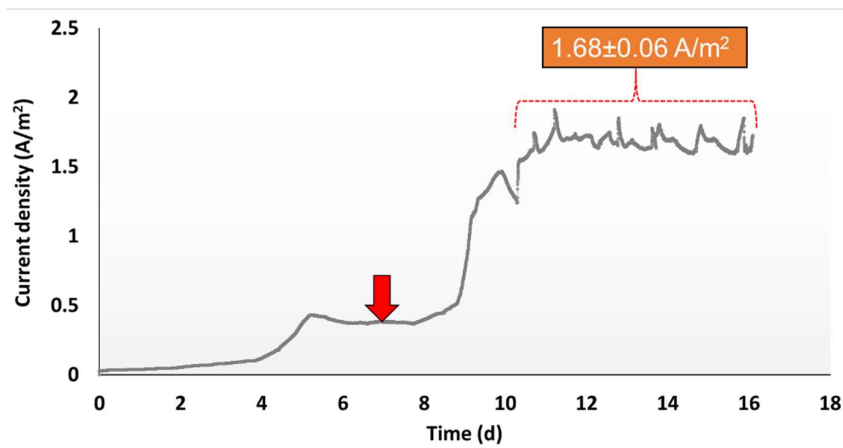
Figure 5-1. Current density with time from period of inoculation until steady-state. The arrow shows the time when the operation was switched from batch to continuous mode.
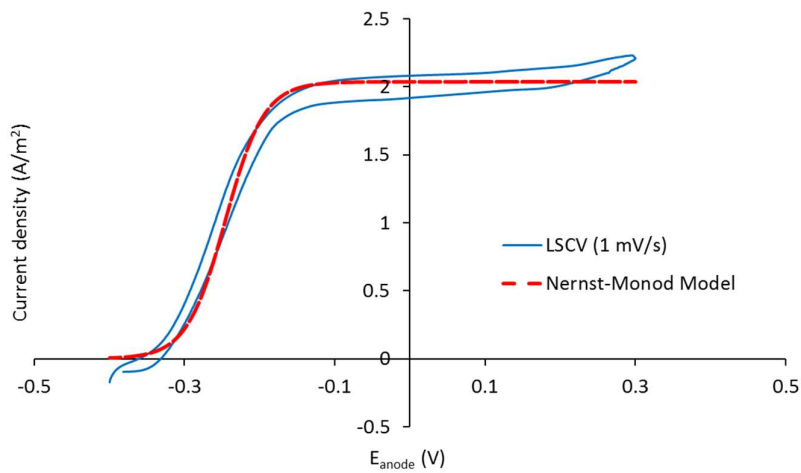
Figure 5-2. LSCV (1 mV/s) and Nernst-Monod Model simulation of biofilm anode at steady-state.

5.3.2 Effects of Substrate Limitation on Biofilm Conductivity in Short Period

Initially, acetate concentration in MEC effluent was ~2,648 mg COD/L, which is substantially higher than the estimated $K_{s,app}$ of 168 mg/L. At this substrate non-limiting condition, the measured K_{bio} was 0.51 ± 0.06 mS/cm (1.86 A/m^2) (Figure 5-3), which is close to the average K_{bio} (0.48 ± 0.05 mS/cm) at the steady state. After mineral medium lacking acetate was fed to the MxC continuously (~ 6h), the acetate concentration in effluent substantially decreased to ~7 mg COD /L, reducing current density by 0.17 A/m^2 (Figure 5-3). At this low substrate concentration, the measured K_{bio} was still high at 0.56 ± 0.02 mS/cm. This result proves that substrate limitation does not influence biofilm conductivity in a short period of time (~ 6 h), which is consistent with the literature reporting no substrate effects on K_{bio} during batch operation of MxCs (Malvankar et al., 2011).
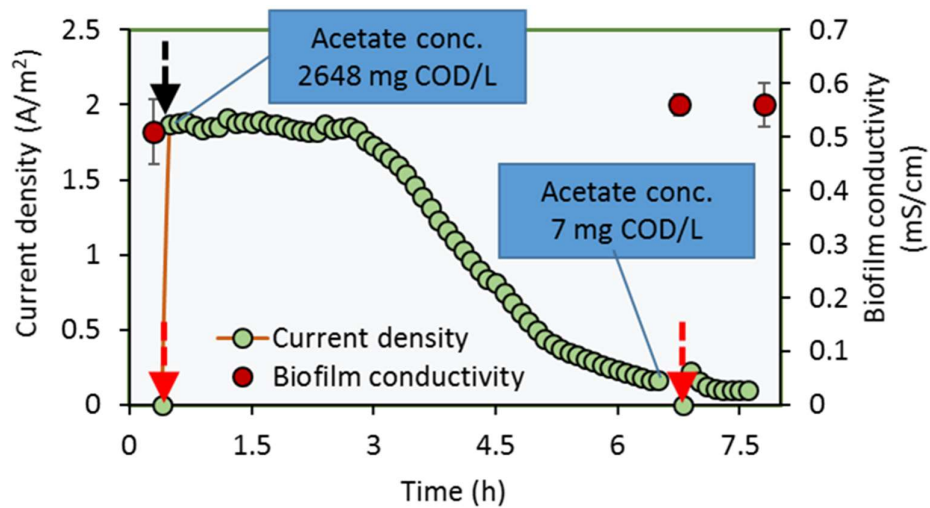
Figure 5-3. Current density and biofilm conductivity at short-term substrate limited condition. The red arrows show the time when MxC was switched from open circuit to the closed-circuit mode (3-electrode operation with potentiostat) after biofilm conductivity measurement; the black arrow shows the time when the pump was started for continuous feeding of nutrient medium lacking acetate.

5.3.3 Effects of Substrate Limitation on Biofilm Conductivity in Long Starvation

Figure 5-4 shows the changes of current density and K_{bio} in the MxC run at starvation and acetate-spiking conditions. The MxC was operated for 4-5 days at starvation phase (i.e., the absence of exogenous electron donor). The endogenous decay current was stable at 0.03 ± 0.01 A/m^2 during this period. The current density sharply increased up to 1.17-1.28 A/m^2 after acetate spiking in which acetate concentration was 238 ± 42 mg COD/L in anolyte. This peak current density, close to the steady-state current density in the continuous MxC, gradually decreased to 0.01-0.03 A/m^2 after 3.5-7 days, due to acetate depletion with time. The trend of current decrease and increase to substrate concentration was repeated in three batch cycles, indicating ARB were able to respire by transferring acetate electrons to the anode, despite of long starvation from 4 to 5 days. This result is consistent with the literature (Gao et al., 2014; Mahmoud et al., 2016). Average biofilm thickness was 123-142 μm, which means biofilm thickness did not cause a significant substrate gradient throughout the biofilm during experiments (Table E-1).

Substantial decrease of K_{bio} was observed at the end of each starvation period. K_{bio} ranged from 0.10 to 0.16 mS/cm at endogenous decay conditions, which was 66-79% lower than the steady-state K_{bio} 0.48 mS/cm. Interestingly, high K_{bio} (0.53-0.57 mS/cm) was recovered after acetate spiking (2-3 days after endogenous growth conditions), evidently proving that the metabolic activity of ARB influences K_{bio}. The literature (Malvankar et al., 2011) claimed that K_{bio} would be independent of ARB's metabolic activity by showing negligible substrate effect on K_{bio} or metal-like nature of microbial nanowires. However, the literature only measured K_{bio} dynamics in a short period of time (20-24 hours). Nanowires does not need to the sole EET route (Snider et al., 2012, El-Naggar et al., 2010) for conductive biofilm anodes. Intracellular or membrane bound proteins associated with electron transfer might be associated with EET, and this work clearly shows the close relationship between ARB's activity (depressed and stimulated with substrate) and K_{bio}. For instance, intracellular cyclic diguanylate (c-di-GMP), a ubiquitous signalling and sensing protein in bacteria, has been identified to be liable for activating Type IV pili (i.e., nanowires) in *Geobacter* spp. and *Pseudomonas* spp., by protein-protein interactions (Skotnicka et al., 2016; Hengge, 2009; Leang et al., 2013). More studies are required to identify which genes and proteins regulate biofilm conductivity in biofilm anodes, but this work is the first to demonstrate that the metabolic activity of ARB is closely related to biofilm conductivity.
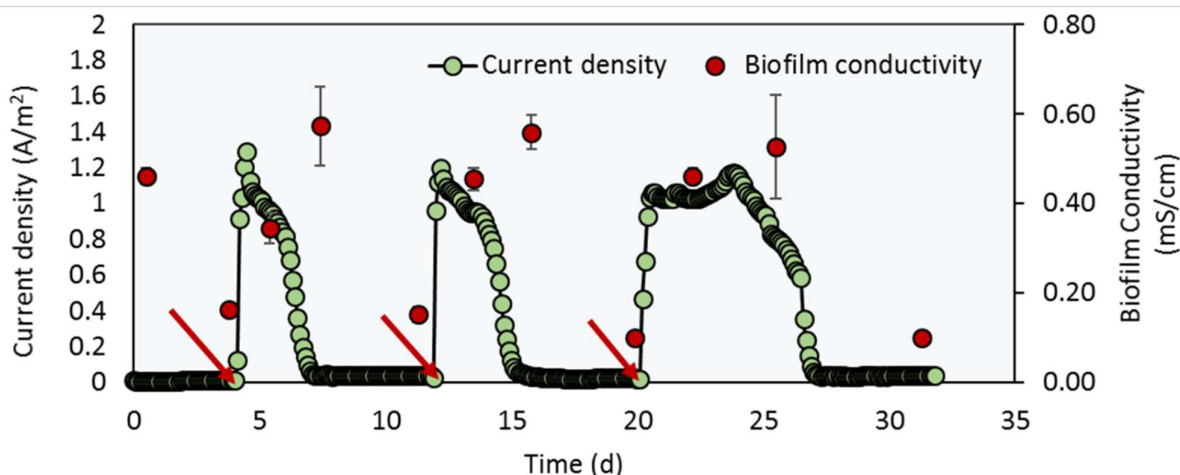
Figure 5-4. Current density and biofilm conductivity in response to acetate medium injection after 4-5 days of the starvation period. The red arrows show the time when acetate was injected into the anode chamber.

5.4   Conclusions

Biofilm conductivity was stable under steady-state conditions, and it did not change at low substrate concentrations in a short period of time (~ 6 hours). For long endogenous decay conditions (4-5 days), biofilm conductivity dynamically decreased from 0.53±0.02 mS/cm to 0.14±0.03 mS/cm, but it was recovered to 0.55 mS/cm after acetate spiking. The decreasing and increasing pattern of biofilm conductivity was consistent in three batch cycles. This study proves that the metabolic activity of ARB is correlated with biofilm conductivity.

Chapter 6

Ohmic Resistance Affects microbial Community and Electrochemical Kinetics in a Multi-anode Microbial Electrochemical Cell

A version of this chapter, co-authored by Dhar, B.R., Ryu, H., Santo Domingo, J. W., and Lee, H.S., has been submitted to Journal of Power Sources for peer-review and publication.

Contributions statement: Dhar, B.R. designed the study, fabricated the reactors, performed all laboratory experiments and analyses, and contributed to data interpretation and manuscript preparation. Ryu, H. and Santo Domingo, J. W conducted microbial community analysis. Lee, H.S. supervised this project.

6.1 Introduction

Current society needs sustainable biotechnologies to build a green cycle at the intersection of economy, environment, and energy. Microbial electrochemical cells (MxCs) that produce value-added chemicals from organic waste and wastewater can be one of the biotechnologies to catalyze establishment of the green circle (Logan et al., 2015; Escapa et al., 2016; He et al., 2015). MxCs should produce high current density (the fast yield of value-added products) with an acceptable range of exogenous energy supply to deploy MxCs in field. Anode kinetics primarily limit current density in external energy dependent-MxCs, since catalysts and exogenous energy efficiently accelerate abiotic reaction rates associated with ohmic and cathodic limitations (Logan et al., 2015; Logan and Rabaey, 2012; Escapa et al., 2016; He et al., 2015; Ghasemi et al., 2013; Santoro et al., 2015). While the anode reaction rates significantly depend on biological kinetic parameters, nanomaterials and new designs have been applied for anodes to improve anodic rate (Logan et al., 2015; Xie et al., 2012; He et al., 2012; Ghasemi et al., 2013). These approaches increased current density by 10-25 A/m^2 (Xie et al., 2012; He et al., 2012), but they would not be readily applicable for large-scale MxCs, due to expensive costs or scale-up issues (Logan et al., 2015; Escapa et al., 2016; He et al., 2015; Ghadge and Ghangrekar, 2015). Multi-anode configurations employing inexpensive electrodes could be a technically robust and economically promising option for scale up of MxCs (Ahn and Logan, 2012; Lanas and Logan, 2013; Hutchinson et al., 2011; Ren et al., 2014; Ghadge and Ghangrekar, 2015; Ahn et al., 2014; Jiang et al., 2011; Jiang and Li, 2009), since multiple electrodes can improve anode kinetics by increasing surface area for mass

transfer and biofilm formation (Ahn and Logan, 2012; Dewan et al., 2008; Ghadge and Ghangrekar, 2015; Ahn et al., 2014). However, literature has shown non-linear or sometimes trivial increase of current density in multi-anode MxCs over single-anode ones (Lanas and Logan, 2013; Hutchinson et al., 2011; Jiang et al., 2011; Jiang and Li, 2009).

Small increase of current density indicates minor contribution to current density from additional anodes in multi-anode MxCs, implying sluggish anode kinetics on the anodes. No studies, however, have explored anode kinetics for individual anodes in the MxCs. Each anode would have heterogeneous conditions for electron transfer in the MxCs, such as mixing conditions, local substrate concentration, local pH, and ionic resistance between anodes which might cause negligible contribution of multiple anodes to current density. While many parameters can create heterogeneity in multiple anodes, it seems evident that ionic resistance exists between anodes: unique feature of multi-anode configuration against single anode. Ohmic resistance (mainly ionic resistance) can change electric potential of individual anodes in multi-anode MxCs when electrode distance is far from each other. In this circumstance, anode potential of individual anodes would not be equivalent in multi-anode MxCs, leading to different electron transfer kinetics on each anode. Anode potential is a key parameter for enrichment of kinetically efficient anode-respiring bacteria (ARB) in biofilm anodes from mixed-culture inocula (Torres et al., 2009; Commault et al., 2013; Kumar et al., 2013), although other factors (e.g., electrode materials and structures, substrate type and concentration, pH, and temperature) can affect ARB community structure in biofilm anodes (Logan et al., 2015; Escapa et al., 2016; He et al., 2015; Ghasemi et al., 2013; Santoro et al., 2015; Logan and Rabaey, 2012; Lee et al., 2009; Torres et al., 2008a; Parameswaran et al., 2013). For example, *Geobacter* genus, one of the most kinetically efficient ARB, became dominant in biofilm anodes and generated high current density (~ 10 A/m^2), when mixed culture was inoculated at negative anode potential (-0.05 to -0.15 V vs. standard hydrogen electrode (SHE) (Torres et al., 2009; Commault et al., 2013). In comparison, more diverse ARB community was established at positive anode potential (+0.2 to +0.37 V vs. SHE), which showed lower current density (0.6-2 A/m^2) in MxCs (Torres et al., 2009; Kumar et al., 2013).

Improvement of current density using multiple anodes is based on the assumption that individual anodes generate comparable current density, increasing overall current density in multi-anode MxCs. If different microbial communities are built on individual anodes in multi-anode MxCs, biological and electrochemical kinetics may not be conserved for each anode.

Then, current density generated from individual anodes is inconsistent, and multi-anode MxCs would not improve current density much. To maximize the advantage of multi-anode MxCs (e.g., more anode surface area per volumes of MxCs), we should understand anode kinetics on individual anodes in the MxCs.

This study was conducted to characterize microbial community and anode kinetics in individual anode biofilms for a multi-anode MxC. First, current density in each anode was quantified. Second, dominant ARB in biofilm anodes were identified by targeting 16S rRNA. Third, E_{KA} values for individual anode biofilms were characterized to evaluate electrochemical kinetics, and finally the implication of ohmic energy loss and its impacts on performance of multi-anode MxCs was summarized.

6.2   Methods

6.2.1   Configuration of Multi-anode Microbial Electrochemical Cell (MxC)

The dual chamber multi-anode microbial electrochemical cell (MxC) was built with plexiglass (Fig. 6-1a). High-density carbon fibers (2293-A, 24A Carbon Fiber, Fibre Glast Development Corp., Ohio, USA) that were connected with stainless steel current collectors were used as the anode module (Fig. 6-1c). Prior to use, the carbon fibers were pretreated for 3 days with nitric acid (1N), acetone (1N) and ethanol (1N) for 1 day in series, and then washed with MilliQ water (18.2 MΩ-cm). Three anode modules (anode-1, anode-2, and anode-3) were installed in an anode chamber to improve current density per membrane surface area in the dual-chamber MxC (Fig. 6-1a) and they were connected via copper wires. An anion exchange membrane (AMI-7001, Membranes International Inc., USA) was used as separator between the anode and the cathode chamber, and the geometric surface area of the membrane was 28.1 cm^2. Current density was expressed per the membrane surface area (Dhar et al., 2013, 2015; An and Lee, 2013). A reference electrode (Ag/AgCl reference electrode, MF-2052, Bioanalytical System Inc., USA) was placed between anode-1 and anode-2; all anode potentials are reported against standard hydrogen electrode (SHE). The distance between the reference electrode and anode-1 was 1.27 cm. The distances of the reference electrode from anode-2 and anode-3 were 3.81 cm and 6.35 cm, respectively (Figure 6-1a). A stainless steel mesh was employed for the cathode (Type 304, McMaster Carr, OH, USA) (Fig. 6-1b). The working volumes of the anode and cathode chamber were 300 mL and 100 mL, respectively.
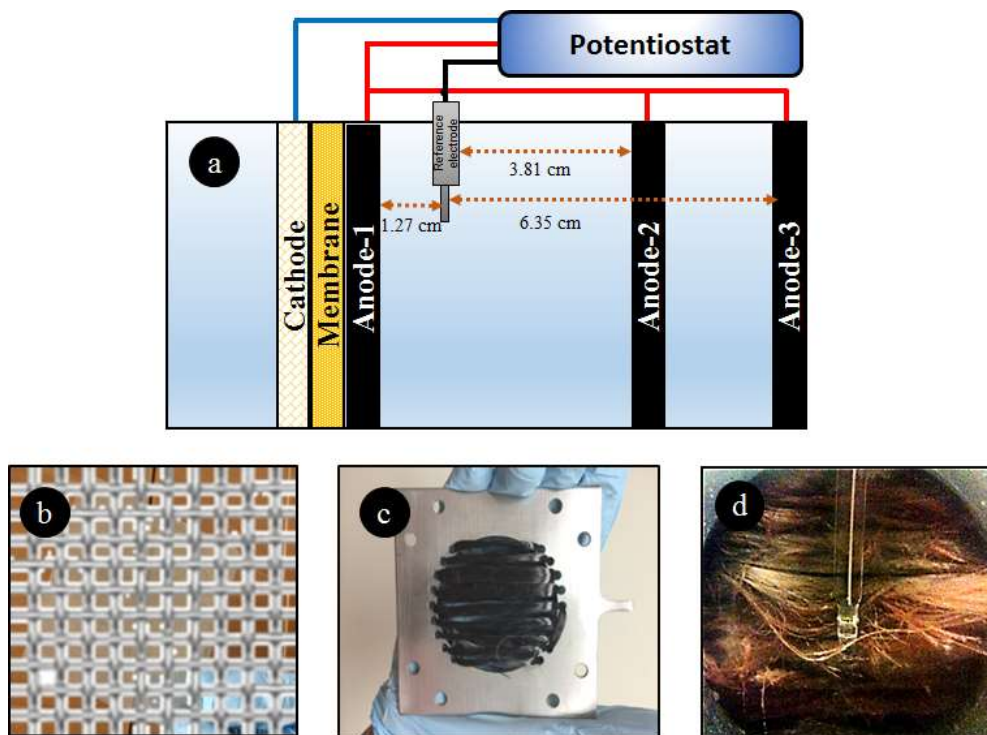
Figure 6-1. (a) Schematic of multi-anode MxC configuration and experimental set-up, (b) cathode (stainless steel mesh), (c) anode module (carbon fibers integrated with a stainless steel current collector), (d) digital photograph of ARB biofilm grown on carbon fiber anode.

6.2.2 Inoculation and Operating Conditions

The MxC equipped with three anodes was inoculated using 30 mL of anolyte from a mother MxC, which had been run with acetate medium (Dhar et al., 2013) for over 1 year. The anode chamber was sparged with ultra-pure nitrogen (99.999%) for 20 min, and then the anode potential was set at -0.1 V vs. SHE using a potentiostat (BioLogic, VSP, Gamble Technologies, Canada). Current and applied voltage was recorded at every 120 s using EC-Lab for windows v 10.32 software in a personal computer connected to the potentiostat (BioLogic, VSP, Gamble Technologies, Canada). The MxC was operated in a temperature-controlled room at 25°C. The anolyte was circulated using a peristaltic pump (Master Flex® L/S economy variable-speed drive, Cole-Parmer, Canada) at a flow rate of 25 mL/min for mixing. The cathode chamber was filled with tap water where hydrogen gas is produced, which allows us to focus on anodic

71

reactions in the MxC (Lee et al., 2009). The MxC was operated in batch mode for 3 days, and then it was switched to continuous mode. In continuous mode, acetate medium (100 mM phosphate buffer) was fed to the MxC at a flow rate of 15 mL/h using a peristaltic pump (Master Flex® L/S digital drive, Model 7523-80, Cole-Parmer, Canada) to maintain hydraulic residence time (HRT) of 20 h in the anode chamber. The average COD concentration of acetate medium was 2,300±40 mg COD/L.

At constant operating conditions, first the MxC was operated with three anode modules (anode-1, anode-2, and anode-3 for phase-1), then two modules (anode-1 and anode-2 for phase-2), and finally one module (anode-1 for phase-3). To avoid oxygen exposure to ARB, anode modules were removed and reassembled in an anaerobic chamber (COY Type B Vinyl Anaerobic Chamber, COY Lab Products, USA). To evaluate the current density and estimate electrochemical kinetics for individual anode modules in phase-1 and phase-2, the external connections between the anode modules were temporally disconnected and the MxC was operated with each anode.

6.2.3 Microbial Community Analysis

For microbial community analysis, biofilm samples were collected from each anode electrode with a sterilized spatula. Microbial community structures were analyzed by targeting 16S rRNA. Total RNA were extracted from three anode biofilm samples as previously described with some minor modifications (Pitkänen et al., 2013). Briefly, the AllPrep DNA/RNA Mini Kit (Qiagen GmbH, Hilden, Germany) was used to extract total nucleic acid. RNA was further purified using Ambion TURBO DNA-free DNase kit (Life Technologies, Grand Island, NY). The concentration and purity of RNA were determined using Qubit RNA assay kits and the Qubit 2.0 Fluorometer (Life Technologies). Barcoded 16S rRNA gene targeting primers (i.e., 515F and 806R) and the targeted product (i.e., 291 bp) was sequenced in both directions using an Illumina MiSeq PE250 approach (Caporaso et al., 2011). Sequence reads (16S rRNA-based) were processed and analyzed using Mothur software (Schloss et al., 2009). Sequence reads that did not fit the following criteria were discarded from further analyses: did not form contigs, deviated considerably from the expected PCR size product, identified as chimeras, had ambiguous bases, and had homopolymers greater than 7 bases long. Sequence reads were grouped at a 97 % similarity and the consensus sequences were then identified using Mothur and the Silva database as a reference (Quast et a., 2013). Excel was used to determine the overall relative abundance of representative sequences at different taxonomic levels (e.g., class,

order, family, genus). Rare members (less than 10 sequences) were excluded for the calculation of the relative abundance. Sequences were analyzed using Blast (http://www.ncbi.nlm.nih.gov/BLAST) and RDP classifier (Wang et al., 2007) further confirm their phylogenetic affiliation and to classify sequences at a low taxonomic level (genus and species) whenever possible.

6.2.4   Estimation of E_{KA} and Simulation of Current Density with the Nernst-Monod Equation

The one-dimensional Nernst-Monod model was used to estimate half-saturation anode potential (E_{KA}) for each anode module in three phases, which represents electrochemical kinetic features of ARB in biofilm anodes (Lee et al., 2009; Torres et al., 2008b; Marcus et al., 2007). E_{KA} was determined using low scanning cyclic voltammetry (LSCV) for anode modules with three-electrode configuration (working, counter and reference electrodes). Anode potential was varied between -0.4 to +0.4 V vs. SHE at a scan rate of 1 mV/s using the potentiostat. The current and anode potential were recorded at every 5 s using EC-Lab for windows v 10.32 software in a personal computer connected with the potentiostat. To ensure the reproducibility of the LSCV data, each CV test was conducted in triplicates, and the average data was reported. Since the potentiostat cannot compensated for ohmic energy loss, the anode potential in the LSCV results were corrected using Eq. (6-1) to account for the ohmic energy loss between working (i.e., anode) and reference electrode (Torres et al., 2008b):

$$\Delta E_{ohm} = -\frac{jL}{\kappa} \qquad (6\text{-}1)$$

Where, κ is the conductivity of the anolyte (15.2 mS/cm), L is the distance between anode and reference electrode (cm). After determination of E_{KA}, the current density in response to anode potential was simulated with the Nernst-Monod equation, described in Eq. (6-2). Acetate concentration was kept at 1,250 to 1,600 mg COD/L during the LSCV experiments to create acetate non-limiting conditions ($S \gg K_s$), given that K_s for ARB is close to 119 mg COD/L (Lee et al., 2009).

$$j = j_{max}\left[\frac{1}{1+\exp\left(-\frac{nF}{RT}(E_{anode}-E_{KA})\right)}\right] \qquad (6-2)$$

Where, j is the current density (A/m^2), j_{max} is the maximum current density (A/m^2), K_s is the half-saturation substrate concentration (g COD/m^3), S is the substrate (acetate) concentration in the bulk liquid (g COD/m^3), R is the ideal gas constant (8.314 J/mol-K), F is the Faraday's constant (96485 C/mol e$^-$), T is the operating temperature of MxC (298.15, K), n is the number of electrons transferred, E_{anode} is the anode potential, and E_{KA} is the half-saturation anode potential (V). For the simulation it was assumed that n=1.

6.2.5   Acetate Quantification

Acetate concentration was analyzed using a gas chromatography (GC) (Model: Hewlett Packard HP 5890 Series II) equipped with a Nukol fused-silica capillary column and flame ionization detector (FID) (Dhar et al., 2015).

6.3   Results and Discussion

6.3.1   Current Density from Individual Anodes

The steady-state current density was the highest at 9.15±0.36 A/m^2 (overall current density) in the MxC equipped with three anode modules (phase-1). The contribution of two anode modules (anode-2 and anode-3) was only 35% of the overall current density (Figure 6-2). The current density for anode-1 (closest to the reference electrode) was consistent at $\sim$ 6 A/m^2 for three phases. In comparison, the current densities for anode-2 (electrode distance 3.81 cm from the reference electrode) and anode-3 (electrode distance 6.35 cm from the reference) were low at 1.4 to 1.7 A/m^2 in phase-1 and phase-2. This result clearly indicates that anode kinetics was not comparable in the three anodes: fast kinetics for anode-1 and sluggish kinetics for anode-2 and anode-3.

6.3.2   Estimation of Anode Potential Corrected for Ionic Resistance in the Multi-anode MxC

In this study, the potentials of three anodes electronically connected with copper wires were set at -0.1 V vs. SHE using the potentiostat, but the potentiostat does not have compensation function of ohmic energy loss for set electric potential (here anode potential). Instead, the potentiostat polarizes counter electrode potential (here cathode potential) to compensate for energy losses. This limited function of the potentiostat indicates that set anode potential (reading potential values) can be different from intrinsic anode potential, when the ionic

74

resistance between anodes and the reference electrode is significant (Torres et al., 2008b; Zhang et al., 2014; Patil et al., 2015). Hence, the electric potentials of individual anodes should be corrected for ohmic energy losses (mainly ionic resistance) for the MxC. Anode potentials corrected for ionic resistance using equation (6-1) are summarized in Table 6-1, which clearly illustrates the deviation of anode potential from the set value of -0.1 V. Deviation of anode potential became significant at phase-1 (three anodes), due to higher current density. For instance, electric potential of anode-3 corrected for ionic resistance was +0.3 V (0.4 V energy loss) at 9.15 A/m^2 (phase-1). In comparison, corrected electric potentials of anode-1 were close to the set value of -0.1 V (-0.04 to -0.01 V), due to close electrode distance and less energy loss. These results indicate that intrinsic anode potential of individual anodes in the multi-anode MxC was actually different from the set potential of -0.1 V because of ionic resistance. Anode potential polarized by ionic resistance (more positive anode potential) can diversify bacterial community in biofilm anodes, which can lower current density in MxCs (Torres et al., 2009; Kumar et al., 2013). High current density was observed only for anode-1, along with small current density for the other two anodes (see Figure 6-2). Calculation of intrinsic anode potentials and the trend of current density suggest that more diverse bacterial community might be built on anode-2 and anode-3 over anode-1, possibly decreasing current density in the two anodes.
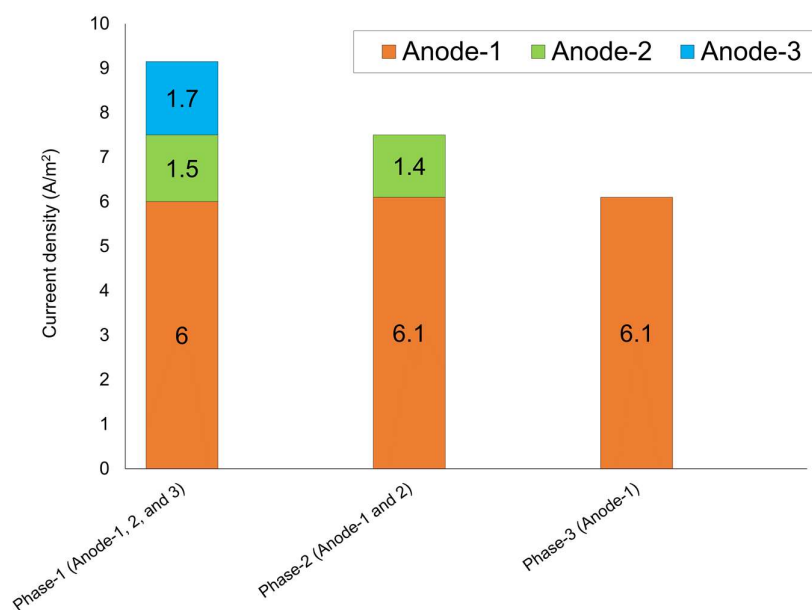
Figure 6-2. Current density from individual anode modules at different experimental phases.

Table 6-1. Anode potentials corrected for ohmic resistances.

Phase	Anode	Electrode distance from reference electrode (cm)	Corrected anode potential (V vs. SHE)	Current density (A/m^2)
1	Anode-1	1.27	-0.01	9.15±0.36
	Anode-2	3.81	+0.14	
	Anode-3	6.35	+0.30	
2	Anode-1	1.27	-0.03	7.5±0.20
	Anode-2	3.81	+0.10	
3	Anode-1	1.27	-0.04	6.1±0.1

6.3.3   Bacterial Community on Individual Anodes

Fig. 6-3 show community structures of bacteria in biofilms on individual anodes identified with a total of 147,468 rRNA sequences; the detailed result for microbial community analysis is provided in Appendix F. The relative abundance of *Geobacter* spp., the most kinetically efficient ARB, was as high as 87% for biofilms on anode-1, which substantially decreased to <1% for biofilms on the other two anodes. Family of *Rhodocyclaceae* became rich at 72% in anode-2, as the population of *Geobacter* spp. decreased. Anode-3 showed the most diverse community structure. Two genera of *Agrobacterium* and *Aeromonas*, and two families of *Rhodocyclaceae* and *Pseudomonadaceae* became abundant in anode-3, and the relative abundance of *Geobacter* spp. in anode-3 was negligible, like that in anode-2. These results support that anode potential changed by ionic resistance substantially influenced bacterial community structures in biofilm anodes. The trend of bacterial community in the biofilms to anode potential is consistent with the literature (Torres et al., 2009; Commault et al., 2013; Kumar et al., 2013), showing abundant *Geobacter* genus at anode-1 (intrinsic anode potential from -0.04 to -0.01 V) but diverse bacterial community at anode-2 and anode-3 (intrinsic anode potential from +0.1 to +0.3 V).

Other dominant bacteria identified in anode-2 and anode-3 would be involved in extracellular electron transfer (EET). Microbial genomes identified EET genes in *Rhodoferax spp.*

(*Rhodocyclaceae*), *Pseudomonas* spp. (*Pseudomonadaceae*), *Aeromonas spp.* homologous to the iron-reducing EET pathway of *Shewanella oneidensis* MR-1 (Finneran et al., 2003; Chaudhuri and Lovley, 2003; Pham et al., 2003; Shi et al., 2012). These microorganisms were relatively abundant for anode-2, and anode-3. The family of *Rhodocyclaceae* are also identified as dominant ARB in biofilm anodes of acetate-fed MxCs, but their EET mechanisms are unclear (Xing et al., 2010; Kouzuma et al., 2013; Song et al., 2015). *Aeromonas spp.* identified as one of the major ARB for anode-3 (19%) can use an exogenous shuttling compound or conductive nanowires for EET (Pham et al., 2003; Chung et al., 2009; Castro et al., 2014a, 2014b). *Agrobacterium* spp. identified for anode-3 (4.8%) were also found in anode biofilms fed with acetate (Liu et al., 2012; Hossini et al., 2015; Kenney and Fein, 2011). *Agrobacterium* spp., well known for biofilm formation and production of extracellular polymeric substances, have putative nanowires (Aguilar et al., 2010; Kenney and Fein, 2011). The *Pseudomonadaceae* family (e.g., *Pseudomonas* spp.) has been found to produce conductive nanowires or endogenous shuttling compounds to facilitate EET in MxCs fed with acetate (Malvankar et al., 2011; Wang et al., 2010). It seems that *Agrobacterium spp.*, *Aeromonas spp.*, and some genera from *Rhodocyclaceae* and *Pseudomonadaceae* families would be involved in EET in the MxC. However, lower current densities for anode-2, and anode-3 imply that their kinetic features would be inferior to *Geobacter* genus.
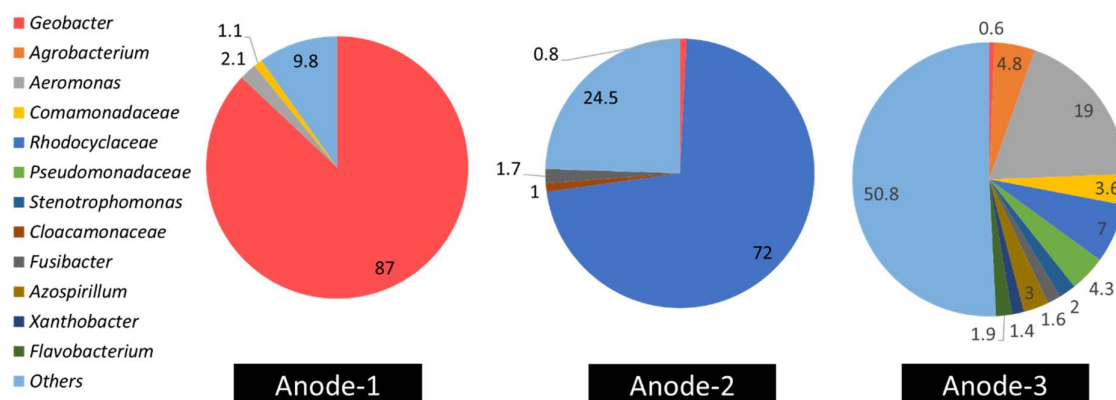
Figure 6-3. Microbial community structure of biofilms on individual anode electrodes.

6.3.4 Estimation of Half-saturation Anode Potential (E_{KA}) for Individual Anode Biofilms

Fig. 6-4 shows the forward scan LSCV patterns (the average of triplicate tests) for individual anode modules. E_{KA} tended to increase (more positive) as the maximum current density (j_{max}) decreased: high E_{KA} with low j_{max}. E_{KA} ranged from -0.251±0.001 to -0.242±0 V (vs. SHE) for anode-1 (j_{max} 7.1±0.15 A/m^2), which was as high as -0.134±0.001 V for anode-3 (j_{max} 1.88±0.07 A/m^2). More negative E_{KA} allows ARB to generate saturated current density with small energy loss, based on the Nernst-Monod equation (Lee et al., 2009; Marcus et al., 2007; Torres et al., 2008b). The highest catalytic function (the highest j_{max} and the lowest E_{KA}) was found for the biofilms on anode-1 with the largest population of *Geobacter* spp. Low j_{max} and high E_{KA} were observed for anode-2 and anode-3, along with increase of *Agrobacterium* spp., *Aeromonas* spp., and *Rhodocyclaceae* and *Pseudomonadaceae* families. High E_{KA} for anode-2 and anode-3 implies inferior electrochemical kinetics for these four ARB candidates. E_{KA} values for anode-1 and anode-2 were consistent to phase 1 to phase 3, indicating that electrochemical kinetics of biofilm anodes was conserved during the experiment (see Fig.6-4).

Estimated E_{KA} values were used to simulate current density against anode potential using the Nernst-Monod model (Eq. 6-2) under substrate non-limiting conditions. As shown in Fig. 6-4, sigmoidal patterns of Nernst-Monod simulations well match experimental LSCVs for anode-1, implying that conduction-based EET might occur for the anode (Lee et al., 2009; Torres et al., 2008b, 2009; Renslow et al., 2013). In comparison, the simulated polarization curves were deviated from experimental LSCVs for anode-2 and anode-3, suggesting EET mechanisms other than conduction or significant energy loss in EET (e.g., poor biofilm conductivity) for anode-2 and anode-3 (Lee et al., 2009; Torres et al., 2008b, 2009; Renslow et al., 2013).
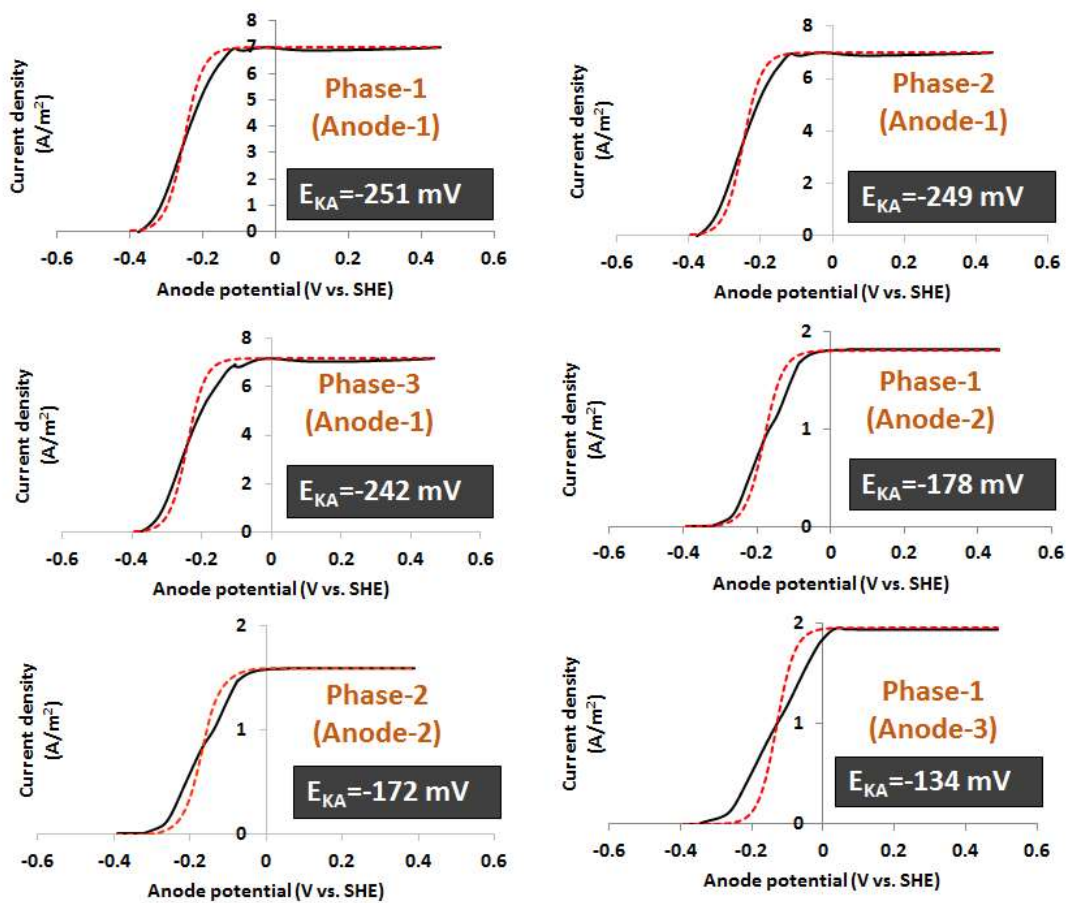
Figure 6-4. Experimental and simulated current density profiles to anode potential. The black lines indicate experimental LSCVs at a scan rate of 1 mV/s for the steady-state MxC. The dotted red line indicates simulations with estimated E_{KA} and the Nernst-Monod equation.

6.4 Conclusions

Multi-anode configurations improved current density, but current density did not increase proportional to the number of anodes, mainly due to different bacteria communities established on individual anodes. Ohmic energy loss that depends on current density, electrolyte resistance and electrode distance changed intrinsic anode potential of each anode in the multi-anode MxC, which significantly shifted biofilm community among three anodes. *Geobacter* genus was only rich at anode-1 close to the reference electrode, while its population substantially decreased in biofilms on anode-2 and anode-3 distant from the reference electrode. Lower current density and relatively higher E_{KA} were observed for anode-2 and anode-3. This study clearly shows that the benefit of multi-anode MxCs will be realized when kinetically efficient ARB (e.g., *Geobacter*) are equally distributed to multiple anodes. Enrichment of the ARB for individual anodes followed by assembly of multiple anodes is recommended for improving current density in multi-anode MxCs.

Chapter 7

Conclusions and Recommendations for Future Research

7.1   Conclusions

This dissertation provides a systematic characterization of extracellular electron transfer (EET) in MxCs. The unique contribution of this research included elucidating the fundamental roles of three important environmental parameters (i.e., anode potential, pH, and substrate) on EET kinetics and biofilm conductivity in MxCs. These three parameters were selected primarily due to the fact that they are important factors influencing intracellular electron transfer kinetics and metabolic activity of ARB in biofilm anodes. To exclusively study the effects of one individual parameter, anode biofilms and MxCs were run to create non-limiting conditions for the other two factors.   The research goals were achieved via *in situ* biofilm conductivity (K_{bio}) measurement, estimation of biological and electrochemical kinetic parameters, microbial community analyses, microscopic visualization of biofilm anodes, and pH gradient measurement throughout the biofilms using pH-microelectrode. Furthermore, the Nernst-Monod Model was used to qualitatively interpret the experimental results.   Following comprehensive characterization of three environmental factors on EET kinetics and K_{bio}, this study further explored the implication of ohmic resistance for anode kinetics and current density in a multi-anode MxC to tackle scale-up issues of MxCs. Based on the results of this study, the following key conclusions can be drawn:

Anode potential changes EET players in a biofilm anode rather than biofilm conductivity. High biofilm conductivity (0.96-1.24 mS/cm) was kept to E_{anode} change from -0.2 V to +0.2 V vs. SHE, although the steady-state current density significantly decreased from 2.05 to 0.35 A/m^2 in a mixed-culture MxC, enriched with *Geobacter* genus. Substantial increase of *Treponema*'s population was observed in biofilm anodes at E_{anode} +0.2 V, which reduced intracellular electron transfer kinetics associated with the maximum specific substrate-utilization rate by a factor of ten approximately. This result suggests that fast EET kinetics would be maintained at E_{anode} dynamic conditions in a highly conductive biofilm anode, although E_{anode} can influence IET kinetics, as a result of shift of main EET players in the biofilm anode.

Protons accumulation adversely impacts metabolic activity and biofilm conductivity. An acidic pH between 6.5 to 6.7 in a thick (>100 μm) biofilm anode appears to have an adverse impact on both metabolic activity of ARB and K_{bio}. The decrease of phosphate buffer concentration in acetate medium from 100 mM to 2.5 mM significantly reduced cell viability and K_{bio} in the biofilm anode, along with a substantial drop of current density from 2.38 to 0.64 A/m^2 in an MxC. The decrease of K_{bio} at acidic pH in the biofilm anode indicates conductive EET mechanisms more than metal-like conduction via nanowires would exist in the conductive biofilm.

Biofilm conductivity changes after long-term substrate starvation. Biofilm conductivity (K_{bio}) was dynamically changed over time in response to long starvation phase followed by acetate spiking. The absence of exogenous electron donor for 4-5 days substantially decreased an average K_{bio} from 0.53±0.02 mS/cm to 0.14±0.03 mS/cm. However, this reduced K_{bio} was recovered in the presence of exogenous electron donor, indicating ARB's metabolic activity plays an important role in biofilm conductivity. K_{bio} dynamics to substrate suggests that the activity of ARB should be closely related to EET in biofilm anodes, which well accords to K_{bio} change to pH.

Ohmic energy loss influences selection of microbial communities and electron transfer kinetics in a multi-anode MxC. Microbial community analysis using 16S rRNA Illumina sequencing showed that *Geobacter* genus was abundant (87%) only on the biofilm anode closest to a reference electrode (low ohmic energy loss) in which current density was the highest among three anodes in the multi-anode MxC. In comparison, *Geobacter* populations were less than 1% for biofilms on other two anodes distant from the reference electrode (high ohmic energy loss), generating small current density. Half-saturation anode potential (E_{KA}) was the lowest at -0.251 to -0.242 V (vs. standard hydrogen electrode) for the closest biofilm anode to the reference electrode, while E_{KA} was as high as -0.134 V for the farthest anode. These results proved that electric potential of individual anodes changed by ohmic energy loss shifts biofilm communities on individual anodes and consequently influences electron transfer kinetics on each anode in the multi-anode MxC.

In summary, the results presented substantiate the importance of environmental parameters on EET kinetics and biofilm conductivity. Among three environmental parameters, anode potential seems to indirectly influence EET pathways and kinetics by shifting microbial community structures probably to non-Ohmic EET players. In comparison, protons

accumulation and substrate limitations showed direct influence on K_{bio}. Three parameters also deteriorated intracellular kinetics parameters (e.g., $q_{max,app}X_f$) or inhibited metabolic activity, significantly limiting current density in MxCs. This observation indicates that sluggish ARB's catabolism would be the major obstruction for electron transfer from a soluble electron donor to the anode. Overall, this dissertation established a methodical approach for characterizing EET, and identifying kinetic limitations in biofilm anodes. This approach can be potentially used in future EET research. The results provide more fundamental insights into EET in multi-species biofilm anodes. Furthermore, the knowledge derived from this research can be potentially translated into better engineering designs for MxCs or can be also used to develop better mathematical models for electron transport in biofilm anodes.

7.2   Recommendations for Future Work

Throughout this dissertation work, several specific areas for potential future research were identified which will be of interest to the MxC researchers focusing on EET in biofilm anodes. The following recommendations are suggested to extend the fundamental understanding of EET in biofilm anodes.

- This study investigated the effects of substrate, pH, and anode potential on EET kinetics and biofilm conductivity in mixed-culture biofilms, enriched with *Geobacter* species. The role of these parameters established from this study should be further validated for pure-culture of ARB, which would help to optimize their EET kinetics against these environmental factors in the multi-species environment.

- The change of biofilm conductivity due to proton accumulation and long-term substrate limitations in this study suggested multiple mechanisms (i.e., microbial nanowires, extracellular cofactors, outer membrane c-type cytochromes, etc.) may be involved in Ohmic conduction in biofilm anodes. For instance, long-term substrate limitation exhibits the possibility that intracellular proteins regulated by ARB's metabolism or closely associated with ARB's activity may affect biofilm conductivity directly or indirectly.

- This study showed high biofilm conductivity was conserved to the change of anode potential, despite of microbial community shift and substantial decrease of current density at higher E_{anode}. It seems that there might be threshold population of kinetically efficient ARB (e.g., *Geobacter*) in biofilm anodes providing high biofilm conductivity. Future

research is required to quantitatively assess biofilm conductivity dynamics as *Geobacter*'s population changes in biofilm anode.

- The Nernst-Monod model well represented experimental LSCVs for highly conductive biofilm anodes and qualitatively described EET kinetic limitations or deterioration of K_{bio}. However, the model does not have K_{bio} terms, and hence the model did not accurately describe LSCVs for the biofilm anodes having low K_{bio}. The Nernst-Monod model should be further extended to incorporate K_{bio} for better quantitative assessment of EET kinetics.

- Finally, future research should focus on the development of more efficient multi-anode MxC designs that is economical and scalable for large-scale application. Strategies should be developed to enrich kinetically efficient ARB (e.g., *Geobacter* spp.) throughout multiple anodes.

References

References for Chapter 1

An, J. and Lee, H.S., 2013. Implication of endogenous decay current and quantification of soluble microbial products (SMP) in microbial electrolysis cells. *RSC Advances*, *3*(33), pp.14021-14028.

Bond, D.R. and Lovley, D.R., 2003. Electricity production by Geobacter sulfurreducens attached to electrodes. *Applied and environmental microbiology*, *69*(3), pp.1548-1555.

Butti, S.K., Velvizhi, G., Sulonen, M.L., Haavisto, J.M., Koroglu, E.O., Cetinkaya, A.Y., Singh, S., Arya, D., Modestra, J.A., Krishna, K.V. and Verma, A., 2016. Microbial electrochemical technologies with the perspective of harnessing bioenergy: Maneuvering towards upscaling. *Renewable and Sustainable Energy Reviews*, *53*, pp.462-476.

El-Naggar, M.Y., Wanger, G., Leung, K.M., Yuzvinsky, T.D., Southam, G., Yang, J., Lau, W.M., Nealson, K.H. and Gorby, Y.A., 2010. Electrical transport along bacterial nanowires from Shewanella oneidensis MR-1. *Proceedings of the National Academy of Sciences*, *107*(42), pp.18127-18131.

Fan, Y., Xu, S., Schaller, R., Jiao, J., Chaplen, F. and Liu, H., 2011. Nanoparticle decorated anodes for enhanced current generation in microbial electrochemical cells. *Biosensors and Bioelectronics*, *26*(5), pp.1908-1912.

Gorby, Y.A., Yanina, S., McLean, J.S., Rosso, K.M., Moyles, D., Dohnalkova, A., Beveridge, T.J., Chang, I.S., Kim, B.H., Kim, K.S. and Culley, D.E., 2006. Electrically conductive bacterial nanowires produced by Shewanella oneidensis strain MR-1 and other microorganisms. *Proceedings of the National Academy of Sciences*, *103*(30), pp.11358-11363.

He, Z., Liu, J., Qiao, Y., Li, C.M. and Tan, T.T.Y., 2012. Architecture engineering of hierarchically porous chitosan/vacuum-stripped graphene scaffold as bioanode for high performance microbial fuel cell. *Nano letters*,*12*(9), pp.4738-4741.

Hernandez, M.E. and Newman, D.K., 2001. Extracellular electron transfer. *Cellular and Molecular Life Sciences CMLS*, *58*(11), pp.1562-1571.

Hutchinson, A.J., Tokash, J.C. and Logan, B.E., 2011. Analysis of carbon fiber brush loading in anodes on startup and performance of microbial fuel cells. *Journal of Power Sources*, *196*(22), pp.9213-9219.

Jiang, D. and Li, B., 2009. Granular activated carbon single-chamber microbial fuel cells (GAC-SCMFCs): a design suitable for large-scale wastewater treatment processes. *Biochemical Engineering Journal*, *47*(1), pp.31-37.

Jiang, D., Curtis, M., Troop, E., Scheible, K., McGrath, J., Hu, B., Suib, S., Raymond, D. and Li, B., 2011. A pilot-scale study on utilizing multi-anode/cathode microbial fuel cells (MAC MFCs) to enhance the power production in wastewater treatment. *international journal of hydrogen energy*,*36*(1), pp.876-884.

Kim, H.J., Park, H.S., Hyun, M.S., Chang, I.S., Kim, M. and Kim, B.H., 2002. A mediator-less microbial fuel cell using a metal reducing bacterium, Shewanella putrefaciens. *Enzyme and Microbial Technology*, *30*(2), pp.145-152.

Lanas, V. and Logan, B.E., 2013. Evaluation of multi-brush anode systems in microbial fuel cells. *Bioresource technology*, *148*, pp.379-385.

Lee, H.S., Vermaas, W.F. and Rittmann, B.E., 2010. Biological hydrogen production: prospects and challenges. *Trends in biotechnology*, *28*(5), pp.262-271.

Li, C., Zhang, L., Ding, L., Ren, H. and Cui, H., 2011. Effect of conductive polymers coated anode on the performance of microbial fuel cells (MFCs) and its biodiversity analysis. *Biosensors and Bioelectronics*, *26*(10), pp.4169-4176.

Liu, Y. and Bond, D.R., 2012. Long-Distance Electron Transfer by G. sulfurreducens Biofilms Results in Accumulation of Reduced c-Type Cytochromes. *ChemSusChem*, *5*(6), pp.1047-1053.

Logan, B.E. and Rabaey, K., 2012. Conversion of wastes into bioelectricity and chemicals by using microbial electrochemical technologies. *Science*,*337*(6095), pp.686-690.

Logan, B.E., Hamelers, B., Rozendal, R., Schröder, U., Keller, J., Freguia, S., Aelterman, P., Verstraete, W. and Rabaey, K., 2006. Microbial fuel cells: methodology and technology. *Environmental science & technology*, *40*(17), pp.5181-5192.

Logan, B.E., Wallack, M.J., Kim, K.Y., He, W., Feng, Y. and Saikaly, P.E., 2015. Assessment of microbial fuel cell configurations and power densities. *Environmental Science & Technology Letters*, *2*(8), pp.206-214.

Malvankar, N.S. and Lovley, D.R., 2014. Microbial nanowires for bioenergy applications. *Current opinion in biotechnology*, *27*, pp.88-95.

Malvankar, N.S., Tuominen, M.T. and Lovley, D.R., 2012. Biofilm conductivity is a decisive variable for high-current-density Geobacter sulfurreducens microbial fuel cells. *Energy & Environmental Science*, *5*(2), pp.5790-5797.

Malvankar, N.S., Vargas, M., Nevin, K.P., Franks, A.E., Leang, C., Kim, B.C., Inoue, K., Mester, T., Covalla, S.F., Johnson, J.P. and Rotello, V.M., 2011. Tunable metallic-like conductivity in microbial nanowire networks. *nature nanotechnology*, *6*(9), pp.573-579.

Marcus, A.K., Torres, C.I. and Rittmann, B.E., 2007. Conduction-based modeling of the biofilm anode of a microbial fuel cell. *Biotechnology and Bioengineering*, *98*(6), pp.1171-1182.

Marsili, E., Baron, D.B., Shikhare, I.D., Coursolle, D., Gralnick, J.A. and Bond, D.R., 2008. Shewanella secretes flavins that mediate extracellular electron transfer. *Proceedings of the National Academy of Sciences*, *105*(10), pp.3968-3973.

Pirbadian, S. and El-Naggar, M.Y., 2012. Multistep hopping and extracellular charge transfer in microbial redox chains. *Physical Chemistry Chemical Physics*, *14*(40), pp.13802-13808.

Pirbadian, S., Barchinger, S.E., Leung, K.M., Byun, H.S., Jangir, Y., Bouhenni, R.A., Reed, S.B., Romine, M.F., Saffarini, D.A., Shi, L. and Gorby, Y.A., 2014. Shewanella oneidensis MR-1 nanowires are outer membrane and periplasmic extensions of the extracellular electron transport components. *Proceedings of the National Academy of Sciences*, *111*(35), pp.12883-12888.

Rabaey, K. and Rozendal, R.A., 2010. Microbial electrosynthesis—revisiting the electrical route for microbial production. *Nature Reviews Microbiology*,*8*(10), pp.706-716.

Rabaey, K., Boon, N., Höfte, M. and Verstraete, W., 2005. Microbial phenazine production enhances electron transfer in biofuel cells. *Environmental science & technology*, *39*(9), pp.3401-3408.

Reguera, G., McCarthy, K.D., Mehta, T., Nicoll, J.S., Tuominen, M.T. and Lovley, D.R., 2005. Extracellular electron transfer via microbial nanowires. *Nature*, *435*(7045), pp.1098-1101.

Renslow, R., Babauta, J., Kuprat, A., Schenk, J., Ivory, C., Fredrickson, J. and Beyenal, H., 2013b. Modeling biofilms with dual extracellular electron transfer mechanisms. *Physical Chemistry Chemical Physics*, *15*(44), pp.19262-19283.

Renslow, R.S., Babauta, J.T., Majors, P.D. and Beyenal, H., 2013b. Diffusion in biofilms respiring on electrodes. *Energy & environmental science*, *6*(2), pp.595-607.

Schröder, U., Harnisch, F. and Angenent, L.T., 2015. Microbial electrochemistry and technology: terminology and classification. *Energy & Environmental Science*, *8*(2), pp.513-519.

Snider, R.M., Strycharz-Glaven, S.M., Tsoi, S.D., Erickson, J.S. and Tender, L.M., 2012. Long-range electron transport in Geobacter sulfurreducens biofilms is redox gradient-driven. *Proceedings of the National Academy of Sciences*, *109*(38), pp.15467-15472.

Strycharz-Glaven, S.M., Snider, R.M., Guiseppi-Elie, A. and Tender, L.M., 2011. On the electrical conductivity of microbial nanowires and biofilms. *Energy & Environmental Science*, *4*(11), pp.4366-4379.

Sun, D., Cheng, S., Wang, A., Li, F., Logan, B.E. and Cen, K., 2015. Temporal-Spatial Changes in Viabilities and Electrochemical Properties of Anode Biofilms. *Environmental science & technology*, *49*(8), pp.5227-5235.

Torres, C.I., 2014. On the importance of identifying, characterizing, and predicting fundamental phenomena towards microbial electrochemistry applications. *Current opinion in biotechnology*, *27*, pp.107-114.

Torres, C.I., Kato Marcus, A. and Rittmann, B.E., 2008a. Proton transport inside the biofilm limits electrical current generation by anode-respiring bacteria. *Biotechnology and Bioengineering*, *100*(5), pp.872-881.

Torres, C.I., Krajmalnik-Brown, R., Parameswaran, P., Marcus, A.K., Wanger, G., Gorby, Y.A. and Rittmann, B.E., 2009. Selecting anode-respiring bacteria based on anode potential: phylogenetic, electrochemical, and microscopic characterization. *Environmental science & technology*, *43*(24), pp.9519-9524.

Torres, C.I., Marcus, A.K. and Rittmann, B.E., 2007. Kinetics of consumption of fermentation products by anode-respiring bacteria. *Applied microbiology and biotechnology*, *77*(3), pp.689-697.

Torres, C.I., Marcus, A.K., Lee, H.S., Parameswaran, P., Krajmalnik-Brown, R. and Rittmann, B.E., 2010. A kinetic perspective on extracellular electron transfer by anode-respiring bacteria. *FEMS Microbiology Reviews*, *34*(1), pp.3-17.

Torres, C.I., Marcus, A.K., Parameswaran, P. and Rittmann, B.E., 2008b. Kinetic experiments for evaluating the Nernst− Monod model for anode-respiring bacteria (ARB) in a biofilm anode. *Environmental science & technology*, *42*(17), pp.6593-6597.

Xie, X., Ye, M., Hu, L., Liu, N., McDonough, J.R., Chen, W., Alshareef, H.N., Criddle, C.S. and Cui, Y., 2012. Carbon nanotube-coated macroporous sponge for microbial fuel cell electrodes. *Energy & Environmental Science*,*5*(1), pp.5265-5270.

Yoho, R.A., Popat, S.C. and Torres, C.I., 2014. Dynamic Potential-Dependent Electron Transport Pathway Shifts in Anode Biofilms of Geobacter sulfurreducens. *ChemSusChem*, *7*(12), pp.3413-3419.

Zhang, C., Su, H., Baeyens, J. and Tan, T., 2014. Reviewing the anaerobic digestion of food waste for biogas production. *Renewable and Sustainable Energy Reviews*, *38*, pp.383-392.

Zhou, M., Chi, M., Luo, J., He, H. and Jin, T., 2011. An overview of electrode materials in microbial fuel cells. *Journal of Power Sources*, *196*(10), pp.4427-4435.

References for Chapter 2

Aelterman, P., Freguia, S., Keller, J., Verstraete, W. and Rabaey, K., 2008. The anode potential regulates bacterial activity in microbial fuel cells. Applied microbiology and biotechnology, 78(3), pp.409-418.

Ahn, Y. and Logan, B.E., 2010. Effectiveness of domestic wastewater treatment using microbial fuel cells at ambient and mesophilic temperatures. Bioresource Technology, 101(2), pp.469-475.

Ahn, Y. and Logan, B.E., 2012. A multi-electrode continuous flow microbial fuel cell with separator electrode assembly design. *Applied microbiology and biotechnology*, *93*(5), pp.2241-2248.

Ahn, Y., Hatzell, M.C., Zhang, F. and Logan, B.E., 2014. Different electrode configurations to optimize performance of multi-electrode microbial fuel cells for generating power or treating domestic wastewater. *Journal of Power Sources*, *249*, pp.440-445.

An, J. and Lee, H.S., 2013. Implication of endogenous decay current and quantification of soluble microbial products (SMP) in microbial electrolysis cells. *RSC Advances*, *3*(33), pp.14021-14028.

Atci, E., Babauta, J.T., Sultana, S.T. and Beyenal, H., 2016. Microbiosensor for the detection of acetate in electrode-respiring biofilms. *Biosensors and Bioelectronics*, *81*, pp.517-523.

Babauta, J.T., Nguyen, H.D. and Beyenal, H., 2011. Redox and pH microenvironments within Shewanella oneidensis MR-1 biofilms reveal an electron transfer mechanism. *Environmental science & technology*, *45*(15), pp.6654-6660.

Babauta, J.T., Nguyen, H.D., Harrington, T.D., Renslow, R. and Beyenal, H., 2012. pH, redox potential and local biofilm potential microenvironments within Geobacter sulfurreducens biofilms and their roles in electron transfer.*Biotechnology and bioengineering*, *109*(10), pp.2651-2662.

Bae, W. and Rittmann, B.E., 1996. A structured model of dual-limitation kinetics. *Biotechnology and bioengineering*, *49*(6), pp.683-689.

Bond, D.R. and Lovley, D.R., 2003. Electricity production by Geobacter sulfurreducens attached to electrodes. *Applied and environmental microbiology*, *69*(3), pp.1548-1555.

Bond, D.R. and Lovley, D.R., 2005. Evidence for involvement of an electron shuttle in electricity generation by Geothrix fermentans. *Applied and environmental microbiology*, *71*(4), pp.2186-2189.

Boyd, D.A., Snider, R.M., Erickson, J.S., Roy, J.N., Strycharz-Glaven, S.M., Tender, L.M., Beyenal, H. and Babauta, J., 2015. Theory of Redox Conduction and the Measurement of Electron Transport Rates Through Electrochemically Active Biofilms. *Biofilms in Bioelectrochemical Systems: From Laboratory Practice to Data Interpretation*, p.177.

Brutinel, E.D. and Gralnick, J.A., 2012. Shuttling happens: soluble flavin mediators of extracellular electron transfer in Shewanella. *Applied microbiology and biotechnology*, *93*(1), pp.41-48.

Chae, K.J., Choi, M.J., Kim, K.Y., Ajayi, F.F., Park, W., Kim, C.W. and Kim, I.S., 2010. Methanogenesis control by employing various environmental stress conditions in two-chambered microbial fuel cells. *Bioresource technology*, *101*(14), pp.5350-5357.

Commault, A.S., Lear, G., Packer, M.A. and Weld, R.J., 2013. Influence of anode potentials on selection of Geobacter strains in microbial electrolysis cells. *Bioresource technology*, *139*, pp.226-234.

Dhar, B.R. and Lee, H.S., 2014. Evaluation of limiting factors for current density in microbial electrochemical cells (MXCs) treating domestic wastewater. *Biotechnology Reports*, *4*, pp.80-85.

Dhar, B.R., Elbeshbishy, E., Hafez, H. and Lee, H.S., 2015. Hydrogen production from sugar beet juice using an integrated biohydrogen process of dark fermentation and microbial electrolysis cell. *Bioresource technology*, *198*, pp.223-230.

Dhar, B.R., Gao, Y., Yeo, H. and Lee, H.S., 2013. Separation of competitive microorganisms using anaerobic membrane bioreactors as pretreatment to microbial electrochemical cells. *Bioresource technology*, *148*, pp.208-214.

El-Naggar, M.Y., Wanger, G., Leung, K.M., Yuzvinsky, T.D., Southam, G., Yang, J., Lau, W.M., Nealson, K.H. and Gorby, Y.A., 2010. Electrical transport along bacterial nanowires from Shewanella oneidensis MR-1. *Proceedings of the National Academy of Sciences*, *107*(42), pp.18127-18131.

Fan, Y., Hu, H. and Liu, H., 2007. Enhanced Coulombic efficiency and power density of air-cathode microbial fuel cells with an improved cell configuration. *Journal of Power Sources*, *171*(2), pp.348-354.

Feng, Y., Wang, X., Logan, B.E. and Lee, H., 2008. Brewery wastewater treatment using air-cathode microbial fuel cells. *Applied microbiology and biotechnology*, *78*(5), pp.873-880.

Franks, A.E., Nevin, K.P., Jia, H., Izallalen, M., Woodard, T.L. and Lovley, D.R., 2009. Novel strategy for three-dimensional real-time imaging of microbial fuel cell communities: monitoring the inhibitory effects of proton accumulation within the anode biofilm. *Energy & Environmental Science*, *2*(1), pp.113-119.

Freguia, S., Rabaey, K., Yuan, Z. and Keller, J., 2008. Syntrophic processes drive the conversion of glucose in microbial fuel cell anodes. *Environmental science & technology*, *42*(21), pp.7937-7943.

Friman, H., Schechter, A., Ioffe, Y., Nitzan, Y. and Cahan, R., 2013. Current production in a microbial fuel cell using a pure culture of Cupriavidus basilensis growing in acetate or phenol as a carbon source. *Microbial biotechnology*, *6*(4), pp.425-434.

Gao, Y., An, J., Ryu, H. and Lee, H.S., 2014b. Microbial Fuel Cells as Discontinuous Portable Power Sources: Syntropic Interactions with Anode-Respiring Bacteria. *ChemSusChem*, *7*(4), pp.1026-1029.

Gao, Y., Ryu, H., Santo Domingo, J.W. and Lee, H.S., 2014a. Syntrophic interactions between H 2-scavenging and anode-respiring bacteria can improve current density in microbial electrochemical cells. *Bioresource technology*, *153*, pp.245-253.

Ghadge, A.N. and Ghangrekar, M.M., 2015. Performance of low cost scalable air–cathode microbial fuel cell made from clayware separator using multiple electrodes. *Bioresource technology*, *182*, pp.373-377.

Gorby, Y.A., Yanina, S., McLean, J.S., Rosso, K.M., Moyles, D., Dohnalkova, A., Beveridge, T.J., Chang, I.S., Kim, B.H., Kim, K.S. and Culley, D.E., 2006. Electrically conductive bacterial nanowires produced by Shewanella oneidensis strain MR-1 and other microorganisms. *Proceedings of the National Academy of Sciences*, *103*(30), pp.11358-11363.

Harnisch, F., Wirth, S. and Schröder, U., 2009. Effects of substrate and metabolite crossover on the cathodic oxygen reduction reaction in microbial fuel cells: platinum vs. iron (II) phthalocyanine based electrodes.*Electrochemistry Communications*, *11*(11), pp.2253-2256.

He, Z., Liu, J., Qiao, Y., Li, C.M. and Tan, T.T.Y., 2012. Architecture engineering of hierarchically porous chitosan/vacuum-stripped graphene scaffold as bioanode for high performance microbial fuel cell. *Nano letters*,*12*(9), pp.4738-4741.

He, Z., Liu, J., Qiao, Y., Li, C.M. and Tan, T.T.Y., 2012. Architecture engineering of hierarchically porous chitosan/vacuum-stripped graphene scaffold as bioanode for high performance microbial fuel cell. *Nano letters*,*12*(9), pp.4738-4741.

Hernandez, M.E. and Newman, D.K., 2001. Extracellular electron transfer. *Cellular and Molecular Life Sciences CMLS*, *58*(11), pp.1562-1571.

Hutchinson, A.J., Tokash, J.C. and Logan, B.E., 2011. Analysis of carbon fiber brush loading in anodes on startup and performance of microbial fuel cells. *Journal of Power Sources*, *196*(22), pp.9213-9219.

Ishii, S.I., Suzuki, S., Norden-Krichmar, T.M., Tenney, A., Chain, P.S., Scholz, M.B., Nealson, K.H. and Bretschger, O., 2013. A novel metatranscriptomic approach to identify gene expression dynamics during extracellular electron transfer. *Nature communications*, *4*, p.1601.

Jiang, D., Curtis, M., Troop, E., Scheible, K., McGrath, J., Hu, B., Suib, S., Raymond, D. and Li, B., 2011. A pilot-scale study on utilizing multi-anode/cathode microbial fuel cells (MAC MFCs) to enhance the power production in wastewater treatment. *international journal of hydrogen energy*,*36*(1), pp.876-884.

Kim, B.H., Park, H.S., Kim, H.J., Kim, G.T., Chang, I.S., Lee, J. and Phung, N.T., 2004. Enrichment of microbial community generating electricity using a fuel-cell-type electrochemical cell. *Applied Microbiology and Biotechnology*,*63*(6), pp.672-681.

Kim, H.J., Park, H.S., Hyun, M.S., Chang, I.S., Kim, M. and Kim, B.H., 2002. A mediator-less microbial fuel cell using a metal reducing bacterium, Shewanella putrefaciens. *Enzyme and Microbial Technology*, *30*(2), pp.145-152.

Kim, K.Y., Yang, W. and Logan, B.E., 2015. Impact of electrode configurations on retention time and domestic wastewater treatment efficiency using microbial fuel cells. *Water research*, *80*, pp.41-46.

Kim, M.S. and Lee, Y.J., 2010. Optimization of culture conditions and electricity generation using Geobacter sulfurreducens in a dual-chambered microbial fuel-cell. *international journal of hydrogen energy*, *35*(23), pp.13028-13034.

Korth, B., Rosa, L.F., Harnisch, F. and Picioreanu, C., 2015. A framework for modeling electroactive microbial biofilms performing direct electron transfer.*Bioelectrochemistry*, *106*, pp.194-206.

Lebedev, N., Strycharz-Glaven, S.M. and Tender, L.M., 2014. Spatially Resolved Confocal Resonant Raman Microscopic Analysis of Anode-Grown Geobacter sulfurreducens Biofilms. *ChemPhysChem*, *15*(2), pp.320-327.

Lee, H.S., Parameswaran, P., Kato-Marcus, A., Torres, C.I. and Rittmann, B.E., 2008. Evaluation of energy-conversion efficiencies in microbial fuel cells (MFCs) utilizing fermentable and non-fermentable substrates. *Water Research*, *42*(6), pp.1501-1510.

Lee, H.S., Torres, C.I. and Rittmann, B.E., 2009. Effects of substrate diffusion and anode potential on kinetic parameters for anode-respiring bacteria.*Environmental science & technology*, *43*(19), pp.7571-7577.

Li, C., Zhang, L., Ding, L., Ren, H. and Cui, H., 2011. Effect of conductive polymers coated anode on the performance of microbial fuel cells (MFCs) and its biodiversity analysis. *Biosensors and Bioelectronics*, *26*(10), pp.4169-4176.

Liu, Y. and Bond, D.R., 2012. Long-Distance Electron Transfer by G. sulfurreducens Biofilms Results in Accumulation of Reduced c-Type Cytochromes. *ChemSusChem*, *5*(6), pp.1047-1053.

Liu, Y., Kim, H., Franklin, R. and Bond, D.R., 2010. Gold line array electrodes increase substrate affinity and current density of electricity-producing G. sulfurreducens biofilms. *Energy & Environmental Science*, *3*(11), pp.1782-1788.

Logan, B.E. and Rabaey, K., 2012. Conversion of wastes into bioelectricity and chemicals by using microbial electrochemical technologies. *Science*,*337*(6095), pp.686-690.

Logan, B.E., Hamelers, B., Rozendal, R., Schröder, U., Keller, J., Freguia, S., Aelterman, P., Verstraete, W. and Rabaey, K., 2006. Microbial fuel cells: methodology and technology. *Environmental science & technology*, *40*(17), pp.5181-5192.

Logan, B.E., Wallack, M.J., Kim, K.Y., He, W., Feng, Y. and Saikaly, P.E., 2015. Assessment of microbial fuel cell configurations and power densities.*Environmental Science & Technology Letters*, *2*(8), pp.206-214.

Lovley, D.R. and Malvankar, N.S., 2015. Seeing is believing: novel imaging techniques help clarify microbial nanowire structure and function.*Environmental microbiology*, *17*(7), pp.2209-2215.

Lovley, D.R., 2006. Bug juice: harvesting electricity with microorganisms.*Nature Reviews Microbiology*, *4*(7), pp.497-508.

Lu, L., Xing, D., Ren, N. and Logan, B.E., 2012. Syntrophic interactions drive the hydrogen production from glucose at low temperature in microbial electrolysis cells. *Bioresource technology*, *124*, pp.68-76.

Mahmoud, M., Parameswaran, P., Torres, C.I. and Rittmann, B.E., 2016. Relieving the fermentation inhibition enables high electron recovery from landfill leachate in a microbial electrolysis cell. *RSC Advances*, *6*(8), pp.6658-6664.

Malvankar, N.S., Lau, J., Nevin, K.P., Franks, A.E., Tuominen, M.T. and Lovley, D.R., 2012c. Electrical conductivity in a mixed-species biofilm. *Applied and environmental microbiology*, *78*(16), pp.5967-5971.

Malvankar, N.S., Tuominen, M.T. and Lovley, D.R., 2012a. Biofilm conductivity is a decisive variable for high-current-density Geobacter sulfurreducens microbial fuel cells. *Energy & Environmental Science*, *5*(2), pp.5790-5797.

Malvankar, N.S., Tuominen, M.T. and Lovley, D.R., 2012b. Lack of cytochrome involvement in long-range electron transport through conductive biofilms and nanowires of Geobacter sulfurreducens. *Energy & Environmental Science*,*5*(9), pp.8651-8659.

Malvankar, N.S., Vargas, M., Nevin, K.P., Franks, A.E., Leang, C., Kim, B.C., Inoue, K., Mester, T., Covalla, S.F., Johnson, J.P. and Rotello, V.M., 2011. Tunable metallic-like conductivity in microbial nanowire networks. *nature nanotechnology*, *6*(9), pp.573-579.

Marcus, A.K., Torres, C.I. and Rittmann, B.E., 2007. Conduction-based modeling of the biofilm anode of a microbial fuel cell. *Biotechnology and Bioengineering*, *98*(6), pp.1171-1182.

Marcus, A.K., Torres, C.I. and Rittmann, B.E., 2010. Evaluating the impacts of migration in the biofilm anode using the model PCBIOFILM. *Electrochimica Acta*, *55*(23), pp.6964-6972.

Marcus, A.K., Torres, C.I. and Rittmann, B.E., 2011. Analysis of a microbial electrochemical cell using the proton condition in biofilm (PCBIOFILM) model.*Bioresource technology*, *102*(1), pp.253-262.

Marsili, E., Baron, D.B., Shikhare, I.D., Coursolle, D., Gralnick, J.A. and Bond, D.R., 2008. Shewanella secretes flavins that mediate extracellular electron transfer. *Proceedings of the National Academy of Sciences*, *105*(10), pp.3968-3973.

Matsuda, S., Liu, H., Kato, S., Hashimoto, K. and Nakanishi, S., 2011. Negative faradaic resistance in extracellular electron transfer by anode-respiring Geobacter sulfurreducens cells. *Environmental science & technology*, *45*(23), pp.10163-10169.

Mehta, T., Coppi, M.V., Childers, S.E. and Lovley, D.R., 2005. Outer membrane c-type cytochromes required for Fe (III) and Mn (IV) oxide reduction in Geobacter sulfurreducens. *Applied and Environmental Microbiology*, *71*(12), pp.8634-8641.

Mehta-Kolte, M.G. and Bond, D.R., 2012. Geothrix fermentans secretes two different redox-active compounds to utilize electron acceptors across a wide range of redox potentials. *Applied and environmental microbiology*, *78*(19), pp.6987-6995.

Nam, J.Y., Tokash, J.C. and Logan, B.E., 2011. Comparison of microbial electrolysis cells operated with added voltage or by setting the anode potential. *international journal of hydrogen energy*, *36*(17), pp.10550-10556.

Nguyen, H.D., Renslow, R., Babauta, J., Ahmed, B. and Beyenal, H., 2012. A voltammetric flavin microelectrode for use in biofilms. *Sensors and Actuators B: Chemical*, *161*(1), pp.929-937.

Okamoto, A., Nakamura, R., Nealson, K.H. and Hashimoto, K., 2014b. Bound Flavin Model Suggests Similar Electron-Transfer Mechanisms in Shewanella and Geobacter. *ChemElectroChem*, *1*(11), pp.1808-1812.

Okamoto, A., Saito, K., Inoue, K., Nealson, K.H., Hashimoto, K. and Nakamura, R., 2014a. Uptake of self-secreted flavins as bound cofactors for extracellular electron transfer in Geobacter species. *Energy Environ. Sci.*,*7*(4), pp.1357-1361.

Ozkaya, B., Akoglu, B., Karadag, D., Acı, G., Taskan, E. and Hasar, H., 2012. Bioelectricity production using a new electrode in a microbial fuel cell.*Bioprocess and biosystems engineering*, *35*(7), pp.1219-1227.

Pant, D., Van Bogaert, G., Diels, L. and Vanbroekhoven, K., 2010. A review of the substrates used in microbial fuel cells (MFCs) for sustainable energy production. *Bioresource technology*, *101*(6), pp.1533-1543.

Parameswaran, P., Torres, C.I., Kang, D.W., Rittmann, B.E. and Krajmalnik-Brown, R., 2012. The role of homoacetogenic bacteria as efficient hydrogen scavengers in microbial electrochemical cells (MXCs). *Water Science & Technology*, *65*(1).

Parameswaran, P., Torres, C.I., Lee, H.S., Krajmalnik-Brown, R. and Rittmann, B.E., 2009. Syntrophic interactions among anode respiring bacteria (ARB) and Non-ARB in a biofilm anode: electron balances. *Biotechnology and bioengineering*, *103*(3), pp.513-523.

Parameswaran, P., Torres, C.I., Lee, H.S., Rittmann, B.E. and Krajmalnik-Brown, R., 2011. Hydrogen consumption in microbial electrochemical systems (MXCs): the role of homo-acetogenic bacteria. *Bioresource technology*, *102*(1), pp.263-271.

Parameswaran, P., Zhang, H., Torres, C.I., Rittmann, B.E. and Krajmalnik-Brown, R., 2010. Microbial community structure in a biofilm anode fed with a fermentable substrate: the significance of hydrogen scavengers.*Biotechnology and bioengineering*, *105*(1), pp.69-78.

Pirbadian, S. and El-Naggar, M.Y., 2012. Multistep hopping and extracellular charge transfer in microbial redox chains. *Physical Chemistry Chemical Physics*, *14*(40), pp.13802-13808.

Pirbadian, S. and El-Naggar, M.Y., 2012. Multistep hopping and extracellular charge transfer in microbial redox chains. *Physical Chemistry Chemical Physics*, *14*(40), pp.13802-13808.

Pirbadian, S., Barchinger, S.E., Leung, K.M., Byun, H.S., Jangir, Y., Bouhenni, R.A., Reed, S.B., Romine, M.F., Saffarini, D.A., Shi, L. and Gorby, Y.A., 2014. Shewanella oneidensis MR-1 nanowires are outer membrane and periplasmic extensions of the extracellular electron transport components.*Proceedings of the National Academy of Sciences*, *111*(35), pp.12883-12888.

Rabaey, K., Boon, N., Höfte, M. and Verstraete, W., 2005. Microbial phenazine production enhances electron transfer in biofuel cells.*Environmental science & technology*, *39*(9), pp.3401-3408.

Rabaey, K., Boon, N., Siciliano, S.D., Verhaege, M. and Verstraete, W., 2004. Biofuel cells select for microbial consortia that self-mediate electron transfer.*Applied and environmental microbiology*, *70*(9), pp.5373-5382.

Reguera, G., McCarthy, K.D., Mehta, T., Nicoll, J.S., Tuominen, M.T. and Lovley, D.R., 2005. Extracellular electron transfer via microbial nanowires.*Nature*, *435*(7045), pp.1098-1101.

Reguera, G., Nevin, K.P., Nicoll, J.S., Covalla, S.F., Woodard, T.L. and Lovley, D.R., 2006. Biofilm and nanowire production leads to increased current in Geobacter sulfurreducens fuel cells. *Applied and environmental microbiology*, *72*(11), pp.7345-7348.

Ren, L., Ahn, Y., Hou, H., Zhang, F. and Logan, B.E., 2014. Electrochemical study of multi-electrode microbial fuel cells under fed-batch and continuous flow conditions. *Journal of Power Sources*, *257*, pp.454-460.

Renslow, R., Babauta, J., Kuprat, A., Schenk, J., Ivory, C., Fredrickson, J. and Beyenal, H., 2013b. Modeling biofilms with dual extracellular electron transfer mechanisms. *Physical Chemistry Chemical Physics*, *15*(44), pp.19262-19283.

Renslow, R.S., Babauta, J.T., Majors, P.D. and Beyenal, H., 2013a. Diffusion in biofilms respiring on electrodes. *Energy & environmental science*, *6*(2), pp.595-607.

Rismani-Yazdi, H., Carver, S.M., Christy, A.D. and Tuovinen, O.H., 2008. Cathodic limitations in microbial fuel cells: an overview. *Journal of Power Sources*, *180*(2), pp.683-694.

Schmitz, S., Nies, S., Wierckx, N., Blank, L.M. and Rosenbaum, M.A., 2015. Engineering mediator-based electroactivity in the obligate aerobic bacterium Pseudomonas putida KT2440. *Frontiers in microbiology*, *6*.

Snider, R.M., Strycharz-Glaven, S.M., Tsoi, S.D., Erickson, J.S. and Tender, L.M., 2012. Long-range electron transport in Geobacter sulfurreducens biofilms is redox gradient-driven. *Proceedings of the National Academy of Sciences*, *109*(38), pp.15467-15472.

Srikanth, S., Mohan, S.V. and Sarma, P.N., 2010. Positive anodic poised potential regulates microbial fuel cell performance with the function of open and closed circuitry. *Bioresource technology*, *101*(14), pp.5337-5344.

Strycharz-Glaven, S.M., Snider, R.M., Guiseppi-Elie, A. and Tender, L.M., 2011. On the electrical conductivity of microbial nanowires and biofilms.*Energy & Environmental Science*, *4*(11), pp.4366-4379.

Sun, D., Cheng, S., Wang, A., Li, F., Logan, B.E. and Cen, K., 2015. Temporal-Spatial Changes in Viabilities and Electrochemical Properties of Anode Biofilms. *Environmental science & technology*, *49*(8), pp.5227-5235.

Torres, C.I., Kato Marcus, A. and Rittmann, B.E., 2008a. Proton transport inside the biofilm limits electrical current generation by anode-respiring bacteria. *Biotechnology and Bioengineering*, *100*(5), pp.872-881.

Torres, C.I., Krajmalnik-Brown, R., Parameswaran, P., Marcus, A.K., Wanger, G., Gorby, Y.A. and Rittmann, B.E., 2009. Selecting anode-respiring bacteria based on anode

potential: phylogenetic, electrochemical, and microscopic characterization. *Environmental science & technology*, *43*(24), pp.9519-9524.

Torres, C.I., Marcus, A.K. and Rittmann, B.E., 2007. Kinetics of consumption of fermentation products by anode-respiring bacteria. *Applied microbiology and biotechnology*, *77*(3), pp.689-697.

Torres, C.I., Marcus, A.K., Lee, H.S., Parameswaran, P., Krajmalnik-Brown, R. and Rittmann, B.E., 2010. A kinetic perspective on extracellular electron transfer by anode-respiring bacteria. *FEMS Microbiology Reviews*, *34*(1), pp.3-17.

Torres, C.I., Marcus, A.K., Parameswaran, P. and Rittmann, B.E., 2008b. Kinetic experiments for evaluating the Nernst− Monod model for anode-respiring bacteria (ARB) in a biofilm anode. *Environmental science & technology*, *42*(17), pp.6593-6597.

Velasquez-Orta, S.B., Head, I.M., Curtis, T.P., Scott, K., Lloyd, J.R. and von Canstein, H., 2010. The effect of flavin electron shuttles in microbial fuel cells current production. *Applied microbiology and biotechnology*, *85*(5), pp.1373-1381.

Von Canstein, H., Ogawa, J., Shimizu, S. and Lloyd, J.R., 2008. Secretion of flavins by Shewanella species and their role in extracellular electron transfer.*Applied and Environmental Microbiology*, *74*(3), pp.615-623.

Wei, J., Liang, P., Cao, X. and Huang, X., 2010. A new insight into potential regulation on growth and power generation of Geobacter sulfurreducens in microbial fuel cells based on energy viewpoint. *Environmental science & technology*, *44*(8), pp.3187-3191.

Xie, X., Ye, M., Hu, L., Liu, N., McDonough, J.R., Chen, W., Alshareef, H.N., Criddle, C.S. and Cui, Y., 2012. Carbon nanotube-coated macroporous sponge for microbial fuel cell electrodes. *Energy & Environmental Science*,*5*(1), pp.5265-5270.

Xie, X., Ye, M., Hu, L., Liu, N., McDonough, J.R., Chen, W., Alshareef, H.N., Criddle, C.S. and Cui, Y., 2012. Carbon nanotube-coated macroporous sponge for microbial fuel cell electrodes. *Energy & Environmental Science*,*5*(1), pp.5265-5270.

Yoho, R.A., Popat, S.C. and Torres, C.I., 2014. Dynamic Potential-Dependent Electron Transport Pathway Shifts in Anode Biofilms of Geobacter sulfurreducens. *ChemSusChem*, *7*(12), pp.3413-3419.

Yong, Y.C., Cai, Z., Yu, Y.Y., Chen, P., Jiang, R., Cao, B., Sun, J.Z., Wang, J.Y. and Song, H., 2013. Increase of riboflavin biosynthesis underlies enhancement of extracellular electron transfer of Shewanella in alkaline microbial fuel cells. *Bioresource technology*, *130*, pp.763-768.

Zhou, M., Chi, M., Luo, J., He, H. and Jin, T., 2011. An overview of electrode materials in microbial fuel cells. *Journal of Power Sources*, *196*(10), pp.4427-4435.

References for Chapter 3

Aelterman, P., Freguia, S., Keller, J., Verstraete, W. and Rabaey, K., 2008. The anode potential regulates bacterial activity in microbial fuel cells. *Applied microbiology and biotechnology*, *78*(3), pp.409-418.

Bonanni, P.S., Bradley, D.F., Schrott, G.D. and Busalmen, J.P., 2013. Limitations for current production in Geobacter sulfurreducens biofilms. *ChemSusChem*, *6*(4), pp.711-720.

Bond, D.R. and Lovley, D.R., 2005. Evidence for involvement of an electron shuttle in electricity generation by Geothrix fermentans. *Applied and environmental microbiology*, *71*(4), pp.2186-2189.

Caporaso, J.G., Lauber, C.L., Walters, W.A., Berg-Lyons, D., Lozupone, C.A., Turnbaugh, P.J., Fierer, N. and Knight, R., 2011. Global patterns of 16S rRNA diversity at a depth of millions of sequences per sample. *Proceedings of the National Academy of Sciences*, *108*(Supplement 1), pp.4516-4522.

Chae, K.J., Choi, M.J., Lee, J.W., Kim, K.Y. and Kim, I.S., 2009. Effect of different substrates on the performance, bacterial diversity, and bacterial viability in microbial fuel cells. *Bioresource Technology*, *100*(14), pp.3518-3525.

Commault, A.S., Lear, G., Packer, M.A. and Weld, R.J., 2013. Influence of anode potentials on selection of Geobacter strains in microbial electrolysis cells. *Bioresource technology*, *139*, pp.226-234.

Crittenden, S.R., Sund, C.J. and Sumner, J.J., 2006. Mediating electron transfer from bacteria to a gold electrode via a self-assembled monolayer. *Langmuir*, *22*(23), pp.9473-9476.

Dhar, B.R., Gao, Y., Yeo, H. and Lee, H.S., 2013. Separation of competitive microorganisms using anaerobic membrane bioreactors as pretreatment to microbial electrochemical cells. *Bioresource technology*, *148*, pp.208-214.

Esteve-Núñez, A., Rothermich, M., Sharma, M. and Lovley, D., 2005. Growth of Geobacter sulfurreducens under nutrient-limiting conditions in continuous culture. *Environmental microbiology*, *7*(5), pp.641-648.

Franks, A.E., Nevin, K.P., Jia, H., Izallalen, M., Woodard, T.L. and Lovley, D.R., 2009. Novel strategy for three-dimensional real-time imaging of microbial fuel cell communities: monitoring the inhibitory effects of proton accumulation within the anode biofilm. *Energy & Environmental Science*, *2*(1), pp.113-119.

Gao, Y., An, J., Ryu, H. and Lee, H.S., 2014b. Microbial Fuel Cells as Discontinuous Portable Power Sources: Syntropic Interactions with Anode-Respiring Bacteria. *ChemSusChem*, *7*(4), pp.1026-1029.

Gao, Y., Ryu, H., Santo Domingo, J.W. and Lee, H.S., 2014a. Syntrophic interactions between H 2-scavenging and anode-respiring bacteria can improve current density in microbial electrochemical cells. *Bioresource technology*, *153*, pp.245-253.

Hamelers, H.V., Ter Heijne, A., Stein, N., Rozendal, R.A. and Buisman, C.J., 2011. Butler–Volmer–Monod model for describing bio-anode polarization curves. *Bioresource technology*, *102*(1), pp.381-387.

Ishii, S.I., Shimoyama, T., Hotta, Y. and Watanabe, K., 2008. Characterization of a filamentous biofilm community established in a cellulose-fed microbial fuel cell. *Bmc Microbiology*, *8*(1), p.1.

Kankare, J. and Kupila, E.L., 1992. In-situ conductance measurement during electropolymerization. *Journal of Electroanalytical Chemistry*, *322*(1), pp.167-181.

Kim, M.S. and Lee, Y.J., 2010. Optimization of culture conditions and electricity generation using Geobacter sulfurreducens in a dual-chambered microbial fuel-cell. *international journal of hydrogen energy*, *35*(23), pp.13028-13034.

Kumar, A., Siggins, A., Katuri, K., Mahony, T., O'Flaherty, V., Lens, P. and Leech, D., 2013. Catalytic response of microbial biofilms grown under fixed anode potentials depends on electrochemical cell configuration. *Chemical engineering journal*, *230*, pp.532-536.

Lee, H.S., Parameswaran, P., Kato-Marcus, A., Torres, C.I. and Rittmann, B.E., 2008. Evaluation of energy-conversion efficiencies in microbial fuel cells (MFCs) utilizing fermentable and non-fermentable substrates. *Water Research*, *42*(6), pp.1501-1510.

Lee, H.S., Torres, C.I. and Rittmann, B.E., 2009. Effects of substrate diffusion and anode potential on kinetic parameters for anode-respiring bacteria.*Environmental science & technology*, *43*(19), pp.7571-7577.

Liu, H., Matsuda, S., Kato, S., Hashimoto, K. and Nakanishi, S., 2010. Redox-Responsive Switching in Bacterial Respiratory Pathways Involving Extracellular Electron Transfer. *ChemSusChem*, *3*(11), pp.1253-1256.

Logan, B.E. and Rabaey, K., 2012. Conversion of wastes into bioelectricity and chemicals by using microbial electrochemical technologies. *Science*,*337*(6095), pp.686-690.

Logan, B.E., Wallack, M.J., Kim, K.Y., He, W., Feng, Y. and Saikaly, P.E., 2015. Assessment of microbial fuel cell configurations and power densities. *Environmental Science & Technology Letters*, *2*(8), pp.206-214.

Lovley, D.R., 2008. Extracellular electron transfer: wires, capacitors, iron lungs, and more. *Geobiology*, *6*(3), pp.225-231.

Malvankar, N.S. and Lovley, D.R., 2014. Microbial nanowires for bioenergy applications. *Current opinion in biotechnology*, *27*, pp.88-95.

Malvankar, N.S., Lau, J., Nevin, K.P., Franks, A.E., Tuominen, M.T. and Lovley, D.R., 2012. Electrical conductivity in a mixed-species biofilm. *Applied and environmental microbiology*, *78*(16), pp.5967-5971.

Malvankar, N.S., Tuominen, M.T. and Lovley, D.R., 2012a. Biofilm conductivity is a decisive variable for high-current-density Geobacter sulfurreducens microbial fuel cells. *Energy & Environmental Science*, *5*(2), pp.5790-5797.

Malvankar, N.S., Vargas, M., Nevin, K.P., Franks, A.E., Leang, C., Kim, B.C., Inoue, K., Mester, T., Covalla, S.F., Johnson, J.P. and Rotello, V.M., 2011. Tunable metallic-like conductivity in microbial nanowire networks. *nature nanotechnology*, *6*(9), pp.573-579.

Marcus, A.K., Torres, C.I. and Rittmann, B.E., 2007. Conduction-based modeling of the biofilm anode of a microbial fuel cell. *Biotechnology and Bioengineering*, *98*(6), pp.1171-1182.

Marsili, E., Baron, D.B., Shikhare, I.D., Coursolle, D., Gralnick, J.A. and Bond, D.R., 2008. Shewanella secretes flavins that mediate extracellular electron transfer. *Proceedings of the National Academy of Sciences*, *105*(10), pp.3968-3973.

Marsili, E., Sun, J. and Bond, D.R., 2010. Voltammetry and growth physiology of Geobacter sulfurreducens biofilms as a function of growth stage and imposed electrode potential. *Electroanalysis*, *22*(7-8), pp.865-874.

Matsuda, S., Liu, H., Kato, S., Hashimoto, K. and Nakanishi, S., 2011. Negative faradaic resistance in extracellular electron transfer by anode-respiring Geobacter sulfurreducens cells. *Environmental science & technology*, *45*(23), pp.10163-10169.

Miceli III, J.F., Parameswaran, P., Kang, D.W., Krajmalnik-Brown, R. and Torres, C.I., 2012. Enrichment and analysis of anode-respiring bacteria from diverse anaerobic inocula. *Environmental science & technology*, *46*(18), pp.10349-10355.

Parameswaran, P., Bry, T., Popat, S.C., Lusk, B.G., Rittmann, B.E. and Torres, C.I., 2013. Kinetic, electrochemical, and microscopic characterization of the thermophilic, anode-respiring bacterium Thermincola ferriacetica.*Environmental science & technology*, *47*(9), pp.4934-4940.

Patil, S.A., Surakasi, V.P., Koul, S., Ijmulwar, S., Vivek, A., Shouche, Y.S. and Kapadnis, B.P., 2009. Electricity generation using chocolate industry wastewater and its treatment in activated sludge based microbial fuel cell and analysis of developed microbial community in the anode chamber.*Bioresource technology*, *100*(21), pp.5132-5139.

Pitkänen, T., Ryu, H., Elk, M., Hokajärvi, A.M., Siponen, S., Vepsäläinen, A., Räsänen, P. and Santo Domingo, J.W., 2013. Detection of fecal bacteria and source tracking identifiers in environmental waters using rRNA-based RT-qPCR and rDNA-based qPCR assays. *Environmental science & technology*,*47*(23), pp.13611-13620.

Quast, C., Pruesse, E., Yilmaz, P., Gerken, J., Schweer, T., Yarza, P., Peplies, J. and Glöckner, F.O., 2013. The SILVA ribosomal RNA gene database project: improved data processing and web-based tools. *Nucleic acids research*, *41*(D1), pp.D590-D596.

Rabaey, K. and Rozendal, R.A., 2010. Microbial electrosynthesis—revisiting the electrical route for microbial production. *Nature Reviews Microbiology*,*8*(10), pp.706-716.

Rabaey, K., Boon, N., Höfte, M. and Verstraete, W., 2005. Microbial phenazine production enhances electron transfer in biofuel cells.*Environmental science & technology*, *39*(9), pp.3401-3408.

Reguera, G., McCarthy, K.D., Mehta, T., Nicoll, J.S., Tuominen, M.T. and Lovley, D.R., 2005. Extracellular electron transfer via microbial nanowires. *Nature*, *435*(7045), pp.1098-1101.

Ren, H., Tian, H., Lee, H.S., Park, T., Leung, F.C., Ren, T.L. and Chae, J., 2015. Regulating the respiration of microbe: A bio-inspired high performance microbial supercapacitor with graphene based electrodes and its kinetic features. *Nano Energy*, *15*, pp.697-708.

Renslow, R., Babauta, J., Kuprat, A., Schenk, J., Ivory, C., Fredrickson, J. and Beyenal, H., 2013. Modeling biofilms with dual extracellular electron transfer mechanisms. *Physical Chemistry Chemical Physics*, *15*(44), pp.19262-19283.

Rismani-Yazdi, H., Christy, A.D., Dehority, B.A., Morrison, M., Yu, Z. and Tuovinen, O.H., 2007. Electricity generation from cellulose by rumen microorganisms in microbial fuel cells. *Biotechnology and bioengineering*,*97*(6), pp.1398-1407.

Schloss, P.D., Westcott, S.L., Ryabin, T., Hall, J.R., Hartmann, M., Hollister, E.B., Lesniewski, R.A., Oakley, B.B., Parks, D.H., Robinson, C.J. and Sahl, J.W., 2009. Introducing mothur: open-source, platform-independent, community-supported software for describing and comparing microbial communities. *Applied and environmental microbiology*, *75*(23), pp.7537-7541.

Sherafatmand, M. and Ng, H.Y., 2015. Using sediment microbial fuel cells (SMFCs) for bioremediation of polycyclic aromatic hydrocarbons (PAHs).*Bioresource technology*, *195*, pp.122-130.

Snider, R.M., Strycharz-Glaven, S.M., Tsoi, S.D., Erickson, J.S. and Tender, L.M., 2012. Long-range electron transport in Geobacter sulfurreducens biofilms is redox gradient-driven. *Proceedings of the National Academy of Sciences*, *109*(38), pp.15467-15472.

Srikanth, S., Mohan, S.V. and Sarma, P.N., 2010. Positive anodic poised potential regulates microbial fuel cell performance with the function of open and closed circuitry. *Bioresource technology*, *101*(14), pp.5337-5344.

Strycharz-Glaven, S.M. and Tender, L.M., 2012. Study of the mechanism of catalytic activity of G. sulfurreducens biofilm anodes during biofilm growth.*ChemSusChem*, *5*(6), pp.1106-1118.

Strycharz-Glaven, S.M., Snider, R.M., Guiseppi-Elie, A. and Tender, L.M., 2011. On the electrical conductivity of microbial nanowires and biofilms.*Energy & Environmental Science*, *4*(11), pp.4366-4379.

Torres, C.I., Kato Marcus, A. and Rittmann, B.E., 2008b. Proton transport inside the biofilm limits electrical current generation by anode-respiring bacteria. *Biotechnology and Bioengineering*, *100*(5), pp.872-881.

Torres, C.I., Krajmalnik-Brown, R., Parameswaran, P., Marcus, A.K., Wanger, G., Gorby, Y.A. and Rittmann, B.E., 2009. Selecting anode-respiring bacteria based on anode potential: phylogenetic, electrochemical, and microscopic characterization. *Environmental science & technology*, *43*(24), pp.9519-9524.

Torres, C.I., Marcus, A.K. and Rittmann, B.E., 2007. Kinetics of consumption of fermentation products by anode-respiring bacteria. *Applied microbiology and biotechnology*, *77*(3), pp.689-697.

Torres, C.I., Marcus, A.K., Lee, H.S., Parameswaran, P., Krajmalnik-Brown, R. and Rittmann, B.E., 2010. A kinetic perspective on extracellular electron transfer by anode-respiring bacteria. *FEMS Microbiology Reviews*, *34*(1), pp.3-17.

Torres, C.I., Marcus, A.K., Parameswaran, P. and Rittmann, B.E., 2008a. Kinetic experiments for evaluating the Nernst− Monod model for anode-respiring bacteria (ARB) in a biofilm anode. *Environmental science & technology*, *42*(17), pp.6593-6597.

Wang, L., Wu, Y., Zheng, Y., Liu, L. and Zhao, F., 2015. Efficient degradation of sulfamethoxazole and the response of microbial communities in microbial fuel cells. *RSC Advances*, *5*(69), pp.56430-56437.

Wang, Q., Garrity, G.M., Tiedje, J.M. and Cole, J.R., 2007. Naive Bayesian classifier for rapid assignment of rRNA sequences into the new bacterial taxonomy. *Applied and environmental microbiology*, *73*(16), pp.5261-5267.

Wardman, C., Nevin, K.P. and Lovley, D.R., 2014. Real-time monitoring of subsurface microbial metabolism with graphite electrodes. *Frontiers in microbiology*, *5*.

Xia, C., Xu, M., Liu, J., Guo, J. and Yang, Y., 2015. Sediment microbial fuel cell prefers to degrade organic chemicals with higher polarity. *Bioresource technology*, *190*, pp.420-423.

Yun, J., Malvankar, N.S., Ueki, T. and Lovley, D.R., 2015. Functional environmental proteomics: elucidating the role of a c-type cytochrome abundant during uranium bioremediation. *The ISME journal*, 10(2), 310-20

References for Chapter 4

Babauta, J.T., Nguyen, H.D. and Beyenal, H., 2011. Redox and pH microenvironments within Shewanella oneidensis MR-1 biofilms reveal an electron transfer mechanism. *Environmental science & technology*, *45*(15), pp.6654-6660.

Babauta, J.T., Nguyen, H.D., Harrington, T.D., Renslow, R. and Beyenal, H., 2012. pH, redox potential and local biofilm potential microenvironments within Geobacter sulfurreducens biofilms and their roles in electron transfer.*Biotechnology and bioengineering*, *109*(10), pp.2651-2662.

Bonanni, P.S., Bradley, D.F., Schrott, G.D. and Busalmen, J.P., 2013. Limitations for current production in Geobacter sulfurreducens biofilms.*ChemSusChem*, *6*(4), pp.711-720.

Bond, D.R., Strycharz-Glaven, S.M., Tender, L.M. and Torres, C.I., 2012. On electron transport through Geobacter biofilms. *ChemSusChem*, *5*(6), pp.1099-1105.

Dhar, B.R. and Lee, H.S., 2013. Membranes for bioelectrochemical systems: challenges and research advances. *Environmental technology*, *34*(13-14), pp.1751-1764.

Dhar, B.R. and Lee, H.S., 2014. Evaluation of limiting factors for current density in microbial electrochemical cells (MXCs) treating domestic wastewater. *Biotechnology Reports*, *4*, pp.80-85.

Dhar, B.R., Elbeshbishy, E., Hafez, H. and Lee, H.S., 2015. Hydrogen production from sugar beet juice using an integrated biohydrogen process of dark fermentation and microbial electrolysis cell. *Bioresource technology*,*198*, pp.223-230.

Dhar, B.R., Gao, Y., Yeo, H. and Lee, H.S., 2013. Separation of competitive microorganisms using anaerobic membrane bioreactors as pretreatment to microbial electrochemical cells. *Bioresource technology*, *148*, pp.208-214.

El-Naggar, M.Y., Wanger, G., Leung, K.M., Yuzvinsky, T.D., Southam, G., Yang, J., Lau, W.M., Nealson, K.H. and Gorby, Y.A., 2010. Electrical transport along bacterial nanowires from Shewanella oneidensis MR-1. *Proceedings of the National Academy of Sciences*, *107*(42), pp.18127-18131.

Franks, A.E., Nevin, K.P., Jia, H., Izallalen, M., Woodard, T.L. and Lovley, D.R., 2009. Novel strategy for three-dimensional real-time imaging of microbial fuel cell communities: monitoring the inhibitory effects of proton accumulation within the anode biofilm. *Energy & Environmental Science*,*2*(1), pp.113-119.

Gao, Y., An, J., Ryu, H. and Lee, H.S., 2014. Microbial Fuel Cells as Discontinuous Portable Power Sources: Syntropic Interactions with Anode-Respiring Bacteria. *ChemSusChem*, *7*(4), pp.1026-1029.

He, Z., Huang, Y., Manohar, A.K. and Mansfeld, F., 2008. Effect of electrolyte pH on the rate of the anodic and cathodic reactions in an air-cathode microbial fuel cell. *Bioelectrochemistry*, *74*(1), pp.78-82.

Kankare, J. and Kupila, E.L., 1992. In-situ conductance measurement during electropolymerization. *Journal of Electroanalytical Chemistry*, *322*(1), pp.167-181.

Kim, M.S. and Lee, Y.J., 2010. Optimization of culture conditions and electricity generation using Geobacter sulfurreducens in a dual-chambered microbial fuel-cell. *international journal of hydrogen energy*, *35*(23), pp.13028-13034.

Lebedev, N., Strycharz-Glaven, S.M. and Tender, L.M., 2014. Spatially Resolved Confocal Resonant Raman Microscopic Analysis of Anode-Grown Geobacter sulfurreducens Biofilms. *ChemPhysChem*, *15*(2), pp.320-327.

Lee, H.S., Torres, C.I. and Rittmann, B.E., 2009. Effects of substrate diffusion and anode potential on kinetic parameters for anode-respiring bacteria.*Environmental science & technology*, *43*(19), pp.7571-7577.

Malvankar, N.S. and Lovley, D.R., 2012d. Microbial nanowires: a new paradigm for biological electron transfer and bioelectronics. *ChemSusChem*,*5*(6), pp.1039-1046.

Malvankar, N.S., Tuominen, M.T. and Lovley, D.R., 2012a. Biofilm conductivity is a decisive variable for high-current-density Geobacter sulfurreducens microbial fuel cells. *Energy & Environmental Science*, *5*(2), pp.5790-5797.

Malvankar, N.S., Tuominen, M.T. and Lovley, D.R., 2012b. Lack of cytochrome involvement in long-range electron transport through conductive biofilms and nanowires of Geobacter sulfurreducens. *Energy & Environmental Science*,*5*(9), pp.8651-8659.

Malvankar, N.S., Tuominen, M.T. and Lovley, D.R., 2012c. Comment on "On electrical conductivity of microbial nanowires and biofilms" by SM Strycharz-Glaven, RM Snider, A. Guiseppi-Elie and LM Tender, Energy Environ. Sci., 2011, 4, 4366. *Energy & Environmental Science*, *5*(3), pp.6247-6249.

Malvankar, N.S., Vargas, M., Nevin, K.P., Franks, A.E., Leang, C., Kim, B.C., Inoue, K., Mester, T., Covalla, S.F., Johnson, J.P. and Rotello, V.M., 2011. Tunable metallic-like conductivity in microbial nanowire networks. *nature nanotechnology*, *6*(9), pp.573-579.

Marcus, A.K., Torres, C.I. and Rittmann, B.E., 2007. Conduction-based modeling of the biofilm anode of a microbial fuel cell. *Biotechnology and Bioengineering*, *98*(6), pp.1171-1182.

Marcus, A.K., Torres, C.I. and Rittmann, B.E., 2010. Evaluating the impacts of migration in the biofilm anode using the model PCBIOFILM. *Electrochimica Acta*, *55*(23), pp.6964-6972.

Marcus, A.K., Torres, C.I. and Rittmann, B.E., 2011. Analysis of a microbial electrochemical cell using the proton condition in biofilm (PCBIOFILM) model.*Bioresource technology*, *102*(1), pp.253-262.

Nakahara, Y., Kimura, K. and Inokuchi, H., 1977. Electrical conductivity of cytochrome c anhydrous film. *Chemical Physics Letters*, *47*(2), pp.251-254.

Nakahara, Y., Kimura, K., Inokuchi, H. and Yagi, T., 1979. Electrical conductivity of solid state proteins: simple proteins and cytochrome c 3 as anhydrous film. *Chemistry Letters*, *8*(8), pp.877-880.

Pierra, M., Carmona-Martínez, A.A., Trably, E., Godon, J.J. and Bernet, N., 2015. Specific and efficient electrochemical selection of Geoalkalibacter subterraneus and Desulfuromonas acetoxidans in high current-producing biofilms. *Bioelectrochemistry*, *106*, pp.221-225.

Pirbadian, S., Barchinger, S.E., Leung, K.M., Byun, H.S., Jangir, Y., Bouhenni, R.A., Reed, S.B., Romine, M.F., Saffarini, D.A., Shi, L. and Gorby, Y.A., 2015. Bacterial Nanowires of Shewanella Oneidensis MR-1 are Outer Membrane and Periplasmic Extensions of the Extracellular Electron Transport Components. *Biophysical Journal*, *108*(2), p.368a.

Renslow, R., Babauta, J., Kuprat, A., Schenk, J., Ivory, C., Fredrickson, J. and Beyenal, H., 2013a. Modeling biofilms with dual extracellular electron transfer mechanisms. *Physical Chemistry Chemical Physics*, *15*(44), pp.19262-19283.

Renslow, R.S., Babauta, J.T., Majors, P.D. and Beyenal, H., 2013b. Diffusion in biofilms respiring on electrodes. *Energy & environmental science*, *6*(2), pp.595-607.

Snider, R.M., Strycharz-Glaven, S.M., Tsoi, S.D., Erickson, J.S. and Tender, L.M., 2012. Long-range electron transport in Geobacter sulfurreducens biofilms is redox gradient-driven. *Proceedings of the National Academy of Sciences*, *109*(38), pp.15467-15472.

Torres, C.I., Kato Marcus, A. and Rittmann, B.E., 2008b. Proton transport inside the biofilm limits electrical current generation by anode-respiring bacteria. *Biotechnology and Bioengineering*, *100*(5), pp.872-881.

Torres, C.I., Krajmalnik-Brown, R., Parameswaran, P., Marcus, A.K., Wanger, G., Gorby, Y.A. and Rittmann, B.E., 2009. Selecting anode-respiring bacteria based on anode potential: phylogenetic, electrochemical, and microscopic characterization. *Environmental science & technology*, *43*(24), pp.9519-9524.

Torres, C.I., Marcus, A.K., Lee, H.S., Parameswaran, P., Krajmalnik-Brown, R. and Rittmann, B.E., 2010. A kinetic perspective on extracellular electron transfer by anode-respiring bacteria. *FEMS Microbiology Reviews*, *34*(1), pp.3-17.

Torres, C.I., Marcus, A.K., Parameswaran, P. and Rittmann, B.E., 2008a. Kinetic experiments for evaluating the Nernst− Monod model for anode-respiring bacteria (ARB) in a biofilm anode. *Environmental science & technology*, *42*(17), pp.6593-6597.

Xiao, K., Malvankar, N.S., Shu, C., Martz, E., Lovley, D.R. and Sun, X., 2016. Low Energy Atomic Models Suggesting a Pilus Structure that could Account for Electrical Conductivity of Geobacter sulfurreducens Pili. *Scientific Reports*, *6*.

Yoho, R.A., Popat, S.C., Rago, L., Guisasola, A. and Torres, C.I., 2015. Anode biofilms of Geoalkalibacter ferrihydriticus exhibit electrochemical signatures of multiple electron transport pathways. *Langmuir*, *31*(45), pp.12552-12559.

References for Chapter 5

An, J. and Lee, H.S., 2013. Implication of endogenous decay current and quantification of soluble microbial products (SMP) in microbial electrolysis cells. *RSC Advances*, *3*(33), pp.14021-14028.

Bonanni, P.S., Bradley, D.F., Schrott, G.D. and Busalmen, J.P., 2013. Limitations for current production in Geobacter sulfurreducens biofilms.*ChemSusChem*, *6*(4), pp.711-720.

Dhar, B.R. and Lee, H.S., 2014. Evaluation of limiting factors for current density in microbial electrochemical cells (MXCs) treating domestic wastewater. *Biotechnology Reports*, *4*, pp.80-85.

Dhar, B.R., Elbeshbishy, E., Hafez, H. and Lee, H.S., 2015. Hydrogen production from sugar beet juice using an integrated biohydrogen process of dark fermentation and microbial electrolysis cell. *Bioresource technology*,*198*, pp.223-230.

Dhar, B.R., Gao, Y., Yeo, H. and Lee, H.S., 2013. Separation of competitive microorganisms using anaerobic membrane bioreactors as pretreatment to microbial electrochemical cells. *Bioresource technology*, *148*, pp.208-214.

El-Naggar, M.Y., Wanger, G., Leung, K.M., Yuzvinsky, T.D., Southam, G., Yang, J., Lau, W.M., Nealson, K.H. and Gorby, Y.A., 2010. Electrical transport along bacterial nanowires from Shewanella oneidensis MR-1. Proceedings of the National Academy of Sciences, 107(42), pp.18127-18131.

Escapa, A., Mateos, R., Martínez, E.J. and Blanes, J., 2016. Microbial electrolysis cells: An emerging technology for wastewater treatment and energy recovery. From laboratory to pilot plant and beyond. *Renewable and Sustainable Energy Reviews*, *55*, pp.942-956.

Franks, A.E., Nevin, K.P., Jia, H., Izallalen, M., Woodard, T.L. and Lovley, D.R., 2009. Novel strategy for three-dimensional real-time imaging of microbial fuel cell communities: monitoring the inhibitory effects of proton accumulation within the anode biofilm. *Energy & Environmental Science*,*2*(1), pp.113-119.

Gao, Y., An, J., Ryu, H. and Lee, H.S., 2014. Microbial Fuel Cells as Discontinuous Portable Power Sources: Syntropic Interactions with Anode-Respiring Bacteria. *ChemSusChem*, *7*(4), pp.1026-1029.

Hengge, R., 2009. Principles of c-di-GMP signalling in bacteria. Nature Reviews Microbiology, 7(4), pp.263-273.

Kankare, J. and Kupila, E.L., 1992. In-situ conductance measurement during electropolymerization. *Journal of Electroanalytical Chemistry*, *322*(1), pp.167-181.

Leang, C., Malvankar, N.S., Franks, A.E., Nevin, K.P. and Lovley, D.R., 2013. Engineering Geobacter sulfurreducens to produce a highly cohesive conductive matrix with enhanced capacity for current production. Energy & Environmental Science, 6(6), pp.1901-1908.

Lee, H.S., Torres, C.I. and Rittmann, B.E., 2009. Effects of substrate diffusion and anode potential on kinetic parameters for anode-respiring bacteria.*Environmental science & technology*, *43*(19), pp.7571-7577.

Logan, B.E. and Rabaey, K., 2012. Conversion of wastes into bioelectricity and chemicals by using microbial electrochemical technologies. *Science*,*337*(6095), pp.686-690.

Mahmoud, M., Parameswaran, P., Torres, C.I. and Rittmann, B.E., 2016. Relieving the fermentation inhibition enables high electron recovery from landfill leachate in a microbial electrolysis cell. RSC Advances, 6(8), pp.6658-6664.

Malvankar, N.S., Tuominen, M.T. and Lovley, D.R., 2012b. Lack of cytochrome involvement in long-range electron transport through conductive biofilms and nanowires of Geobacter sulfurreducens. *Energy & Environmental Science*,*5*(9), pp.8651-8659.

Marcus, A.K., Torres, C.I. and Rittmann, B.E., 2007. Conduction-based modeling of the biofilm anode of a microbial fuel cell. *Biotechnology and Bioengineering*, *98*(6), pp.1171-1182.

Parameswaran, P., Bry, T., Popat, S.C., Lusk, B.G., Rittmann, B.E. and Torres, C.I., 2013. Kinetic, electrochemical, and microscopic characterization of the thermophilic, anode-respiring bacterium Thermincola ferriacetica.*Environmental science & technology*, *47*(9), pp.4934-4940.

Rabaey, K. and Rozendal, R.A., 2010. Microbial electrosynthesis—revisiting the electrical route for microbial production. *Nature Reviews Microbiology,8*(10), pp.706-716.

Renslow, R., Babauta, J., Kuprat, A., Schenk, J., Ivory, C., Fredrickson, J. and Beyenal, H., 2013. Modeling biofilms with dual extracellular electron transfer mechanisms. *Physical Chemistry Chemical Physics*, *15*(44), pp.19262-19283.

Rinaldi, A., Mecheri, B., Garavaglia, V., Licoccia, S., Di Nardo, P. and Traversa, E., 2008. Engineering materials and biology to boost performance of microbial fuel cells: a critical review. *Energy & Environmental Science,1*(4), pp.417-429.

Skotnicka, D., Petters, T., Heering, J., Hoppert, M., Kaever, V. and Søgaard-Andersen, L., 2016. Cyclic Di-GMP Regulates Type IV Pilus-Dependent Motility in Myxococcus xanthus. *Journal of bacteriology*, *198*(1), pp.77-90.

Snider, R.M., Strycharz-Glaven, S.M., Tsoi, S.D., Erickson, J.S. and Tender, L.M., 2012. Long-range electron transport in Geobacter sulfurreducens biofilms is redox gradient-driven. *Proceedings of the National Academy of Sciences*, *109*(38), pp.15467-15472.

Torres, C.I., Kato Marcus, A. and Rittmann, B.E., 2008b. Proton transport inside the biofilm limits electrical current generation by anode-respiring bacteria. *Biotechnology and Bioengineering*, *100*(5), pp.872-881.

Torres, C.I., Krajmalnik-Brown, R., Parameswaran, P., Marcus, A.K., Wanger, G., Gorby, Y.A. and Rittmann, B.E., 2009. Selecting anode-respiring bacteria based on anode potential: phylogenetic, electrochemical, and microscopic characterization. *Environmental science & technology*, *43*(24), pp.9519-9524.

Torres, C.I., Marcus, A.K., Lee, H.S., Parameswaran, P., Krajmalnik-Brown, R. and Rittmann, B.E., 2010. A kinetic perspective on extracellular electron transfer by anode-respiring bacteria. *FEMS Microbiology Reviews*, *34*(1), pp.3-17.

Torres, C.I., Marcus, A.K., Parameswaran, P. and Rittmann, B.E., 2008a. Kinetic experiments for evaluating the Nernst− Monod model for anode-respiring bacteria (ARB) in a biofilm anode. *Environmental science & technology*, *42*(17), pp.6593-6597.

References for Chapter 6

Aguilar, J., Zupan, J., Cameron, T.A. and Zambryski, P.C., 2010. Agrobacterium type IV secretion system and its substrates form helical arrays around the circumference of virulence-induced cells. *Proceedings of the National Academy of Sciences*, *107*(8), pp.3758-3763.

Ahn, Y. and Logan, B.E., 2012. A multi-electrode continuous flow microbial fuel cell with separator electrode assembly design. *Applied microbiology and biotechnology*, *93*(5), pp.2241-2248.

Ahn, Y., Hatzell, M.C., Zhang, F. and Logan, B.E., 2014. Different electrode configurations to optimize performance of multi-electrode microbial fuel cells for generating power or treating domestic wastewater. *Journal of Power Sources*, *249*, pp.440-445.

An, J. and Lee, H.S., 2013. Implication of endogenous decay current and quantification of soluble microbial products (SMP) in microbial electrolysis cells. *RSC Advances*, *3*(33), pp.14021-14028.

Caporaso, J.G., Lauber, C.L., Walters, W.A., Berg-Lyons, D., Lozupone, C.A., Turnbaugh, P.J., Fierer, N. and Knight, R., 2011. Global patterns of 16S rRNA diversity at a depth of millions of sequences per sample. *Proceedings of the National Academy of Sciences*, *108*(Supplement 1), pp.4516-4522.

Castro, L., Vera, M., Muñoz, J.Á., Blázquez, M.L., González, F., Sand, W. and Ballester, A., 2014b. Aeromonas hydrophila produces conductive nanowires.*Research in microbiology*, *165*(9), pp.794-802.

Castro, L., Zhang, R., Muñoz, J.A., González, F., Blázquez, M.L., Sand, W. and Ballester, A., 2014a. Characterization of exopolymeric substances (EPS) produced by Aeromonas hydrophila under reducing conditions. *Biofouling*,*30*(4), pp.501-511.

Chaudhuri, S.K. and Lovley, D.R., 2003. Electricity generation by direct oxidation of glucose in mediatorless microbial fuel cells. *Nature biotechnology*, *21*(10), pp.1229-1232.

Chung, K. and Okabe, S., 2009. Characterization of electrochemical activity of a strain ISO2-3 phylogenetically related to Aeromonas sp. isolated from a glucose-fed microbial fuel cell. *Biotechnology and bioengineering*, *104*(5), pp.901-910.

Commault, A.S., Lear, G., Packer, M.A. and Weld, R.J., 2013. Influence of anode potentials on selection of Geobacter strains in microbial electrolysis cells. *Bioresource technology*, *139*, pp.226-234.

Dewan, A., Beyenal, H. and Lewandowski, Z., 2008. Scaling up microbial fuel cells. *Environmental science & technology*, *42*(20), pp.7643-7648.

Dhar, B.R., Elbeshbishy, E., Hafez, H. and Lee, H.S., 2015. Hydrogen production from sugar beet juice using an integrated biohydrogen process of dark fermentation and microbial electrolysis cell. *Bioresource technology*,*198*, pp.223-230.

Dhar, B.R., Gao, Y., Yeo, H. and Lee, H.S., 2013. Separation of competitive microorganisms using anaerobic membrane bioreactors as pretreatment to microbial electrochemical cells. *Bioresource technology*, *148*, pp.208-214.

Escapa, A., Mateos, R., Martínez, E.J. and Blanes, J., 2016. Microbial electrolysis cells: An emerging technology for wastewater treatment and energy recovery. From laboratory to pilot plant and beyond. *Renewable and Sustainable Energy Reviews*, *55*, pp.942-956.

Finneran, K.T., Johnsen, C.V. and Lovley, D.R., 2003. Rhodoferax ferrireducens sp. nov., a psychrotolerant, facultatively anaerobic bacterium that oxidizes acetate with the reduction of Fe (III). *International Journal of Systematic and Evolutionary Microbiology*, *53*(3), pp.669-673.

Ghadge, A.N. and Ghangrekar, M.M., 2015. Performance of low cost scalable air–cathode microbial fuel cell made from clayware separator using multiple electrodes. *Bioresource technology*, *182*, pp.373-377.

Ghasemi, M., Ismail, M., Kamarudin, S.K., Saeedfar, K., Daud, W.R.W., Hassan, S.H., Heng, L.Y., Alam, J. and Oh, S.E., 2013. Carbon nanotube as an alternative cathode support and catalyst for microbial fuel cells. *Applied Energy*, *102*, pp.1050-1056.

He, C.S., Mu, Z.X., Yang, H.Y., Wang, Y.Z., Mu, Y. and Yu, H.Q., 2015. Electron acceptors for energy generation in microbial fuel cells fed with wastewaters: A mini-review. *Chemosphere*, *140*, pp.12-17.

He, Z., Liu, J., Qiao, Y., Li, C.M. and Tan, T.T.Y., 2012. Architecture engineering of hierarchically porous chitosan/vacuum-stripped graphene scaffold as bioanode for high performance microbial fuel cell. *Nano letters*,*12*(9), pp.4738-4741.

Hossini, H., Rezaee, A., Ayati, B. and Mahvi, A.H., 2015. Simultaneous nitrification and denitrification using a polypyrrole/microbial cellulose electrode in a membraneless bio-electrochemical system. *RSC Advances*,*5*(89), pp.72699-72708.

Hutchinson, A.J., Tokash, J.C. and Logan, B.E., 2011. Analysis of carbon fiber brush loading in anodes on startup and performance of microbial fuel cells. *Journal of Power Sources*, *196*(22), pp.9213-9219.

Jiang, D. and Li, B., 2009. Granular activated carbon single-chamber microbial fuel cells (GAC-SCMFCs): a design suitable for large-scale wastewater treatment processes. *Biochemical Engineering Journal*, *47*(1), pp.31-37.

Jiang, D., Curtis, M., Troop, E., Scheible, K., McGrath, J., Hu, B., Suib, S., Raymond, D. and Li, B., 2011. A pilot-scale study on utilizing multi-anode/cathode microbial fuel cells (MAC MFCs) to enhance the power production in wastewater treatment. *international journal of hydrogen energy*,*36*(1), pp.876-884.

Kenney, J.P. and Fein, J.B., 2011. Importance of extracellular polysaccharides on proton and Cd binding to bacterial biomass: a comparative study. *Chemical Geology*, *286*(3), pp.109-117.

Kouzuma, A., Kasai, T., Nakagawa, G., Yamamuro, A., Abe, T. and Watanabe, K., 2013. Comparative metagenomics of anode-associated microbiomes developed in rice paddy-field microbial fuel cells. *PloS one*,*8*(11), p.e77443.

Kumar, A., Siggins, A., Katuri, K., Mahony, T., O'Flaherty, V., Lens, P. and Leech, D., 2013. Catalytic response of microbial biofilms grown under fixed anode potentials depends on electrochemical cell configuration. *Chemical engineering journal*, *230*, pp.532-536.

Lanas, V. and Logan, B.E., 2013. Evaluation of multi-brush anode systems in microbial fuel cells. *Bioresource technology*, *148*, pp.379-385.

Lee, H.S., Torres, C.I. and Rittmann, B.E., 2009. Effects of substrate diffusion and anode potential on kinetic parameters for anode-respiring bacteria.*Environmental science & technology*, *43*(19), pp.7571-7577.

Liu, W., Wang, A., Sun, D., Ren, N., Zhang, Y. and Zhou, J., 2012. Characterization of microbial communities during anode biofilm reformation in a two-chambered microbial electrolysis cell (MEC). *Journal of biotechnology*,*157*(4), pp.628-632.

Logan, B.E. and Rabaey, K., 2012. Conversion of wastes into bioelectricity and chemicals by using microbial electrochemical technologies. *Science*,*337*(6095), pp.686-690.

106

Logan, B.E., Wallack, M.J., Kim, K.Y., He, W., Feng, Y. and Saikaly, P.E., 2015. Assessment of microbial fuel cell configurations and power densities.*Environmental Science & Technology Letters*, *2*(8), pp.206-214.

Malvankar, N.S., Vargas, M., Nevin, K.P., Franks, A.E., Leang, C., Kim, B.C., Inoue, K., Mester, T., Covalla, S.F., Johnson, J.P. and Rotello, V.M., 2011. Tunable metallic-like conductivity in microbial nanowire networks. *nature nanotechnology*, *6*(9), pp.573-579.

Marcus, A.K., Torres, C.I. and Rittmann, B.E., 2007. Conduction-based modeling of the biofilm anode of a microbial fuel cell. *Biotechnology and Bioengineering*, *98*(6), pp.1171-1182.

Parameswaran, P., Bry, T., Popat, S.C., Lusk, B.G., Rittmann, B.E. and Torres, C.I., 2013. Kinetic, electrochemical, and microscopic characterization of the thermophilic, anode-respiring bacterium Thermincola ferriacetica.*Environmental science & technology*, *47*(9), pp.4934-4940.

Patil, S.A., Gildemyn, S., Pant, D., Zengler, K., Logan, B.E. and Rabaey, K., 2015. A logical data representation framework for electricity-driven bioproduction processes. *Biotechnology advances*, *33*(6), pp.736-744.

Pham, C.A., Jung, S.J., Phung, N.T., Lee, J., Chang, I.S., Kim, B.H., Yi, H. and Chun, J., 2003. A novel electrochemically active and Fe (III)-reducing bacterium phylogenetically related to Aeromonas hydrophila, isolated from a microbial fuel cell. *FEMS Microbiology Letters*, *223*(1), pp.129-134.

Pitkänen, T., Ryu, H., Elk, M., Hokajärvi, A.M., Siponen, S., Vepsäläinen, A., Räsänen, P. and Santo Domingo, J.W., 2013. Detection of fecal bacteria and source tracking identifiers in environmental waters using rRNA-based RT-qPCR and rDNA-based qPCR assays. *Environmental science & technology*,*47*(23), pp.13611-13620.

Quast, C., Pruesse, E., Yilmaz, P., Gerken, J., Schweer, T., Yarza, P., Peplies, J. and Glöckner, F.O., 2013. The SILVA ribosomal RNA gene database project: improved data processing and web-based tools. *Nucleic acids research*, *41*(D1), pp.D590-D596.

Ren, L., Ahn, Y., Hou, H., Zhang, F. and Logan, B.E., 2014. Electrochemical study of multi-electrode microbial fuel cells under fed-batch and continuous flow conditions. *Journal of Power Sources*, *257*, pp.454-460.

Renslow, R., Babauta, J., Kuprat, A., Schenk, J., Ivory, C., Fredrickson, J. and Beyenal, H., 2013. Modeling biofilms with dual extracellular electron transfer mechanisms. *Physical Chemistry Chemical Physics*, *15*(44), pp.19262-19283.

Santoro, C., Serov, A., Narvaez Villarrubia, C.W., Stariha, S., Babanova, S., Schuler, A.J., Artyushkova, K. and Atanassov, P., 2015. Double-Chamber Microbial Fuel Cell with a Non-Platinum-Group Metal Fe–N–C Cathode Catalyst. *ChemSusChem*, *8*(5), pp.828-834.

Schloss, P.D., Westcott, S.L., Ryabin, T., Hall, J.R., Hartmann, M., Hollister, E.B., Lesniewski, R.A., Oakley, B.B., Parks, D.H., Robinson, C.J. and Sahl, J.W., 2009. Introducing mothur: open-source, platform-independent, community-supported software for describing and comparing microbial communities.*Applied and environmental microbiology*, *75*(23), pp.7537-7541.

Shi, L., Rosso, K.M., Clarke, T.A., Richardson, D.J., Zachara, J.M. and Fredrickson, J.K., 2012. Molecular underpinnings of Fe (III) oxide reduction by Shewanella oneidensis MR-1. *The microbial ferrous wheel: iron cycling in terrestrial, freshwater, and marine environments*, p.46.

Song, Y., Xiao, L., Jayamani, I., He, Z. and Cupples, A.M., 2015. A novel method to characterize bacterial communities affected by carbon source and electricity generation in microbial fuel cells using stable isotope probing and Illumina sequencing. *Journal of microbiological methods*, *108*, pp.4-11.

Torres, C.I., Kato Marcus, A. and Rittmann, B.E., 2008a. Proton transport inside the biofilm limits electrical current generation by anode-respiring bacteria. *Biotechnology and Bioengineering*, *100*(5), pp.872-881.

Torres, C.I., Krajmalnik-Brown, R., Parameswaran, P., Marcus, A.K., Wanger, G., Gorby, Y.A. and Rittmann, B.E., 2009. Selecting anode-respiring bacteria based on anode potential: phylogenetic, electrochemical, and microscopic characterization. *Environmental science & technology*, *43*(24), pp.9519-9524.

Torres, C.I., Marcus, A.K., Parameswaran, P. and Rittmann, B.E., 2008b. Kinetic experiments for evaluating the Nernst− Monod model for anode-respiring bacteria (ARB) in a biofilm anode. *Environmental science & technology*, *42*(17), pp.6593-6597.

Wang, Q., Garrity, G.M., Tiedje, J.M. and Cole, J.R., 2007. Naive Bayesian classifier for rapid assignment of rRNA sequences into the new bacterial taxonomy. *Applied and environmental microbiology*, *73*(16), pp.5261-5267.

Wang, Y., Kern, S.E. and Newman, D.K., 2010. Endogenous phenazine antibiotics promote anaerobic survival of Pseudomonas aeruginosa via extracellular electron transfer. *Journal of bacteriology*, *192*(1), pp.365-369.

Xie, X., Ye, M., Hu, L., Liu, N., McDonough, J.R., Chen, W., Alshareef, H.N., Criddle, C.S. and Cui, Y., 2012. Carbon nanotube-coated macroporous sponge for microbial fuel cell electrodes. *Energy & Environmental Science*,*5*(1), pp.5265-5270.

Xing, D., Cheng, S., Logan, B.E. and Regan, J.M., 2010. Isolation of the exoelectrogenic denitrifying bacterium Comamonas denitrificans based on dilution to extinction. *Applied microbiology and biotechnology*, *85*(5), pp.1575-1587.

Zhang, F., Liu, J., Ivanov, I., Hatzell, M.C., Yang, W., Ahn, Y. and Logan, B.E., 2014. Reference and counter electrode positions affect electrochemical characterization of bioanodes in different bioelectrochemical systems. *Biotechnology and bioengineering*, *111*(10), pp.1931-1939.

**Additional Microscopic Images of Gold Electrodes with Non-conductive Gap**
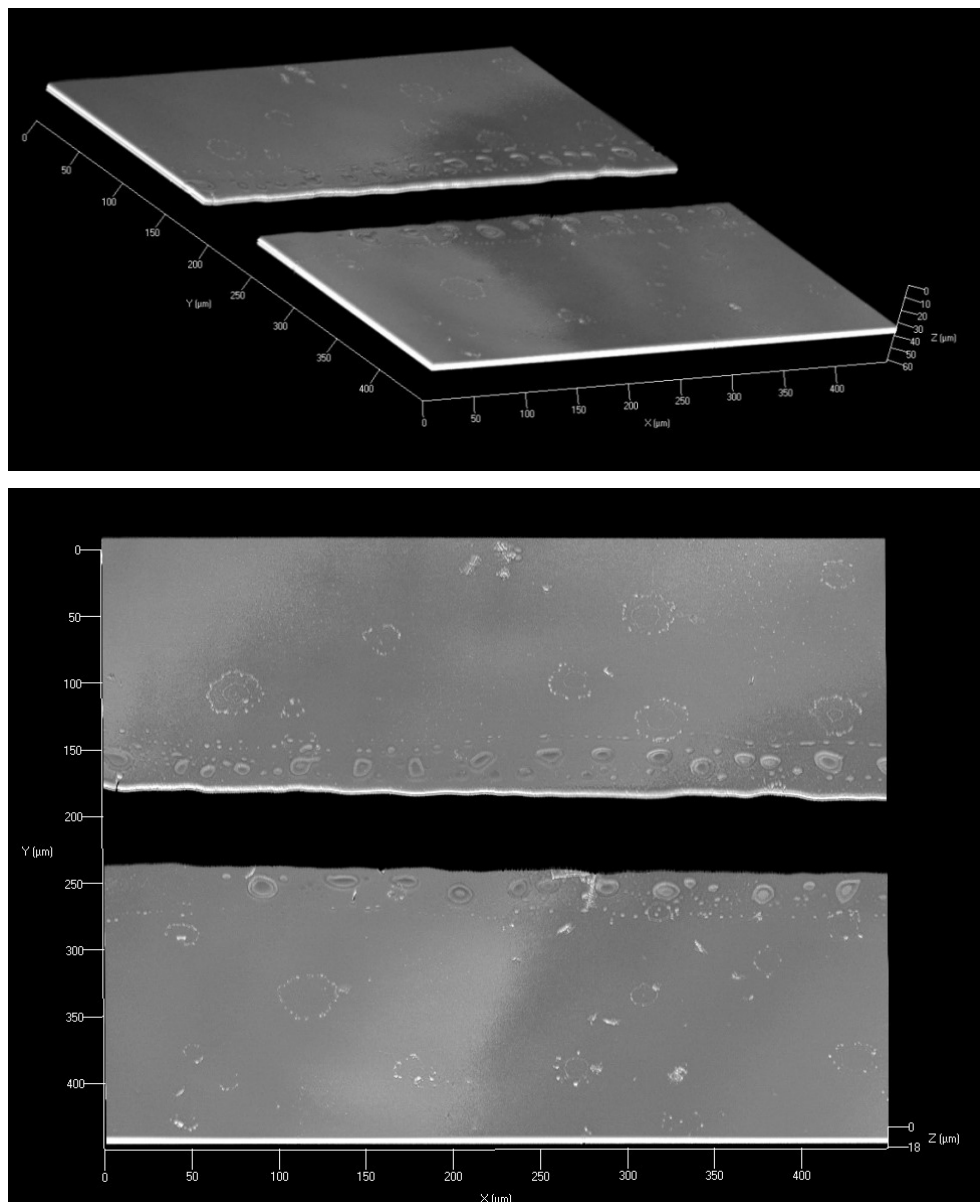
Figure A-1. 3D and 2D confocal laser scanning microscopy (CLSM) images of ~50 µm non-conductive gap between two gold anodes.

**Experimental Set-up for Biofilm Conductivity Measurement**
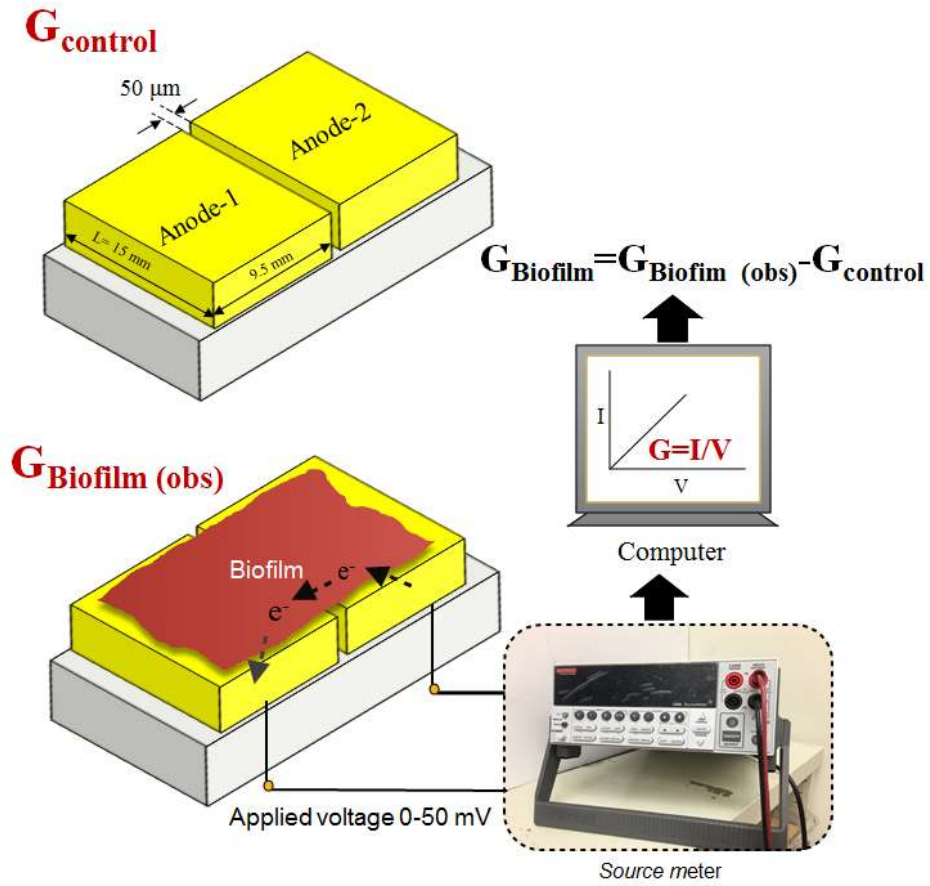
Figure B-1. Experimental set-up for biofilm conductivity measurement.

Appendix C

Supplementary Information for Chapter 3

Table C-1. Distribution of bacterial 16S rRNA during experiments at different anode potentials.

Class	Genus	-0.2 V vs. SHE (n=112689)	+0.2 V vs. SHE (n=45876)
Alpha-Proteobacteria	*Telmatospirillum*	-	68
	Xanthobacter	-	60
Beta-Proteobacteria	*Achromobacter*	-	50
	*Comamonadaceae**	-	164
	*Rhodocyclaceae**	97	436 (1.0%)
Delta-Proteobacteria	*Desulfovibrio*	-	55
	Geobacter	108437 (96%)	20336 (44%)
	Pelobacter	174	191
Epsilon-Proteobacteria	*Campylobacter*	-	90
Gamma-Proteobacteria	*Pseudomonadaceae**	1498 (1.3%)	2451 (5.3%)
Cloacamonae	*Cloacamonaceae**	50	-
Clostridia	*Anaerovorax*	-	79
	Oscillospira	-	54
Elusimicrobia	*Elusimicrobium*	-	228
Spirochaetes	*Treponema*	1100 (1.0%)	18107 (40%)
Synergistia	*Aminiphilus*	67	1507 (3.3%)
	Dethiosulfovibrionaceae	56	159

- (not found or less than 50 sequences)

* Family

Table C-2. Measured biofilm and control conductance for different anode potential conditions using the two-probe measurement method.

E_{anode} (V vs. SHE)	$G_{Biofilm(obs)}$ (mS)	$G_{Control}$ (mS)	$G_{Biofilm}$ (mS)
-0.2	0.79±0.15	0.06±0.008	0.74±0.15
+0.2	0.69±0.14	0.06±0.002	0.63±0.14

Calculation of electron transfer rate for E_{anode} -0.2 V condition

Current, I= 5.85×10^{-4} A

Biofilm thickness, L_f=34 μm =3.4×10^{-5} m

Total surface area of anode electrodes=2.85 cm^2=2.85×10^{-4} m^2

$q_{max,app}X_f$ =648,152 (g COD/m^3-d) (estimated)

Concentration of active biomass in biofilm, X_f= 2.9×10^4 g VSS/m^3

Assuming $q_{max,app}$ is 22 g COD/g VSS-d for *Geobacter* spp.,

Mass of active biofim = (2.85×10^{-4} m^2)×(2.9×10^4 g VSS/m^3)×(3.4×10^{-5} m) =2.8×10^{-4} g VSS=0.28 mg VSS

Assuming 50% of biomass cell (i.e., VSS) is protein,

Mass of protein = 0.14 mg protein

Electron transfer rate= [(5.85×10^{-4} C/sec)×(6.25×10^{18} e$^-$/C)]/ (0.14 mg protein)

=2.6×10^{16} e$^-$/sec-mg protein

Supplementary Information for Chapter 4
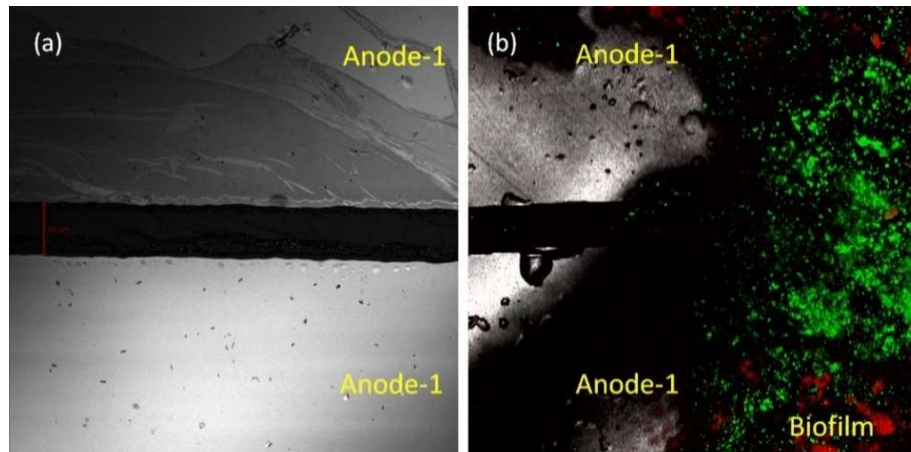
Figure D-1. Confocal laser scanning microscopy (CLSM) images showing (a) 50 μm non-conductive gap between two gold electrodes before biofilm formation (control), and (b) ARB biofilm bridged across non-conductive gap of 50 μm between two gold electrodes.
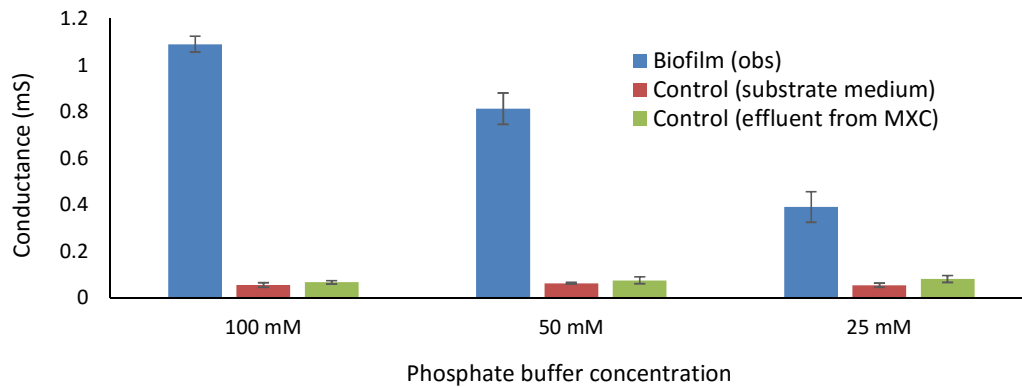

Figure D-2. Measured biofilm and control (substrate medium and effluent from MxC) conductance for different phosphate buffer concentrations.
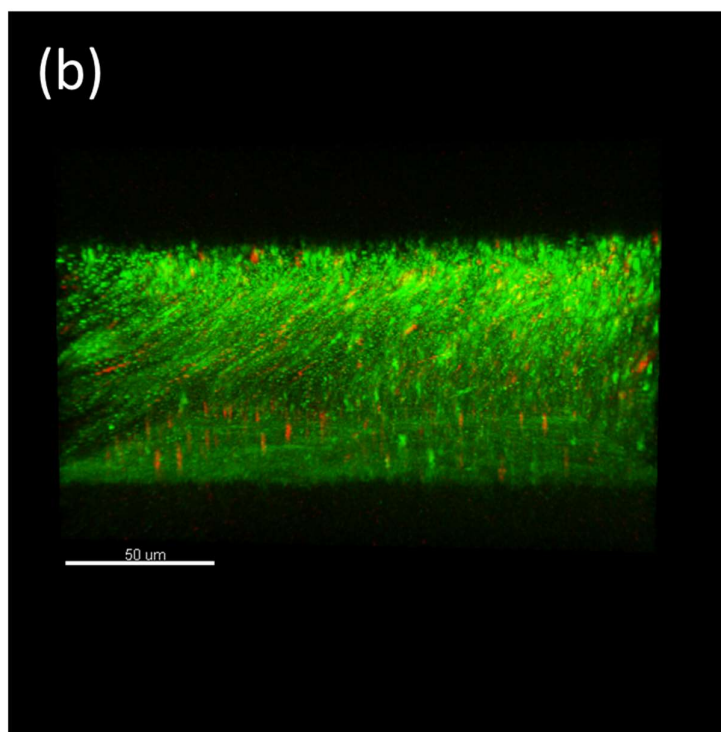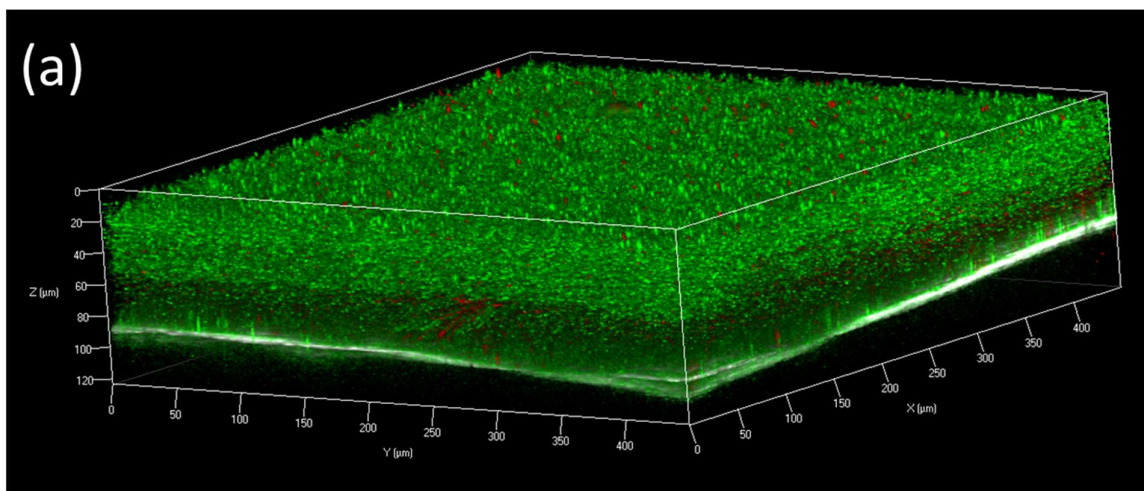
Figure D-3. (a) The 3D CLSM image of biofilm at 100 mM phosphate buffer, (b) representative 2D image prepared using Bitplane Imaris Software (Bitplane USA, Concord MA).
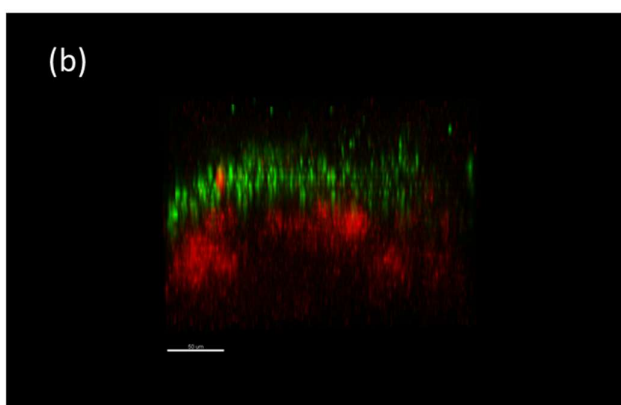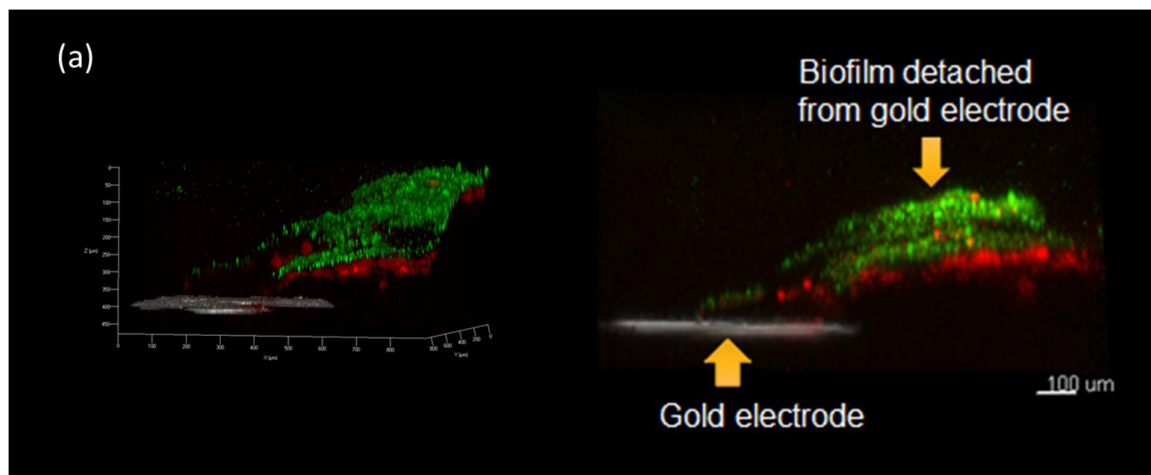
Figure D-4. (a) The CLSM image of biofilm at 2.5 mM phosphate buffer, (b) representative 2D image prepared using Bitplane Imaris Software (Bitplane USA, Concord MA). The biofilm was detached from gold surface during staining process.
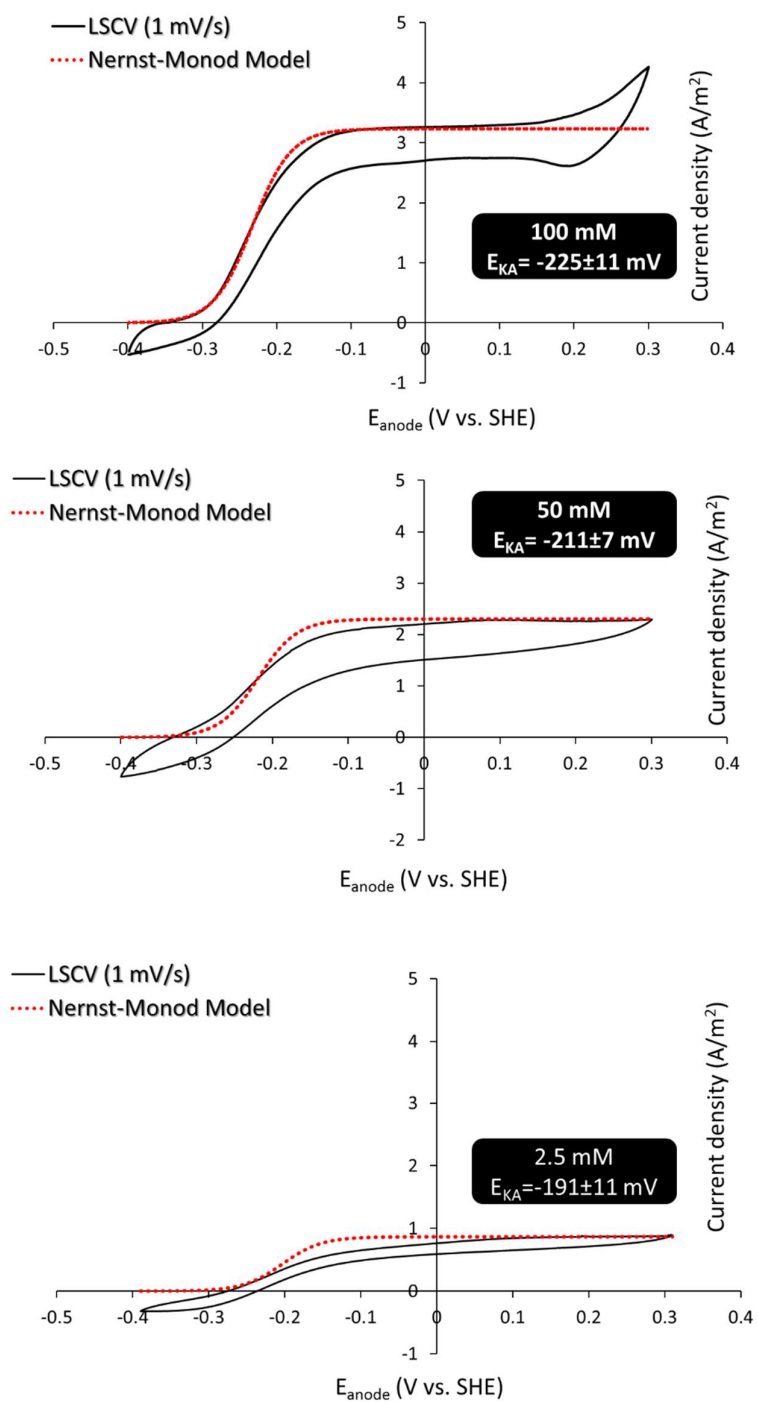
Figure D-5. LSCVs and Nernst-Monod equation simulation using same scale (y-axis) at different phosphate buffer concentration.

Figure D-6. Calibration curve for pH microelectrode.

Appendix E

## Supplementary Information for Chapter 5
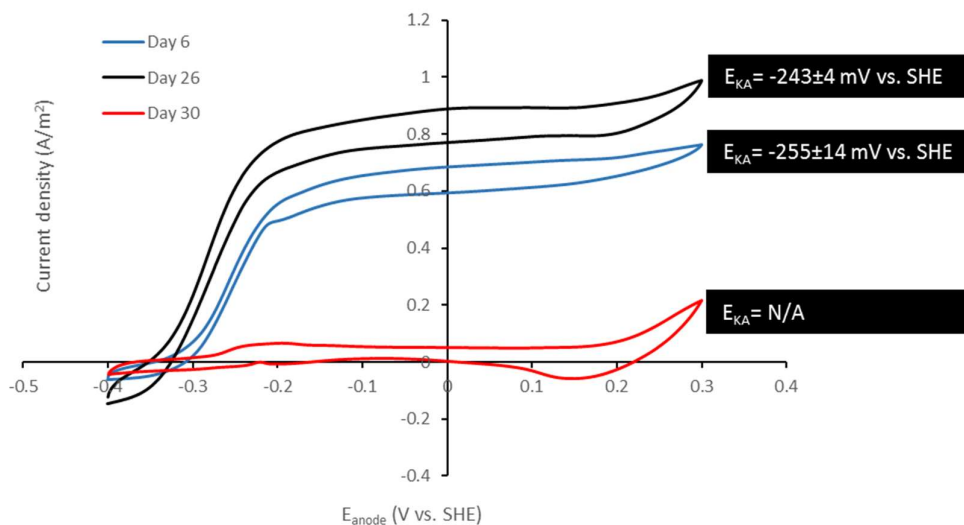
**Figure E-1.** LSCVs during long-term substrate limitation test.
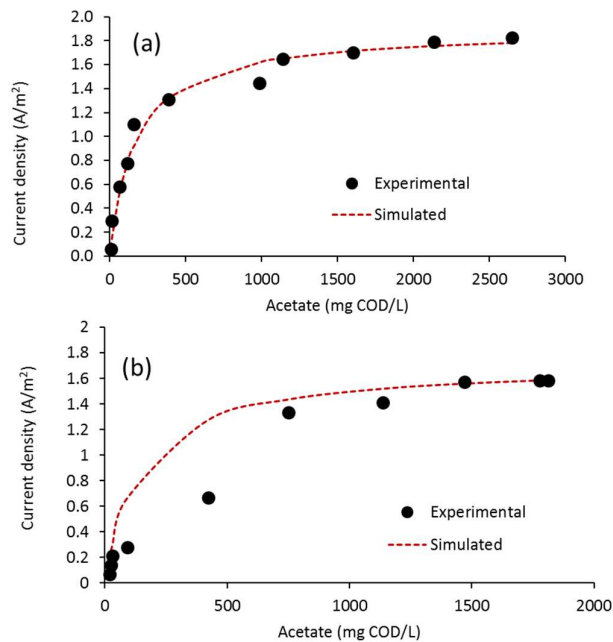
Figure E-2. Observed and simulated current density at different substrate concentration: (a) at steady-state, (b) after long-term substrate limitations tests.

Table E-1: Biofilm thickness measured during long-term substrate limitation test.

Day	Biofilm Thickness (µm)
8	127±33
22	147±19
29	142±26

Table E-2. Estimated biological kinetic parameters.

	Steady-state	After long-term substrate limitation tests
$K_{s,app}$ (g COD/m^3)	168	143
$q_{max,app}X_f$ (g COD/m^3-d)	126,196	111,763

Appendix F

Supplementary Information for Chapter 6

Table F-1. Distribution of bacterial 16S rRNA in multi-anode MxC.

Class	Genus	Anode-1 (n=67242)	Anode-2 (n=52552)	Anode-3 (n=27674)
Alpha-Proteobacteria	*Agrobacterium*	211	-	1332 (4.8%)
	Azospirillum	78	27	820 (3.0%)
	Bosea	65	46	181
	Bravundimonas	-	-	63
	Devosia	-	15	106
	Sphingomonas	65	77	100
	Telmatospirillum	22	-	32
	Xanthobacter	32	-	391 (1.4%)
Beta-Proteobacteria	*Achromobacter*	27	81	103
	*Comamonadaceae**	762 (1.1%)	175	992 (3.6%)
	Comamonas	18	-	32
	*Rhodocyclaceae**	113	37990 (72%)	1946 (7.0%)
Delta-Proteobacteria	*Desulfovibrio*	23	33	61
	Geobacter	58773 (87%)	419 (0.8%)	170 (0.6%)
	Pelobacter	114	-	-
Epsilon-Proteobacteria	*Campylobacter*	-	-	19
	*Helicobacteraceae**	35	165	190
Gamma-Proteobacteria	*Aeromonas*	1437 (2.1%)	-	5208 (19%)
	*Pseudomonadaceae**	149	188	1182 (4.3%)
	Stenotrophomonas	552	181	562 (2.0%)
Bacteroidia	*Blvii28*	-	168	223
	Dysgonomonas	-	-	149
Cloacamonae	*Cloacamonaceae**	73	517 (1.0%)	165
Clostridia	*Anaerovorax*	-	45	55
	*Christensenellaceae**	-	-	17
	Fusibacter	-	910 (1.7%)	448 (1.6%)
	Oscillospira	30	55	106
Elusimicrobia	*Elusimicrobium*	47	-	14
Flavobacteria	*Flavobacterium*	-	-	518 (1.9%)
Opitutae	*Opitutus*	11	174	54
Sphingobacteria	*Sphingobacterium*	-	-	16
Spirochaetes	*Treponema*	27	18	107
Synergistia	*Aminiphilus*	-	50	82
	Dethiosulfovibrionaceae	-	79	201

- (not found or less than 10 sequences)

* Family
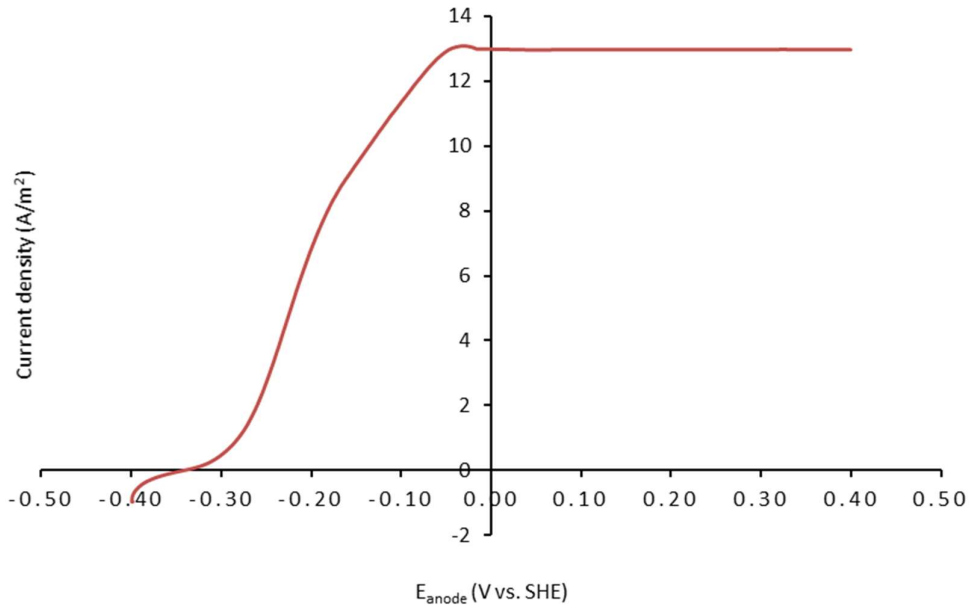
Figure F-1. LSCV for multi-anode MxC when three anode modules were connected together (Phase-1).